

**Clay-Mineral and Grain-Size Distributions in Inner Shelf Sediments off  
Mangalore, Goa, Arabian Sea: Indicators of Sediment Sources and  
Transport Processes**

A Dissertation Report for  
**GEO - 651 Dissertation**  
16 Credits

Submitted in partial fulfilment of Master's Degree  
**M.Sc. in Applied Geology**

by

**SATHEESH LAL K A**

Seat Number: 22P0450020

ABC ID: 183313985025

PRN: 202200097

Under the Supervision of

**Dr. Swati Verma**

Scientist- Geological Oceanography Division  
CSIR-National Institute of Oceanography  
Dona Paula, Goa – 403004.

School of Earth, Ocean, and Atmospheric Sciences  
Applied Geology

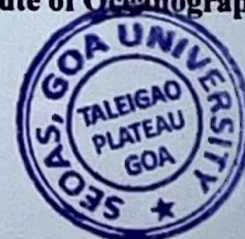


**Goa University**



**CSIR- National Institute of Oceanography**

**April 2024**



**Examined by:**

**Seal of the School**

## DECLARATION BY STUDENT

I hereby declare that the data presented in this Dissertation report entitled "**Clay-Mineral and Grain-Size Distributions in Inner Shelf Sediments off Mangalore, Goa, Arabian Sea: Indicators of Sediment Sources and Transport Processes**" is based on the results of investigations carried out by me in the Discipline of Applied Geology at the School of Earth, Ocean, and Atmospheric Sciences, Goa University and CSIR National Institute of Oceanography, under the Supervision of Dr. Swati Verma, Scientist at CSIR National Institute of Oceanography, and the same has not been submitted elsewhere for the award of a degree or diploma by me. Further, I understand that Goa University or its authorities will not be responsible for the correctness of observations / experimental or other findings given the dissertation.

I hereby authorize the University authorities to upload this dissertation on the dissertation repository or anywhere else as the UGC regulations demand and make it available to any one as needed.

S. Lal  
12/5

Satheesh Lal K A

Student

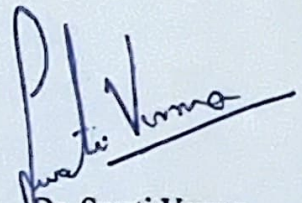
Seat no: 22P0450020

Date: 02 May 2024

Place: Goa University

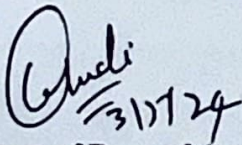
## COMPLETION CERTIFICATE

This is to certify that the dissertation report “Clay-Mineral and Grain-Size Distributions in Inner Shelf Sediments off Mangalore, Goa, Arabian Sea: Indicators of Sediment Sources and Transport Processes” is a bonafide work carried out by Satheesh Lal K A under my supervision in partial fulfilment of the requirements for the award of the degree of Master of Science (Applied Geology) in the Discipline of Applied Geology at the School of Earth, Ocean, and Atmospheric Sciences, Goa University.



Dr. Swati Verma  
Supervisor

Date:



Signature of Dean of the School



School Stamp

Date:

Place: Goa University

**Clay-mineral and grain-size distributions in inner shelf sediments off  
Mangalore, Goa Arabian Sea: Indicators of sediment sources and transport  
processes**

A Dissertation Report for  
**GEO - 651 Dissertation**  
16 Credits

**Submitted in partial fulfilment of Master's Degree  
M.Sc. in Applied Geology**

by

**SATHEESH LAL K A**

Seat Number: 22P0450020

ABC ID: 183313985025

PRN: 202200097

Under the Supervision of

**Dr. Swati Verma**

Scientist- Geological Oceanography Division  
CSIR-National Institute of Oceanography  
Dona Paula, Goa – 403004.

School of Earth, Ocean, and Atmospheric Sciences

Applied Geology



**Goa University**



**CSIR- National Institute of Oceanography**

**April 2024**

Examined by:

Seal of the School

## DECLARATION BY STUDENT

I hereby declare that the data presented in this Dissertation report entitled “Clay-mineral and grain-size distributions in inner shelf sediments off Mangalore, Goa, Arabian Sea: Indicators of sediment sources and transport processes” is based on the results of investigations carried out by me in the Discipline of Applied Geology at the School of Earth, Ocean, and Atmospheric Sciences, Goa University and CSIR National Institute of Oceanography, under the Supervision of Dr. Swati Verma, Scientist at CSIR National Institute of Oceanography, and the same has not been submitted elsewhere for the award of a degree or diploma by me. Further, I understand that Goa University or its authorities will not be responsible for the correctness of observations / experimental or other findings given the dissertation.

I hereby authorize the University authorities to upload this dissertation on the dissertation repository or anywhere else as the UGC regulations demand and make it available to any one as needed.

Satheesh Lal K A

Student

Seat no: 22P0450020

Date:

Place: Goa University

## COMPLETION CERTIFICATE

This is to certify that the dissertation report “Clay-mineral and grain-size distributions in inner shelf sediments off Mangalore, Goa, Arabian Sea: Indicators of sediment sources and transport processes” is a bonafide work carried out by Satheesh Lal K A under my supervision in partial fulfilment of the requirements for the award of the degree of Master of Science (Applied Geology) in the Discipline of Applied Geology at the School of Earth, Ocean, and Atmospheric Sciences, Goa University.

A handwritten signature in blue ink that reads "Swati Verma". The signature is stylized and includes a horizontal line underneath the name.

Dr. Swati Verma  
**Supervisor**

Date:

Signature of Dean of the School

School Stamp

Date:

Place: Goa University

## TABLE OF CONTENTS

Acknowledgement.....	i
List of Tables.....	ii
List of Figures.....	
Abbreviations used	
<b>CHAPTER I: INTRODUCTION.....</b>	<b>1-20</b>
Origin of Ocean.....	2
Grain Size Analysis.....	7
Study Area.....	17
Aim and Objectives.....	20
<b>CHAPTER II: LITERATURE REVIEW.....</b>	<b>21-26</b>
Past studies of clay minerals in World oceans.....	22
Past studies of clay minerals in Arabian Sea.....	24
<b>CHAPTER III: MATERIALS AND METHODOLOGY.....</b>	<b>27-48</b>
Sample Processing.....	28
Laser Particle Size Analyzer.....	29
Instrumentation Of a Laser Particle Size Analyzer.....	32
Statistical Data & Geometric graphical measures.....	35
X-Ray Diffractometer (XRD).....	36
Bulk Mineralogy.....	44
Clay Mineralogy.....	45
Quantitative Analysis – Calculation of Peak areas.....	47
<b>CHAPTER IV: RESULTS AND DISCUSSION.....</b>	<b>49-96</b>
Grain Size Distribution of Gravity Core (GC2).....	49
Grain Size Distribution of Multicore (Mangalore).....	52
Depth Wise Variation of Statistical Data.....	53

Grain-Size Statistics.....	55
Bivariate Plots of Various Statistical Size Parameters.....	59
Clay mineral XRD Graphs of GC2 Core (Mangalore).....	62
SP core bulk XRD Graph.....	77
MC core bulk XRD Graph.....	78
Clay Mineral XRD Graph GC6 Core.....	79
List of Bulk Minerals XRD.....	91
Clay minerals and their $2\theta$ values.....	92
Overall Comparison Between GC2 And GC6 Core Clay Mineralogy.....	93
Variation in clay minerals from the offshore samples.....	94
Discussion.....	95
<b>CHAPTER V: CONCLUSION.....</b>	<b>99-101</b>
<b>CHAPTER VI: REFERENCES.....</b>	<b>102-108</b>

## ACKNOWLEDGEMENTS

I wish to express my indebted gratitude and special thanks to my Dissertation guide Dr. Swati Verma, Scientist, Geological Oceanographic Division, CSIR-National Institute of Oceanography, Goa for his valuable support and guidance to my project work. I express my sincere gratitude to Dr. Aninda Mazumdar, Senior Principal Scientist, Geological Oceanographic Division, National Institute of Oceanography, Goa for the help and wise advice throughout my Dissertation work.

I would like to express my gratitude to the Director Dr. Sunil Kumar Singh, National Institute of Oceanography, for giving me the opportunity in this renowned Institute to carry out my Dissertation work.

I would like to convey my heartfelt thanks to Dr. Anthony Arthur A. Viegas, Vice Dean (Academics), School of Earth, Ocean and Atmospheric Science, Goa University for his assistance during my studies. I would like to convey my sincere appreciation to Dr. Niyati Kalangutkar for her help, and direction in my Dissertation.

My sincere gratitude to Dr. Pooja Ghadi, Dr. Nicole Sequeira, Dr. Poornima Sawant and Mr. Mahesh Mayekar, for the guidance, invaluable advice and support which lead to the completion of this dissertation.

I would also like to thank Mr. Sarankumar, for helping me with the X-ray Diffraction analysis. I would also like to thank all the administrative staffs, Laboratory assistant of School of Earth Ocean and Atmospheric Sciences, Goa University for their assistance. I want to express my gratitude to Ms. Ankita Ghosh, Ms. Anjali, Ms. Kalyani Sivan, Mr. Viplove Rajurkar, Mr. Sai Pavan Kumar, Mr. Shadique, Mr. Jittu Mathai for their assistance with my lab work.

I would like to extend my deepest gratitude to my dear friends, Dipali Sarode, Ansa Antony, Bharath Prasanth, Devanandan P S, Suraj Kumar L M, Mohammed Irfan K I, Meera Narayanankutty, Sneha S, Sharon C, Adithyan Palayi, Bineesh A R, Salmanul Faris, Musharaf A K your unwavering support, laughter, acted as a ray of sunshine during the challenging times. My immense gratitude goes to my family, whose love and prayers for believing in me to pursue my Master's degree.

**LIST OF TABLES**

<b>Table no.</b>	<b>Description</b>	<b>Page. no.</b>
Table 1	Geometric graphical measures (modified by Folk and Ward 1957)	35
Table 2	Percentage of clay minerals in GC2 core	76
Table 3	Percentage of clay minerals in GC6 core	89
Table 4	List of Bulk Minerals XRD	91
Table 5	List of clay minerals and their $2\theta$ values	92
Table 6	List of other clay sized minerals	92

## LIST OF FIGURES

<b>Fig. no.</b>	<b>Description</b>	<b>Page no.</b>
Fig. 1	Thermohaline Circulation Arrows indicating the flow direction of the water (modified from Friedland (2010))	3
Fig. 2	Shepard, F.P., 1954, Nomenclature based on sand-silt-clay ratios.	8
Fig. 3	Grain-size scale for sediments and sedimentary rock (after Udden and Wentworth 1922)	8
Fig. 4	Octahedral structure and tetrahedral structure (Goh et al., 2011).	10
Fig. 5	Structures of Common Clay Minerals (Credit: U.S. Geological Survey).	16
Fig. 6	Map of the study area with blue dot, showing the location of the gravity core made using ODV (SSD070/GC2),(SSD070GC6)	17
Fig. 7	Working Principle of LPSA	31
Fig. 8	Showing the instrumentation of a laser particle size analyser	34
Fig. 9	Braggs law. $\theta$ is the angle between the incident beam and the lattice plane. $\Lambda$ is the wavelength and $d$ is the distance between parallel lattice points.	38
Fig. 10	Schematic of X-ray diffractometer. $\theta$ -angle between the incident beam and a lattice plane	44
Fig. 11 (A – C)	Grain Size Distribution of GC2	50
Fig.12 (A-C)	Graphs of Grain Size Distribution of Multi Core with depth (cm)	51
Fig.13	Plots of Statistical Data	52
Fig.14 (A-C)	(A)Plot of Mean Grain Size Vs sorting (B)- Mean Grain Size Vs Skewness (C)- Mean Grain Size Vs Kurtosis	55-58

Fig. 15	(A)Graphic Skewness vs Graphic Kurtosis; (B)Graphic Skewness vs sorting	59-60
Fig.16 (A-E)	Clay mineral XRD Graph of GC2 0-491 cm	62-66
Fig 17 (A-S)	Percentage of clay minerals in GC2 0-491 cm	67-73
Fig. 18 (A-B)	(A) Bulk mineral XRD Graph of GC2 40-261 cm (B) Bulk mineral XRD Graph of GC2 310-491 cm	74-75
Fig. 19	Bulk mineral XRD Graph of SP 13 0-1 cm, 40-41 cm	77
Fig. 20	Bulk mineral XRD Graph of MC1 0-30 cm	78
Fig. 21 (A-D)	Clay mineral XRD Graph of GC6 4-471 cm	79-82
Fig. 22 (A-Q)	Percentage of clay minerals in GC6 0-471 cm	83-88
Fig. 23	Bulk mineral XRD Graph of SSD070 GC6 84-449 cm	91
Fig. 24 (A-B)	(A) Overall percentage of clay minerals in GC2 core; (B) Overall percentage of clay minerals in GC6 core	93

### ABBREVIATIONS USED

Entity	Abbreviation
Laser Particle Size Analyser	LPSA
X-Ray Diffractometer	XRD
National Institute of Oceanography	NIO
Sindhu Sadhana	SSD
Gravity Core	GC
Multi Core	MC
Spade Core	SP
Full Width Half Maxima	FWHM
Ocean Data Viewer	ODV
Hydrogen Peroxide	H <sub>2</sub> O <sub>2</sub>
Calcium Chloride	CaCl <sub>2</sub>
Hydrochloric Acid	HCl
Acetic Acid	CH <sub>3</sub> COOH
Normality	N
Metre	m
Centimetre	cm
Gram	g
Degree Celsius	°C
Hours	hrs
Percentage	%

## ABSTRACT

Clay mineralogical study and grain size pattern of sediments have indicated their environment of deposition, sediment movement pattern and the dynamic behaviour of sediments. In this study, the grain size and clay mineralogy were carried out on the marine sediment samples collected from the continental shelf offshore Mangalore site, Arabian Sea, India. This study aims to characterize the composition of clay minerals and examine the depth-wise grain-size distribution of sediments to predict the depositional process of inner-shelf sediments and their relation to hydrodynamics to identify the sources and transport pathways. Inner-shelf sediments consist mainly of clay silt and silty clay, with limited amounts of sand. Clay and silt percentages show slight variations, suggesting consistent sediment composition. However, there is a notable increase in clay content and decrease in silt percentages, indicating a change in sediment characteristics and deposition. Utilizing Laser Particle Size Analysis, a modest variability in clay and silt proportions in the upper sediment core (ranging from 0cm to 132cm) is observed, indicating a relatively uniform sediment structure. Conversely, the clay content progressively rises from 20% to 40%, accompanied by a corresponding decrease in silt proportions from 70% to 50%. Grain size distribution analysis reveals poorly sorted sediments but also suggests reworking and redistribution influenced by wave and tidal currents. Identification of clay minerals with X-ray diffraction (XRD) to show the variation of clay mineral assemblages in the shallow marine sediments has provided the presence of illite-smectite, montmorillonite, kaolinite, illite and terrigenous non clay minerals like quartz. Other clay mineral such as chlorite is also present in certain samples. Our study demonstrates that decreasing sorting trend as grain sizes increase to is interpreted to be due to increasing rates of bioturbation and sediment mixing, also indicates weak bottom currents which capable of transporting only the finest silts and clays in suspension and sediment depositional processes.

**CHAPTER I**  
**INTRODUCTION**

## 1. INTRODUCTION

### 1.1 Origin of oceans

The origin of oceans was put forth first in 1912 by Alfred Wegner, a German meteorologist. He put forward the concept of plate tectonics which was originally called the “Theory of continental Drift”. According to this concept there was one supercontinent, Pangaea about 200 million years ago. It existed from the Permian through Jurassic periods. The same was surrounded by a single universal sea Panthalassa. The landmass was later separated into two continents by the Tethys Sea. It began breaking up during the Jurassic period. The landmass on the north of the Tethys was the Laurasia with the Eurasian and the North American continents and landmass to the south of the Tethys was the Gondwana which include African, South American, Australians and Antarctica continents and Indian subcontinent. As continents separated out the Gulf was taken over by various water bodies to be called later as five major oceans (Fig.). These are Arctic, Atlantic, Pacific, Antarctic and Indian Ocean, of these the Indian Ocean is the third largest. It extends between the continents of Africa (to the west) and Australia (to the east), and South Asia (to the north) and Southern Ocean (to the south). The northern Indian Ocean consists of the Arabian Sea (present study area) and the Bay of Bengal (Wegener, Alfred et al., 1912).

#### 1.1.1 The ocean floor

The Ocean floor can be divided into the continental margin and the deep-sea floor. The continental margin consists of the continental shelf, the continental slope, and the continental rise. The continental shelves have a flat topography (0.10 gradient), the average depth being ~130m. They are sites for the deposition of abundant land-derived sediments and biogenic

carbonates. The continental shelf is separated from the continental slope by the shelf edge or shelf break at approximately 200 m depth. The continental shelf and slope together covers ~15% of the total ocean floor, and the continental rise covers about 5%. The material of the slope is predominantly mud, with some rock out crops. Water circulation in the ocean Most important factor in determining the structure of the oceans is the circulation pattern. The water of the oceans move because of three main mechanisms: cooling near the Polar Regions and warming near the equatorial region (Garrison, T. S et al., 2016). This leads to thermohaline circulation (Fig.2) where new water is generated in the Atlantic Ocean gets circulated to Indian Ocean, then moves to the Pacific Ocean and goes back to the Atlantic Ocean via Indian Ocean. There are other forces which move the water, like the force exerted by the winds on the ocean surface, and the tides arising from the gravitational pull of the Moon and the Sun. The rotation of the Earth (360 degrees in 24 hours from west to east) about an axis passing through its poles, the shape of the oceans (long horizontal dimension in comparison to vertical), and the stable stratification (lighter waters overlying denser waters) in the oceans influence the movement of waters in the oceans.

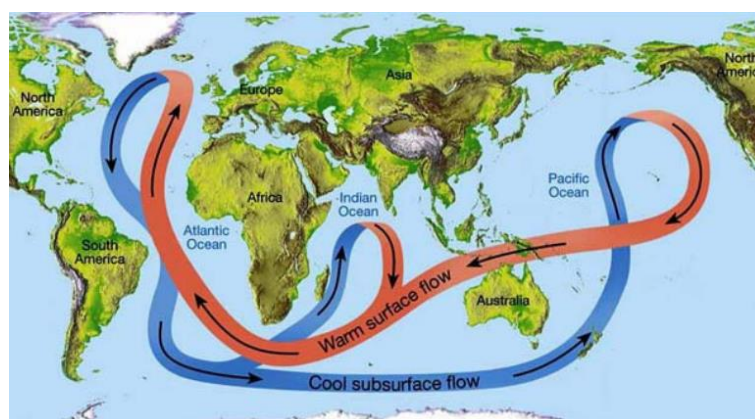


Fig.1: Thermohaline Circulation Arrows indicating the flow direction of the water (modified from Friedland (2010))

### **1.1.2 Origin of the Indian Ocean tectonics**

The northward movements of Indian subcontinent after separating from Gondwana supercontinent essentially led to the formation of Indian Ocean. The movement of the Indian continent from south eastern part of Africa to join Eurasia by destroying the Tethys Sea has made the Indian Ocean tectonics interesting (Torsvik, Trond H., et al. 2008). The Arabian Sea was formed within past roughly 50 million years as the Indian Subcontinent collided with Asia

### **1.1.3 Physiography of the Indian Ocean**

The Indian Ocean is the third largest of the world's Oceanic divisions, covering about 20% of the water on the Earth's surface. This Ocean covers an area of about 73,600,000 Sq Kms bounded by African continent on the west, Australian continent on the east, Asian continent on the north and Atlantic continent on the south. The North Indian Ocean includes the Arabian Sea (to the west of India) and the Bay of Bengal (to the east) The northern Indian Ocean exhibits unique oceanographic characteristics compared to those of its counterparts-the north Atlantic and the north Pacific oceans (Pearson, M.N., et al. 2003). It encompasses world's most productive region, most prominent oxygen minimum zone and largest deep sea fans- the Indus fan and Bengal fan. This uniqueness is said to be result of land-locked boundary on the north, giving rise to monsoons, seasonal reversing currents and there is no source of deep convection of the cold water of polar region.

### **1.1.4 GRAIN SIZE**

Most fine grained fluviially-derived marine sediments are deposited in the near shore and continental margins and only a small amount is transferred to the deep sea (Chester, 1990). The fine-grained sediments are composed mainly of clay and amorphous minerals. The composition and relative abundance of the clay minerals are controlled by their source rocks

and weathering conditions. The characteristics of terrigenous sediments deposited on a continental margin largely reflect the prevailing climatic conditions, hydrography, and geology of the continental source area. A number of studies have shown that clay mineral distributions are particularly sensitive indicators of spatial and temporal changes of the geology and the weathering characteristics on the adjacent continental landmass (Biscaye, 1965; Chauhan et al., 1992; Kolla et al., 1976, 1981; Nair et al., 1982; Staneley and Liyanage, 1986; Weaver, 1989;).

To understand Earth's dynamic history and foresee future changes, it is essential to understand historical environmental circumstances (IPCC, 2013). Insights into climatic variability, sea-level changes, and biological transitions over geological time scales can be gained via paleoenvironmental reconstructions (Clark et al., 2009; Thompson et al., 2002). Analysis of grain size in marine sediments is a potent method for reconstructing paleoenvironments (Blott and Pye, 2001; Balsam et al., 2010). The energy levels, environmental factors, and depositional processes that impacted sediment deposition may all be inferred via grain size analysis. (Manning et al., 2011). Examining the distribution and properties of sediment particles within a sample is part of the grain size analysis process for marine sediments (Folk, 1980). The sedimentary processes and the paleoenvironmental circumstances under which the sediments were formed by measuring metrics including mean grain size, sorting, skewness, and kurtosis (Folk, 1980; Inman and Jenkins, 1999).

The capacity of grain size analysis to provide light on previous climatic and oceanic circumstances as well as its potential for forecasting paleoenvironments (Doe et al., 2017; Smith et al., 2019). However, more study is required to determine if grain size analysis can be used in various maritime environments and to establish reliable connections between certain paleoenvironmental factors and grain size parameters (Maldonado et al., 2018). To understand

the depositional process and environment, including hydrodynamic process, it is crucial to first characterise the grain size of the siliciclastic sediment. This analysis makes some inferences about potential transportation mechanisms and classifies sediment characteristics and depositional settings. To compare different sediment types, the investigated sediments must be split into several groups based on their dimensional ranges. Because there are several categories accepted in scientific literature, the optimal classification to adopt depends on the study's objectives, the kind of sediment being researched, and the quality of the analysis (Pinemet et al.,2009).

Grain size is the most fundamental physical property of sediments. The size and the shape of grain influence flow and compaction properties. Geologist and sedimentologist use information on sediment grain size to study trends in surface processes related to the dynamic conditions of transport and depositions (environment characteristic of clays and clay minerals USGS). Grain size is commonly related to other properties i.e. porosity and permeability which have major economic implications. Particle size influences many properties of particulate materials and is a valuable indicator of quality and performance (Blatt, H., et al. 1980). This is true for powders, suspensions emulsions and aerosols. The size and shape of powders influences flow and compaction properties. Larger more spherical particles will typically flow more easily than smaller or high aspect ratio particles. Smaller particles dissolve more quickly and lead to higher surface suspension viscosities than larger ones (Vinu & Narayana, 2012). Smaller droplet size and higher surface charge will typically improve suspension and emulsion stability. Powder or droplets in the range of 2-5 $\mu$ m aerosolize better and will penetrate into lungs deeper than larger sizes. For these and many other reasons it is important to measure and control the particle size distribution of many products. There is also an industry application specific reason why controlling and measuring particle size is important. In the paint and pigment industries particle size influences appearance properties including gloss and tinctorial

strength particle size of the cocoa powder used in chocolate affects color and flavor. The size and shape of the glass bead used in highway paint impact reflectivity. Cement particle size influences hydration rate and strength. In pharmaceutical industry the size of active ingredients influences critical characteristics including content uniformity, dissolution and absorption rates. Other industries where particle size plays an important role include nanotechnology, proteins, cosmetic polymers, soils, abrasives, fertilizers.

## 1.2 GRAIN SIZE ANALYSIS

The grain size's mean value is the average. This grain size is typically represented in phi or in millimetres. The particle size that falls in the centre of the population is called the median, and it is defined as the size at which half of the total weight of the particle is finer and the other half is rougher than the grain size. The value of phi at the point where the cumulative curve reduces the value of 50% can be directly viewed as the median from the cumulative curve. Sorting is the grain size distribution's standard deviation (the distribution of values around the mean). Kurtosis displays the comparison value between the section's centring on the curve's edge.

A curve's skewness expresses how unequal it is. If Skewness is favourable, the sediment will include more coarse grain than fine grain, and vice versa.

This classification is given by the ratio between sand and mud (silt + clay):

- Sand: sand > 95 %
- Muddy sand: sand 95-70 %; mud 30-5 %
- Very sandy mud: sand 70-30 %; mud 30-70 %
- Sandy mud: sand 30-5 %, mud 70-95 %
- Mud: mud > 95 %

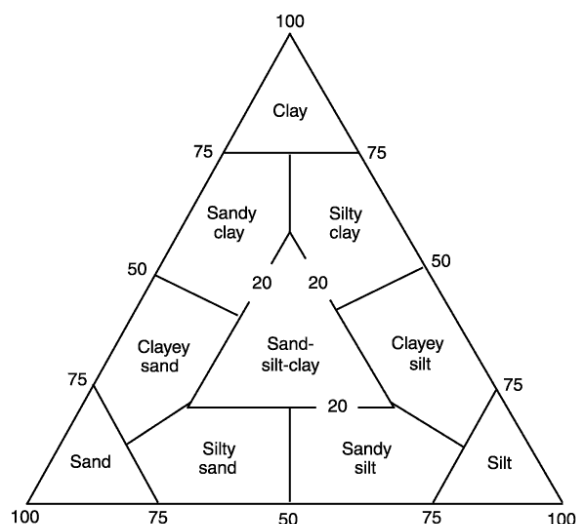


Fig.2: Shepard, F.P., 1954, Nomenclature based on sand-silt-clay ratios.

Laser diffraction measures very small particles (0.02 - 2000 microns), and when a laser beam passes a dispersed particle, it can measure angular variation of the particle. Rock size can be categorised by Udden and Wentworth 1922 below.

mm	phi implying grain size	class term	sediment and rock terms
256	-8	<u>boulders</u>	
128	-7		
64	-6	<u>cobbles</u>	gravels
32	-5		rudite
16	-4	pebbles	rudaceouseds.
8	-3		conglomerates
4	-2		breccias
2	-1	<u>granules</u>	
1	0		
0.5	1		
0.25	2	sand	v.coarse coarse medium fine
0.125	3		v.fine
0.0625	4		coarse medium fine
0.0312	5		
0.0156	6	silt	
0.0078	7		
0.0039	8		
		clay	claystone

Fig.3: Grain-size scale for sediments and sedimentary rock  
(after Udden and Wentworth 1922)

### 1.2.1 CLAY MINERALS

Clay refers to naturally occurring material composed primarily of fine-grained minerals, which is generally plastic at appropriate water contents and will harden when fired or dried. Clay minerals are hydrous aluminium phyllosilicates, sometimes with variable amounts of iron, magnesium, alkali metals, alkaline earths. They are usually less than  $2\mu\text{m}$  in size. Clay minerals are an important group of minerals as they are amongst the most common products of chemical weathering, and thus are the main constituents of the fine-grained sedimentary rocks called mud rocks (including mudstone, claystone, and shale). In fact clay minerals are the main constituent of soils and make up about 40% of the minerals in sedimentary rocks. Their composition largely depends on climate, geology and topography of the area. Clay minerals in sediments, particularly in marine sediments, can be useful indicators of provenance (Reddy., 2001). Clay minerals are hydrous silicate minerals essentially composed of two-dimensional Si bearing tetrahedral and Al-bearing octahedral sheet stacked in a regular array (Fagel et al. 2007). All Clay minerals are hydrous aluminium silicates and are classified as phyllosilicates or layer silicates. Despite considerable chemical and physical variation in their properties, these minerals mostly display platy morphology and perfect (001) cleavage, low specific gravity, low hardness and elastic nature. Clay minerals are believed to be constructed from two modular units:

#### 1. Tetrahedral Sheets

The dominant cation is  $\text{Si}^{4+}$  but  $\text{Al}^{3+}$  substitutes for it frequently and  $\text{Fe}^{3+}$  occasionally. The cation/Oxygen ratio is  $\text{T}_2\text{O}_5$ . This ratio results from the sharing of 3 oxygen atoms in each tetrahedron. Six-fold symmetry is exhibited in undistorted sheets with the Si-O bond distance about  $1.62 \text{ \AA}$  and the O-O distance about  $2.64 \text{ \AA}$ . Al may replace up to half of the Si changing the Al-O distance.

## 2. Octahedral Sheets

It is analogous to two planes of closest-packed oxygen ions with cations occupying the resulting octahedral sites between the two planes. Connections from these to neighbouring oxygen ions form a sheet of edge-linked octahedral extending in two dimensions infinitely.

Most of the minerals in the clay mineral group have a short-range unit cell continuity and consequently do not grow more than 3 or 4 microns in size. Most are less than 2 microns in size with the exception of palygorskite that can grow up to 100 microns in size.

In gibbsite, hydroxyl ions coordinated by aluminium ions like Mg, Al also forms a stable 6-fold coordination polyhedron with hydroxyl but because of the higher charge of the Al ion, only two-thirds as many Al ions may enter the sheet structure. Gibbsite has dioctahedral sheet structure and so does kaolinite, pyrophyllite, muscovite etc. Brucite sheets consist of two layers of hydroxyl ions in hexagonal close packing with Mg ions occupying the interstices. The radius ratio of Mg to hydroxyl is such that the 6-fold coordination of hydroxyl ions bond with Mg for maximum stability. This kind of configuration is called trioctahedral sheet structure. Brucite, antigorite, talc, phlogopite are of the trioctahedral group.

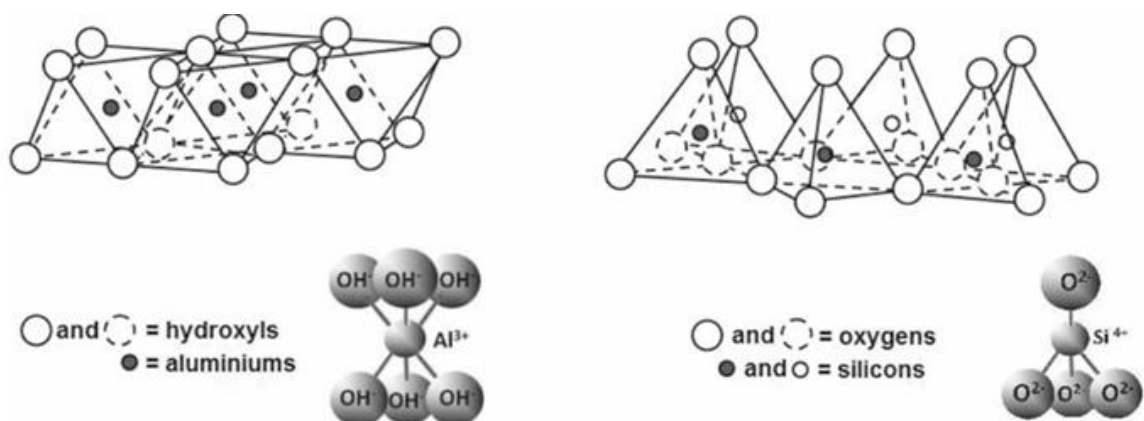


Fig.4: Octahedral structure and tetrahedral structure (Goh et al., 2011).

### 1.2.2 FORMATION OF CLAY MINERALS

Clay minerals have their origin in the weathering and alteration of rocks and minerals over long periods of time. The formation of clay minerals is a complex process that involves the interaction of various geological and chemical factors. Here's a general overview of the origin of clay minerals:

**Weathering:** The process begins with the weathering of primary minerals, such as feldspars, micas, and volcanic glass, which are present in rocks. Weathering occurs due to the exposure of rocks to various physical, chemical, and biological agents, including temperature fluctuations, water, wind, and organisms. These agents break down the rocks into smaller particles and initiate the transformation of primary minerals into clay minerals.

**Chemical alteration:** During weathering, water acts as a solvent, infiltrating the rocks and facilitating chemical reactions. The water interacts with the minerals, leading to ion exchange, dissolution, and precipitation reactions. The breakdown of primary minerals releases ions into the water, which can react with other dissolved species to form new minerals, including clay minerals.

**Hydrolysis:** One of the key processes in clay mineral formation is hydrolysis. Hydrolysis occurs when water molecules react with the silicate minerals, breaking the chemical bonds and altering the mineral structure. This process releases ions such as silicon, aluminium, and various cations into the solution, which can later participate in the formation of clay minerals.

**Ion exchange:** As the primary minerals weather and release ions, these ions can be exchanged with other ions present in the environment. For example, cations like calcium, sodium, and potassium can be exchanged with hydrogen ions in the presence of water. This ion exchange process further contributes to the formation of clay minerals.

**Sedimentation and diagenesis'**: The weathered particles, including the newly formed clay minerals, can be transported by wind or water and eventually settle as sediments. Over time, these sediments can undergo compaction and lithification, transforming into sedimentary rocks. The process of compaction and lithification, known as diagenesis, plays a crucial role in the preservation and transformation of clay minerals. It's important to note that there are various types of clay minerals, including kaolinite, montmorillonite, illite, and others. The specific conditions and mineral compositions during the weathering and alteration process influence the type and characteristics of the resulting clay minerals.

### 1.2.3 CLAY MINERAL CLASSIFICATION

#### **Chlorite Group**

The basic structure of the chlorite group consists of negatively charged mica-like (2:1) layers regularly alternating with positively charged brucite-like (octahedral) sheets. They are described as end members based on their chemistry via substitution of the four elements in the silicate lattice viz. Mg, Fe, Ni, and Mn. The chlorite minerals are common components of low-grade greenschist facies metamorphic rocks, and of igneous rocks as hydrothermal alteration products of ferromanganese minerals. Chlorites are also common constituents of argillaceous sedimentary rocks where these minerals occur in both detrital and authigenic forms. The typical general formula is:  $(\text{Mg,Fe})_3(\text{Si,Al})_4\text{O}_{10}(\text{OH})_2 \cdot (\text{Mg,Fe})_3(\text{OH})_6$ .

#### **Illite Group**

Illite is essentially a group name for non-expanding, clay-sized, dioctahedral, micaceous minerals. It is structurally similar to muscovite in that its basic unit is a layer composed of two inward-pointing silica tetragonal sheets with a central octahedral sheet. However, illite has on average slightly more Si, Mg, Fe, and water and slightly less

tetrahedral Al and interlayer K than muscovite (Poppe et al., 2001). The weaker interlayer forces caused by fewer interlayer cations in illite also allow for more variability in the manner of stacking. Glauconite is the green iron-rich member of this group. Illites form by the weathering of silicates (primarily feldspar), through the alteration of other clay minerals, and during the degradation of muscovite. Formation of illite is generally favored by alkaline conditions and by high concentrations of Al and K. Glauconite forms authigenically in marine environments and occurs primarily in pelletal form. The general formula is given as:  $(K,H_3O)(Al,Mg,Fe)_2(Si,Al)_4O_{10}(OH)_2 \cdot (H_2O)_n$ .

### **Kaolinite Group**

The kaolinite group includes the dioctahedral minerals kaolinite, dickite, nacrite, and halloysite, and the trioctahedral minerals antigorite, chamosite, chrysotile, and cronstedite. The primary structural unit of this group is a layer composed of one octahedral sheet condensed with one tetrahedral sheet (Wada, 1965). In the dioctahedral minerals the octahedral sites are occupied by Al; in the trioctahedral minerals these sites are occupied by Mg and Fe. Kaolinite and halloysite are single-layer structures. Although dickite and nacrite have the same basic structure, the stacking sequence of layers is different in these minerals (Poppe et al., 2001). Kaolinite, dickite, and nacrite occur as plates; halloysite, which can have a single layer of water between its sheets, occurs in a tubular form (Moore and Reynolds, 1997). All members of the kaolinite group form primarily during hydrothermal alteration or weathering of feldspars under acid conditions; but kaolinite and halloysite are probably the only members formed in soils.

### **Smectite Group**

Members of the smectite group include the dioctahedral minerals montmorillonite, beidellite, and nontronite, and the trioctahedral minerals hectorite (Li-rich), saponite (Mg rich), and sauconite (Zn-rich). The basic structural unit is a layer consisting of two inward pointing tetrahedral sheets with a central alumina octahedral sheet (Grim, 1962). The layers are continuous in the a and b directions, but the bonds between layers are weak and have excellent cleavage, allowing water and other molecules to enter between the layers causing expansion in the c-direction. Smectites commonly result from the weathering of basic rocks (Wilson, 1987). Smectite formation is favoured by level to gently sloping terranes that are poorly drained, mildly alkaline (such as in marine environments), and have the high Si and Mg potentials. Other factors that favour the formation of smectites include the availability of Ca and the paucity of K. Poor drainage is necessary because otherwise water can leach away ions (e.g. Mg) freed in the alteration reactions. Smectites are used in industry as fillers, carriers, absorbents, and a component in drilling fluids (Grim, 1962).

### **Vermiculite Group**

The structure of Mg-saturated vermiculite resembles talc in that it contains a central octahedrally-coordinated layer of Mg ions that lie between two inwardly pointing sheets of linked tetrahedra. These silicate layers are normally separated by two sheets of interlayer water molecules arranged in a distorted hexagonal fashion. Progressive removal of this interlayer water results in a series of less hydrated phases that include the 14.36 angstrom lattice with two sheets of water molecules, a 11.59 angstrom lattice with a single sheet of water molecules, and a 9.02 angstrom lattice from which all water has been removed (Gribble, C. D., et al. 2012). In as much as the layers are electrically neutral and interlayer cations occupy only about one third of the available sites, cohesion between the layers is

typically weak (Poppe et al., 2001). Vermiculites are usually formed in sediments by the alteration of micaceous minerals (biotite and chlorite to trioctahedral vermiculite; muscovite to dioctahedral vermiculite). However, vermiculites formed through the alteration of mica are comparatively rare in marine sediments because the K of sea water readily contracts them. Where present, marine vermiculites are probably derived from volcanic material, chlorite, and hornblende (Poppe et al., 2001).

### **Mixed Layer Clays Mixed-layer**

Clay minerals are materials in which different kinds of clay layers alternate with each other. The mixing or interstratification in vertical stacking can be regular (ordered), segregated regular, or random. Commonly described mixed-layer clays include: illite-vermiculite, illite-smectite, chlorite-vermiculite (corrensite), chlorite-smectite, and kaolinite-smectite (Gribble, C. D., et al. 2012). Mixed-layer clays can form by weathering involving the removal or uptake of cations (e.g. K), hydrothermal alteration, or removal of hydroxide interlayers, and, in some cases, may represent an intermediate stage in the formation of swelling minerals from non-swelling minerals or vice-versa (Poppe et al., 2001).

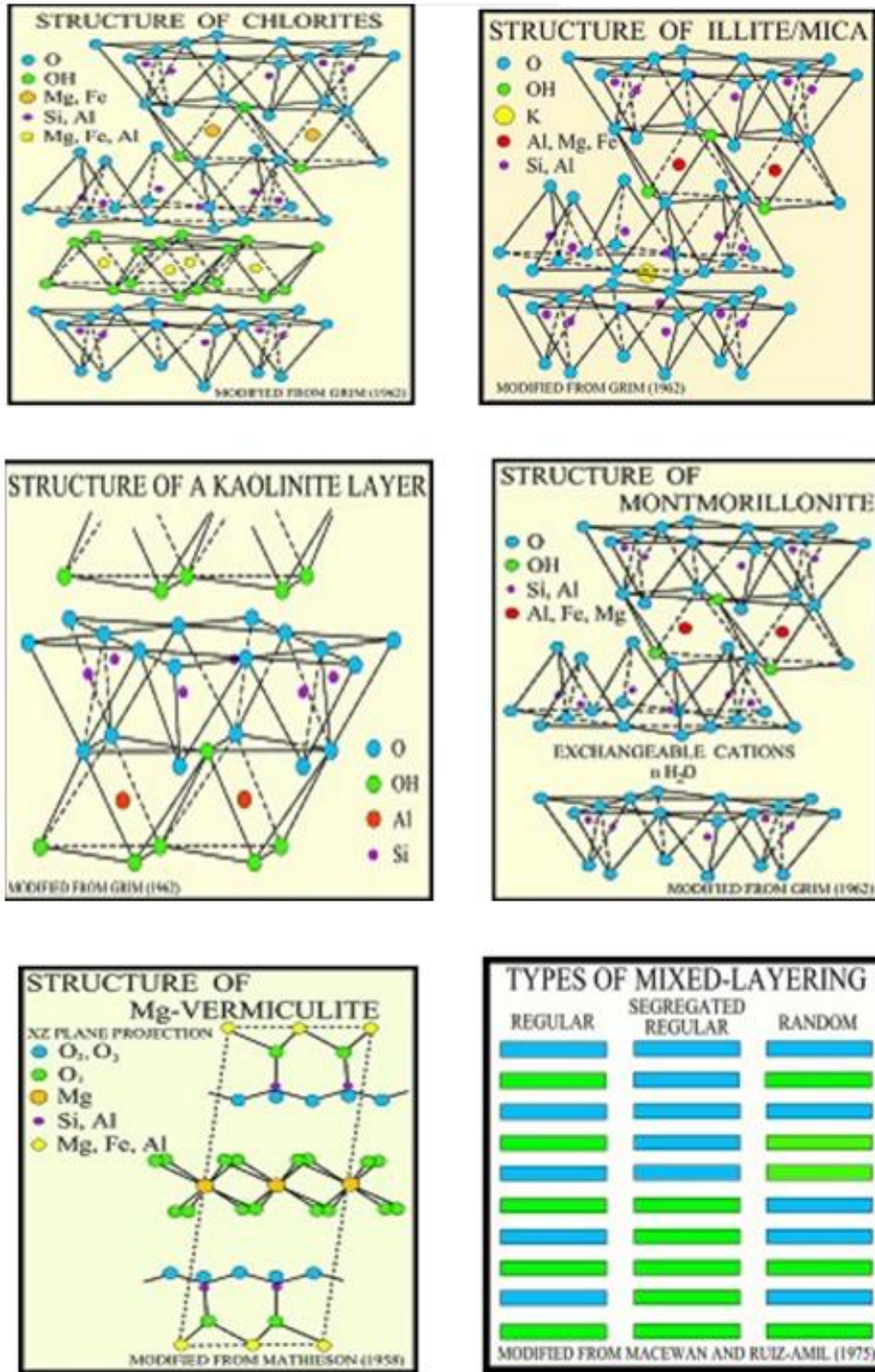


Fig.5: Structures of Common Clay Minerals (Credit: U.S. Geological Survey).

### 1.3 STUDY AREA

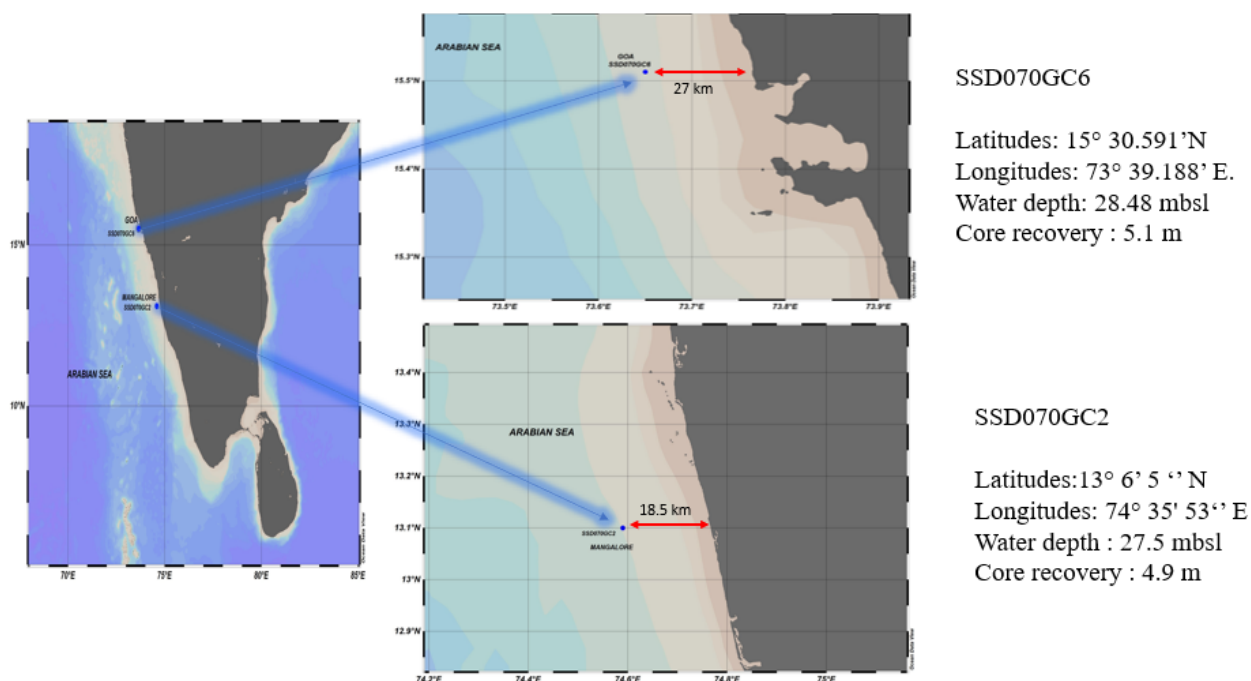


Fig.6: Map of the study area with blue dot, showing the location of the gravity core made using ODV (SSD070/GC2), (SSD070GC6)

#### 1.3.1 ARABIAN SEA

A collision between Asia and the Indian Subcontinent caused the formation of the Arabian Sea some 50 million years ago. Two major basins, the Somalia and Arabian Basins, are formed by the Carlsberg Ridge. In January - February, the Arabian Sea region often has a minimum surface air temperature of 75 to 77 degrees Fahrenheit due to the monsoon season. In June and November, temperatures rise over 82 degrees Fahrenheit. The southwest monsoons are what start the rainy season, which lasts from April to November. The top layer (45 metres) of the water's salinity decreases below 3.5‰ during the rainy season. The northeast monsoons blow across the sea during the dry season, which lasts from November

to March, and the salt level rises to over 3.6% at the surface, especially to the north. The Arabian Sea features a sizable "dead zone" or zone with the lowest oxygen content. The oxygen content of the ocean's OMZ (oxygen minimum zone) is the lowest in the world, particularly in the Gulf of Oman. High temperatures on the Indian Subcontinent and the dumping of untreated sewage into the ocean are two factors contributing to the OMZ.

### **1.3.2 WESTERN CONTINENTAL SHELF OF INDIA**

The sediments of the western continental shelf can be broadly categorized into two types, on the basis of their texture, carbonate and organic matter contents, and radiocarbon ages.

(1) Modern sediments are restricted to the inner shelf and are composed of silt and clay with high organic matter and low carbonate contents. These sediments have been supplied by the Western Ghat rivers since the reinforcement of the southwest monsoon during the Holocene.

(2) Relict carbonate sediments present on the outer shelf are coarse sands, with low organic matter and high carbonate contents. The radiocarbon dates of these carbonates (shells, calcareous algae, limestone) range between 9000 and 11,000 yrs. B.P. suggesting that they are of late Pleistocene age. (Naini et al., 1983).

### **1.3.3 HYDROGRAPHY OF ARABIAN SEA**

The Arabian Sea's climate and surface hydrography are primarily regulated by the cyclically reversing Indian monsoon wind patterns. The hydrography, circulation, distribution of nutrients, and productivity of the surface ocean are all affected differently by the monsoon winds depending on the season and location. (Banse, 1987; Brock et al. 1994; Luis & Kawamura, 2004). Upwelled water from the western Arabian Sea is advected during the summer SW monsoon season (June to September), while convective mixing takes place during the winter NE monsoon season (November to February). During the summer monsoon

season, the Arabian Sea develops a clockwise circulation. (Schott, 1983), and the eastern arm of this anti-cyclonic circulation creates the West India Coastal Current (WICC). in the EAS (Shetye et al. 1991).

#### **1.3.4 GEOLOGY OF THE AREA**

The western continental shelf of India occupies an area of about  $0.3 \times 10^6 \text{ km}^2$ . The continental shelf dips gently to the west with a gradient of 1:400 to 1:3000 to a water depth of 140 m (Mazumdar et al., 2009). The inner shelf is covered with a late Holocene to Recent sediment wedge of silt and clay which pinches out at a water depth of 45-50m. Beyond 50m, and up to the shelf break, the sediment is composed predominantly of calcareous oolitic sand (Nair and Pylee, 1968). The late Holocene sedimentary wedge can be traced all along the west coast (Siddiquie et al., 1981) and it ranges in width from 175km (off Narmada-Tapti) to 25 km off Cochin (Rao and Wagle, 1997). Holocene sea level rise (Hashimi, et al., 1995) resulted in the deposition of this organic rich fine grained sediment wedge (Karisiddaiah et. al., 2002 and Mazumdar et al., 2009)

#### **1.4 OBJECTIVES**

- The objective of this study is to characterize the clay and bulk minerals composition and their distributions in marine sediments using X-ray powder diffraction (XRD) technique to predict depositional process of inner-shelf sediments off Mangalore- Goa, Arabian Sea west coast of India.
- To examine depth-wise grain-size distribution of sediments to predict transportation processes of marine sediments and relation to hydrodynamic conditions

# **CHAPTER II**

## **LITERATURE REVIEW**

## 2.REVIEW OF LITREATURE

### 2.1 Past studies of clay minerals in world oceans

Based on the studies in the World Ocean, in the South Atlantic the composition of recent clays was reported 30 years ago by Biscaye (1965) and as part of world-wide examination by Griffin et. al. (1968), Ratea et. al. (1989) and Windom (1976)

John J. Griffin et. al. (1974) have found the relative amounts of chlorite, montmorillonite, kaolinite and illite in the World Oceans and have discussed about the sources and transport paths of solid phases from the continents to the Oceans. They reported that although all the four clay minerals have continental sources, only montmorillonite forms in the marine environment in significant amounts. Saburo Aoki et. al. (1974) investigated 81 surface samples from Japan Sea and six from four rivers in Japan. They reported that the distribution of clay minerals such as montmorillonite, chlorite, illite and kaolinite are strongly influenced by the supply or transportation, or both, of fine-grained materials by rivers and the Tsushima warm current that flows northeastward in the Japan Sea. Arieh Singer (1984) reported that levels rich in chlorite, illite, palygorskite and quartz are interpreted as corresponding to relatively dry periods, while more humid periods lead to more intensive weathering and consequently to the dominance of clay mineral such as kaolinite. Smectite is taken to indicate a climate with corresponding seasons and a pronounced dry season and using this and similar schemes, the paleoclimatic of areas adjoining the Mediterranean Basin, North Sea, North Atlantic, Southern Arctic, Equatorial and North-West Pacific, and North Phillipine Sea are reconstructed.

Globally warm climate and alternating arid seasons and wet climate are deduced from the widespread abundance of pedegenic smectite at every location from the Atlantic Ocean

and the adjacent sector of the Southern Ocean. Near the Paleocene-Eocene boundary, enhanced humidity at high latitudes and in continental hinterlands was indicated by more abundant kaolinite, while in coastal areas from low and middle latitudes increased aridity resulted in more abundant palygorskite. Christian Robert et. al. (1991).

The vertical change in clay mineral composition and chemical characteristics of smectite in sediment cores from the southern part of the Central Pacific Basin showed that smectite content is highest in the Miocene. In the Pleistocene, however, the smectite concentration decreased, whereas the other three clay minerals illite, kaolinite and chlorite increased, this trend continues into the Holocene. The vertical change in clay mineral composition in the sediment cores may suggest changes in the sources of clay minerals, and may reflect authigenic changes and hence changes in paleoenvironments through geological time. Saburo Aoki et. al. (1991).

Werner et. al. (1992) used clay mineral as sensitive tools for reconstructing climatic conditions. They reported the significance of clay mineral assemblages in the Antarctic Ocean in respect to decipher the pale oceanographic history of the Antarctic Ocean, the glacial history of Antarctica and the sedimentary processes at the Antarctic continental margin. Late Quaternary monsoon oscillations were reconstructed by using clay mineral proxies by Thamban M et. al. (2002). It was reported that the relative low values of humidity proxies and higher illite crystallinity with significant variations indicate that the summer monsoons in General was weaker during the late glaciations. The last deglaciation was characterized by an increased terrigenous input with high values of humidity proxies during 15700-14800 cal yr BP, indicating an early strengthening of summer monsoon activity. Yvonne Hamann et. al. (2009) reported the modern clay mineral distribution around the southeastern Levantine Sea. These showed changes in the late Quaternary clay

mineral distribution in the southeastern Levantine Sea which was caused by changes in the source area.

## **2.2 Past studies of clay minerals in Arabian Sea**

River discharge and Aeolian input are the two main processes, supplying the terrigenous material to the Arabian Sea (Sirocko and Lange, 1991). Most fine-grained fluviially derived marine sediments are deposited in the near shore and continental margin and only a small amount is transported to the deep sea (Chester 1990). The fine-grained sediments are composed mainly of clay minerals and amorphous material. Two distinct sediment types occur on the continental shelf of western India: Modern clastic clays on the inner shelf and relict sandy sediments on the outer shelf (Nair and Pylee, 1968; Hashimi et al., 1982). The continental slope is covered by silty clays which are an admixture of dominant terrigenous and biogenic components.

In the eastern Arabian Sea, rivers are the principal agents of transport of detrital sediments. The Indus River is the largest one (2900km length, ~966000km<sup>2</sup> drainage area), bringing enormous amounts of sediments (Haq and Milliman, 1984). The Deccan Traps has a maximum thickness of 1200-1700m in central and NW India and covers an area of 500,000 km<sup>2</sup>. It is overlain by Quaternary Sediments in Coastal Saurashtra. Several Rivers debouch into the Gulf of Khambat (Kessarkar et al, 2003). The Sabarmati River rises in the Aravali mountain range comprising Precambrian gneisses and schists and before entering the Gulf they flow through Quaternary formations. The rocks in the drainage basin of the Mahi River are similar to those of the Sabarmati, but its tributaries also flow through Deccan Traps. (Kessarkar et al, 2003). In Saurashtra and the drainage basins of Sabarmati and Mahi a semiarid climate prevails and has rainfall ranging from 500 to 1000 mm/yr.

The rocks in the drainage basin of the Narmada River (1300km long, ~93000km<sup>2</sup> drainage area) are complex. These rocks comprise of Precambrian gneisses (Banded Gneissic Complex), Vindhyan and Satpuras (Deccan Traps plateau basalts) in the upper and middle reaches and Quaternary alluvium in the lower reaches. The Tapi is a moderate River (700km long) largely flowing through Satpuras. Several workers (e.g. Subramanian, 1980; Naidu et al., 1985) have reported smectite as an abundant clay mineral in the suspended and bed loads of the Narmada and Tapi Rivers. South of Tapi, the Western Ghats mountain range is found to be composed of two major rock types: the Deccan Traps basalts and Precambrian gneisses and schists. The former comes between Tapi and Mormugao and the latter comes between Mormugao and Cape Comorin. The Western Ghats has a humid tropical climate with a maximum rainfall of ~3000mm. They are drained by several rivers that bring sediments into the coastal Arabian Sea. Here the coastal region is occupied by recent alluvium and the Warkala beds of tertiary age. The Indus originates in the Himalayas and carries the glacial weathering products of Precambrian rocks and semi-arid to arid rocks of Pakistan and NW India (Krishnan, 1968). Illite and chlorite are the major clay mineral assemblages in the Indus discharge (Nair et al., 1982; Konta, 1985).

Clay minerals have been studied by various workers (Nair et al., 1982; Stewart et al., 1986; Mattait et al., 1973; Rao and Rao, 1995; Chauhan and Gujar, 1996; Thamban et al., 2002; Kessarkar et al., 2003) along the western continental shelf and have reported different clay mineral assemblages and provenance of the sediments. Kolla et al. (1976 & 1981) has conducted detailed studies of clay minerals in surface sediments of the Arabian Sea. On the basis of geographic patterns of clay mineral abundances, they concluded that:

1. Smectites are derived from the Deccan Traps of India;
2. Kaolinites in the northern Arabian Sea are probably derived from tropical soils of Southern India;
3. Illite and chlorite

are derived either from the Himalayan complex and supplied to the Indus Fan and adjacent areas by the Indus River, or from soils in the Iran-Makran region and supplied to the Gulf of Oman by northwest winds; and 4. Palygorskite (a fibrous clay) is derived from soils of the Arabian Peninsula and Somalia, and supplied to the Arabian Sea by westerly and south westerly winds. Smectite, illite, chlorite and kaolinite are the major constituents of Indus delta, where the sediments are derived from the glacial Himalayas and semiarid to arid soils (Kumar et al., 2010) Kolla et al (1976, 1981) also reported that smectite-rich sediments in the deeper Arabian Sea are derived from the Deccan Traps. The weathering of gneissic rocks (Precambrian source of southern India) provides high amount of kaolinite, poorly crystalline illite and gibbsite. These gneissic rocks are lateritized at places. The study on distribution and dispersal of clay minerals on the western continental shelf of India by Nair et al., 1982b are transported by the Indus River to the northern Arabian Sea. The influence of Indus River is largely restricted to the north of Gulf of Kutch because the macro tidal currents in these zones act as barriers for long shore sediment transport to the south.

**CHAPTER III**  
**MATERIALS AND METHODOLOGY**

### **3. MATERIAL AND METHODOLOGY**

The gravity core used in this investigation was collected during a special cruise by the National Institute of Oceanography (NIO) research vessel Sindhu Sadhana. The gravity core samples were packed in an air tight cylindrical PVC container. Then the core samples were taken to the wet lab for sub-sampling. The core section is laid down on a table, and with the help of a measuring tape, the accurate length is noted down. Then it was sub-sampled, which was collected in the pre-labelled (core section and actual depth) container.

#### **3.1 SAMPLE PROCESSING**

The samples were first collected from the cold storage according to their marking scale of depth resolutions, then transferred to the well- labelled 50 ml centrifuge vials by weighing the sample at 1.8– 2 g using the weighing machine SSP-300.

##### **3.2.1 DECARBONATION**

Samples are then transferred into centrifuge tubes. 30ml of 1N Acetic Acid is added to each sample and then is shaken vigorously until the effervescence produced stops. The samples are then thoroughly mixed using a sample shaker and left ideally for 1 hr. After centrifuging, the supernatant acid is decanted from the tubes and an additional 30ml of 1N Acetic Acid is added. In case if effervescence is generated again, the above steps are repeated and if not, the samples are centrifuged after an hour. After centrifuging, the supernatant is decanted and 30ml of distilled water is added. The samples are then further centrifuged. The process is repeated until the acid is completely removed (Check the acidity of the solution after every wash using acid paper)

### **3.2.2 ORGANIC MATTER REMOVAL**

When the samples are acid free then 30ml of 20 % H<sub>2</sub>O<sub>2</sub> is added to each sample followed by a vigorous shake until the effervescence ceases. After using a sample shaker to completely combine the samples, they should ideally be left for overnight. Following centrifugation, 30ml of 20 % H<sub>2</sub>O<sub>2</sub> is added after the supernatant H<sub>2</sub>O<sub>2</sub> is decanted from the tubes. The aforementioned procedures are repeated if effervescence is produced again, and if not, the samples are centrifuged an hour later. The supernatant is decanted after centrifugation, and 30ml of distilled water is added, again centrifuge and decant 3 times.

### **3.2 LASER PARTICLE SIZE ANALYZER**

It is a conventional method for determining grain size because laser diffraction analysis is not the only means of measuring particles. When findings were compared, it became clear that laser diffraction analysis generated enormous volumes of data, small sample sizes, quick computations, and simple reproducibility after a single study. The data is on a digital surface, making manipulation of the results simple.

The relation between particle size, the scattering light's angle, and intensity is the subject of laser diffraction. Larger particles than small ones cause a stronger and more uniform light scattering, respectively. This concept is used by the Laser Diffraction Particle Size Analyzer. In actuality, the analyser just analyses the angle and strength of light scattered from the particles in your sample. It does not detect particle size itself. The scattered light data is then converted into particle size information via an algorithm that is built on the Mie Scattering Theory.

### **3.2.1 WORKING PRINCIPLE OF LPSA**

In the Laser diffraction analyzes, the angular change in light intensity scattered as a laser beam travels through a dispersed particulate sample to determine particle size distributions. Tiny particles scatter light at wide angles away from the laser beam, whereas massive particles do so at tiny angles. The Mie theory of light scattering is then applied to the angular scattering intensity data to determine the size of the particles that produced the scattering pattern. The diameter of a volume-equivalent sphere is used to describe the particle size. The working principle of a laser particle size analyser is based on the measurement of light scattering by particles in a sample.

### **3.2.2 SAMPLE PREPARATION**

The sample is prepared and added to a sample cell of the particle size analyzer. The sample may be a suspension of particles in a liquid or a dispersion of particles in a gas.

### **3.2.3 LASER BEAM INTERACTION**

A laser beam, typically a monochromatic beam of light, is directed into the sample cell. The laser beam passes through the sample, and particles in the path of the laser beam interact with the light

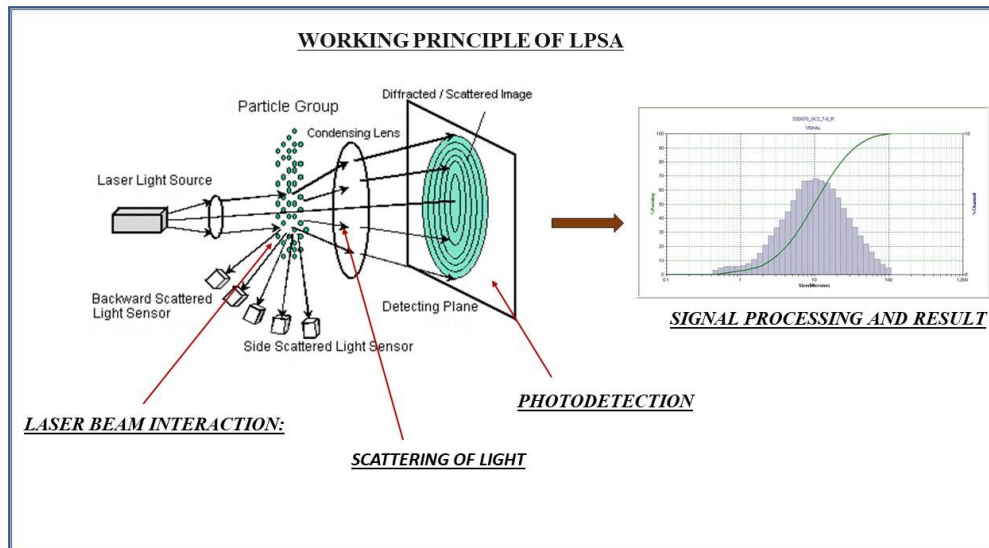


Fig. 7: Working Principle of LPSA

### 3.2.4 SCATTERING OF LIGHT

The laser beam is dispersed in different directions as a result of particle interaction. The size and optical characteristics (refractive index) of the particles affect the scattering pattern. There are two categories of dispersed light:

- A. Forward Scattering: Particles often scatter light at low angles in the forward direction. Information about smaller particles is contained in this forward-scattered light
- B. Side Scattering: Side scattering is the process through which particles disperse light at greater angles. Information about bigger particles is revealed by this light that is dispersed.

### **3.2.5 PHOTODETECTION**

The scattered light is captured by a detector, The detector converts the incoming light signal into an electrical signal proportional to the intensity of the scattered light.

### **3.2.6 SIGNAL PROCESSING**

A detector that is positioned at a specified angle with respect to the laser beam direction gathers the dispersed light. Depending on the desired particle size range, the detector can be positioned for either forward scattering or side scattering observations.

### **3.2.7 DATA ANALYSIS**

The equipment determines the particle size distribution by analysing the electrical output using the relevant algorithms and mathematical models. The algorithms take into consideration elements including the scattering pattern, the intensity of the dispersed light, and calibration data.

### **3.2.8 PARTICLE SIZE DISTRIBUTION OUTPUT**

The last output from the laser particle size analyser is the particle size distribution. A histogram of the distribution may be shown, with the particle sizes shown against the respective frequencies or percentages. Other metrics offered by certain devices include mean particle size, median size, and size range.

## **3.3 INSTRUMENTATION OF A LASER PARTICLE SIZE ANALYZER**

**Laser Source** A monochromatic beam of light is emitted by a laser source, often in the visible or near-infrared spectrum. To enable precise measurements of particle size, the laser's output power and wavelength should be steady.

### **3.3.1 Optical System**

The optical system directs the laser beam's direction using lenses, mirrors, and beam splitters. It aims the laser beam through the sample cell and concentrates the dispersed light onto a detector.

### **3.3.2 Sample Cell**

A compartment where the particles are suspended in liquid is called a sample cell. When a laser beam enters a sample cell, the particles scatter the light in various ways.

### **3.3.3 Detector**

A detector gathers the light that the particles disperse. Depending on the particular instrument design, the detector may be a photodiode, photomultiplier tube (PMT), or avalanche photodiode (APD). It gauges the strength of the light that is dispersed at various angles.

### **3.3.4 SIGNAL PROCESSING AND DATA ANALYSIS**

The detector output is processed to extract information about the particle size distribution. This typically involves amplification, filtering, and conversion of the analog signal into a digital form. The data is then analysed using appropriate algorithms to determine the particle size distribution.

### **3.3.5 SOFTWARE AND DISPLAY**

The instrument is usually connected to a computer that runs dedicated software for data acquisition, control, and analysis. The software allows users to configure measurement parameters, initiate measurements, and visualize the particle size distribution in the form of graphs or tables.

### 3.3.6 CALIBRATION STANDARDS

Laser particle size analyzers need to be calibrated using particles of known sizes to achieve precise readings. To establish a connection between the measured scattered light and particle size, calibration standards made of monodisperse particles of established sizes are utilised.

### 3.3.7 USER INTERFACE

The instrument's user interface, which offers data visualisation, measurement settings, and real-time feedback. It makes it simple for consumers to engage with the device and retrieve measurement findings.

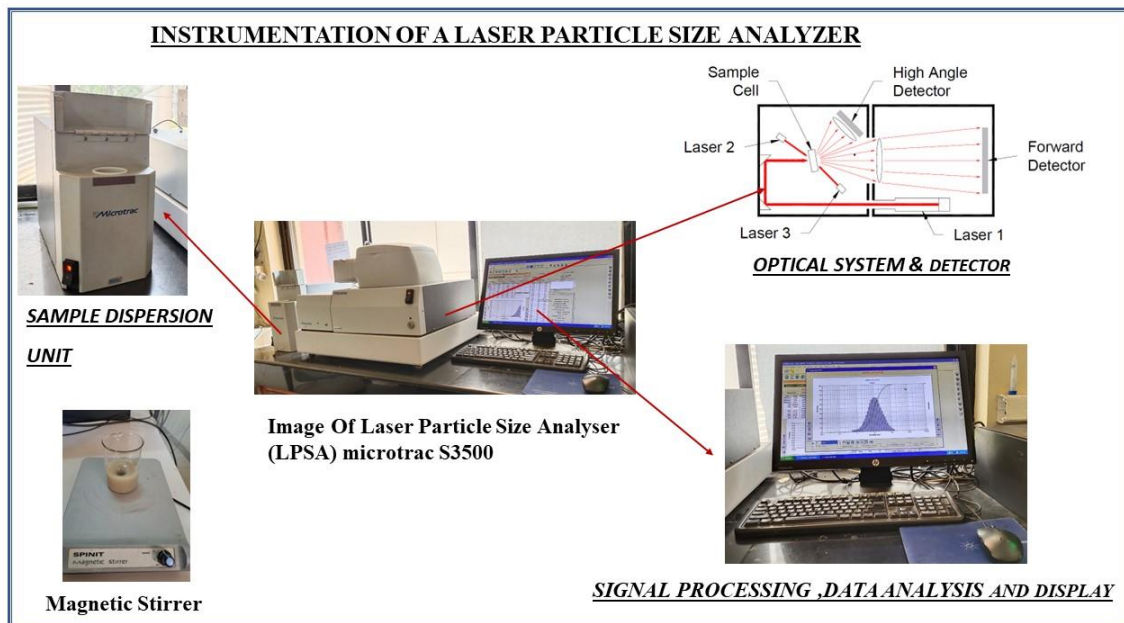


Fig. 8: Showing the instrumentation of a laser particle size analyzer

### 3.4 Statistical Data & Geometric graphical measures

For all samples in this investigation, the findings of the grain size analysis were visually displayed as cumulative curves. Four parameters that were measured were used to describe the grain size distribution: (a) the mean, which is the arithmetic average size of all the particles in the sample; (b) the standard deviation or sorting, which is the percentage and degree of scatter of these sizes around the mean; (c) the skewness, which is the degree of symmetry of the grain size distribution; and (d) the kurtosis, which is the sharpness of the grain size frequency curve. The four statistical measures of grain size mentioned above (MG, SKG), The geometric graphical methods of Folk and Ward (1957) were used to compute the standard deviation ( $s_G$ ), skewness, and kurtosis (KG) for all samples using the metric scale.

Sorting ( $\sigma_G$ )		Skewness ( $SK_G$ )		Kurtosis ( $K_G$ )	
Very well sorted	<1.27	Very fine skewed	-0.3 to -1.0	Very platykurtic	<0.67
Well sorted	1.27-1.41	Fine skewed	-0.1 to -0.3	Platykurtic	0.67-0.90
Moderately well sorted	1.41-1.62	Symmetrical	-0.1 to +0.1	Mesokurtic	0.90-1.11
Moderately sorted	1.62-2.00	Coarse skewed	+0.1 to +0.3	Leptokurtic	1.11-1.50
Poorly sorted	2.00-4.00	Very coarse skewed	+0.3 to +1.0	Very leptokurtic	1.50-3.00
Very poorly sorted	4.00-16.00			Extremely leptokurtic	>3.00
Extremely poor sorted	>16.00				

Table 1: Geometric graphical measures (modified by Folk and Ward 1957)

### 3.5 X-RAY DIFFRACTOMETER (XRD)

#### 3.5.1 X-RAY DIFFRACTION

X-rays are a form of electromagnetic radiation; X-ray wavelengths are  $10^{-2}$  to  $10^{-12}$  m long wavelength X-rays grade into ultraviolet light; shorter wavelengths grade into cosmic and gamma rays. Mineralogists usually give X-ray wavelengths in angstroms (1Å equals  $10^{-10}$  m). The copper radiation commonly used in X-ray studies has  $\lambda = 1.5418\text{Å}$ . Compared to visible light and most other electromagnetic radiation types, X-rays have a higher energy due to their short wavelengths and high frequencies. As noted by Rontgen in 1895, X-rays with high energy may pass through a wide variety of natural materials. High-energy X-rays, often known as hard radiation, are employed in various industrial and manufacturing processes, including the inspection of steel for defects (Perkins, 2013). Soft radiation, or low-energy X-rays, are employed in medical diagnostics and by numerologists. The target electrons release energy in the form of X-rays as they descend in energy. The energy differential between the two levels is inversely proportional to wavelength and directly relates to energy and frequency of X-rays released. Typical X-ray tubes generate distinctive radiation with several wavelengths because some electrons are boosted to greater levels than others and because they do not all return to the same levels. The metal in the X-ray tube target determines the wavelengths of the distinctive radiation. Hence, although polychromatic light from X-ray tubes has a range of wavelengths, the majority of its energy is focused on a few chosen ones. The various typical X-ray wave lengths are denoted by combinations of Greek and English (K, L, and M) letters. Ka stands for the strongest peaks (Dexter Perkins 2002). Most common X-ray investigations employ copper ka radiation. Although copper has a number of distinctive wavelengths, using just one wavelength makes interpreting X-ray diffraction the simplest.

Most X-ray devices incorporate filters, monochromators, or solid-state monochromatic detectors to separate Ka radiation from other wavelengths. CuKa radiation with two approximately similar wavelengths,  $Ka_1 = 1.5401\text{\AA}$  and  $Ka_2 = 1.5443\text{\AA}$ , is released by X-ray tubes. Because of their extreme similarity, the radiation is essentially monochromatic for most purposes even when both wavelengths are present. We thus adopt a weighted average of the  $Ka_1$  and  $Ka_2$  wavelengths and assume a  $\lambda$  value of  $1.5418\text{\AA}$ . The Laue equations are a set of formulas that Von Laue (age) devised to describe diffraction by three-dimensional structures. W. L. Bragg created a mathematical treatment that was clearer and easier to understand.

Although the derivations eliminated some needless complexity, the final equations are just as valid as those of von Laue. Bragg observed that diffracted X-rays behave as though they were reflected from planes within a crystal, despite the fact that diffraction and reflection are two distinct processes. In order to simulate this "reflection," Bragg took into account two parallel atomic planes spaced apart by  $d$  ( $hkl$ ). The monochromatic parallel X-ray beams ABC and DEF strike and reflect off of the planes. Both the incidence angle and the reflection angle are  $i$ . For diffraction to happen, the beams' travel lengths must differ by an integral number of wavelengths, hence the total distances must equal  $n(\lambda)$ ,  $N$  thus equals  $2d\sin(i)$ . In traditional X-ray diffraction investigations, we take the Bragg law's  $n$  to be 1.

Since we cannot discriminate between first-order diffraction by planes with spacing  $d$  and second-order diffraction by a set of planes separated twice as far apart, we will assume first order when discussing X-ray diffraction. The order of diffraction matters in various uses of the Bragg rule. The incident X-ray beam is allowed to impact the sample at a variety of angles in typical X-ray diffraction experiments in order to produce diffraction across a wide range of  $d$ -values that fulfill the Bragg equation (Perkins, 2013). The X-ray beam travels at an angle of  $2$ ,

from the incident beam after diffracting. Diffraction happens at several  $2\theta$  angles because a crystal is made up of numerous atom-filled planes arranged in various orientations. Most of the time X-ray devices used today, the sample is at a fixed location (although it may rotate), and the detector, which measures X-ray intensity, moves through an entire range of angles from near 0 to some high angle. In some diffractometers, the X-ray tube moves as well. If a diffracted beam is to hit the detector, two requirements must be met:

- A family of planes with  $d$  (hkl) must be oriented at an angle ( $\theta$ ) to the incident beam so the Bragg law is satisfied.
- The detector must be located at the correct angle ( $2\theta$ ) from the incident beam to intercept the diffracted X-rays.

Because the angle between the detector and the X-ray beam is  $2\theta$ , mineralogists usually report X-ray data in terms of  $2\theta$  (Dexter Perkins, 2002)

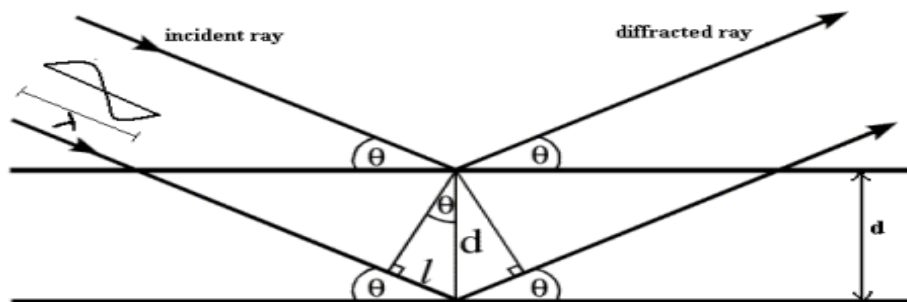


Fig.9: Bragg's law.  $\theta$  is the angle between the incident beam and the lattice plane.  $\lambda$  is the wavelength and  $d$  is the distance between parallel lattice points.

### 3.5.2 Description of X-ray diffractometer

**Diffractometer:** A diffractometer is a measuring instrument for analyzing the structure of a material from the scattering pattern produced when a beam of radiation interacts with it. A typical diffractometer consists of a source of radiation, a monochromator to choose the wavelength, slits to adjust the shape of the beam; goniometer can be used for the fine adjustment of the sample and the detector positions, a sample and a detector.

**X-Ray Generator:** It uses a water-cooled, sealed x-ray tube with 1 to 3 kw output in which a high current is applied to a tungsten filament which gets heated up and emits electrons. These electrons are accelerated by a high voltage applied within the tube to hit the target. Two common targets are Mo and Cu, which have strong K (alpha) x-ray emission at 0.71073 and 1.5418 Å respectively. We used Cu target to produce x-rays.

The x-rays which are produced in the x-ray tube are collimated through the Soller slit and the divergence slit to finally strike the sample. The incident beam is diffracted from the crystallites in the sample which act as specific diffraction gratings. The purpose of a Soller slit is to take a line source of radiation and slice it into smaller, parallel beams; this reduces axial divergence of the beam. The divergence slit limits the radial divergence of the beam and removes scatter.

**Sample Stages:** sample spinners rotate about an axis normal to the sample surface through an angle  $\theta$ . The rotation of the sample is mechanized and occurs through an amount that is preprogrammed into the instrument. The amount of rotation depends upon the purpose of the study and type of minerals to be studied.

**Goniometer:** This device comprises two independent drives that provide accurate and precise motion of the sample stage and detector ( $\theta/2\theta$ ) or the tube and detector ( $\theta/\theta$ ). In either configuration the goniometer may be oriented to keep the sample horizontal or vertical.

**Detectors:** The diffracted beam from the sample passes through the receiving slit and another soller slit to reach the detector. If the sample stage moves through an angle  $\theta$ , then the detector moves through an angle  $2\theta$ . It converts the x-ray signal electronically to a count rate that is processed by the attached computer.

To maintain a constant irradiated area on the sample variable divergence and anti-scatter slits are coupled to Bragg angle. They are essentially valuable for low angles as for clay mineral analysis. By closing down of low angles, scatter from the main beam is attenuated and by opening up at higher angles more diffracted intensity reaches the detector than with small fixed slits. Finally, an x-ray diffraction pattern is obtained recording the intensity of the maxima for the crystallographic structure and the atomic composition of the material. The diffraction patterns are compared to data entries in the International Powder Diffraction File Database. The Joint Commission on Powder Diffraction Standards maintains the database.

### 3.5.3 INTENSITY OF DIFFRACTION

Diffraction at Different Angles: enables us to determine the angle at which diffraction happens for any given value of  $d$ . However, as the positions and types of atoms vary throughout minerals and diffraction patterns rely on atomic arrangement and composition, strong diffraction can only happen when a large number of atoms occupy the  $(hkl)$  planes. Without atoms, there would be no electrons to scatter Xrays. Yet diffraction patterns are also impacted by symmetry (Perkins, 2013). Because high crystal symmetry results in similar atom spacing in all directions, diffraction is caused by fewer  $d$ -values and may thus occur at fewer angles with a reasonably uniform intensity. Because atoms and their spacing vary in all directions, low crystal symmetry results in diffraction occurring in several directions at varying intensities.

Film is often not used in X-ray diffractometers; instead, solid state X-ray detectors and monochromatic light are used.

To measure the intensities of each diffraction peak, the diffractometer moves the detector and spins the crystal. The diffractometer's computers save data straight to disk. For a single crystal, the d-values and intensities of hundreds of distinct peaks may be measured since the procedure is entirely automated. The information required to determine the structure is provided by single-crystal X-ray investigations. There are easier methods available for identifying minerals. The most popular is powder diffraction, which involves X-raying a sample that has been finely powdered and placed in a holder or on a slide. An almost endless number of tiny crystals arranged in random orientations make up a powdered sample

Film is often not used in X-ray diffractometers; instead, solid state X-ray detectors and monochromatic light are used. To measure the intensities of each diffraction peak, the diffractometer moves the detector and spins the crystal. The diffractometer's computers save data straight to disk. For a single crystal, the d-values and intensities of hundreds of distinct peaks may be measured since the procedure is entirely automated. To ascertain crystal structures, we employ the information gleaned from single-crystal diffraction investigations. Knowing a mineral's composition allows us to calculate the number of atoms in each element. Based on the diffraction data, computer algorithms may identify the positions of the atoms in the structure. This procedure is referred to as crystal structure determination (Perkins, 2013). Although the technique of determining crystal structure is complicated, it has been made much simpler since the Braggs identified the first crystal structure in 1913 thanks to automation and high-speed computers. Most mineralogists now utilize an X-ray powder diffractometer in place of a camera, but film was once employed by them to capture powder diffraction patterns. The powdered sample is mounted either in a well within a sample holder or on a slide. When the sample is exposed to a concentrated X-ray beam, the detector rotates in a circular arc, typically

vertically, to measure the diffraction intensities for  $2\theta$  values at angles ranging from extremely low to over  $150^\circ$ . In actuality, the direct X-ray beam bombards the detector, making most diffractometers unable of detecting peaks for angles less than  $1$  or  $2^\circ$ .

Although the highest  $2\theta$  measurement limit is often determined by the needs of the mineralogist, most applications do not require data above  $60^\circ$  to  $70^\circ$ . Before, diffractometers were used in conjunction with strip chart recorders to create diffraction patterns, which usually had between 10 and 50 distinct peaks. After that, a mineralogist would compute d-Values by measuring the diffraction angles on the chart. These days, we attach computers with data analysis and diffraction pattern printing capabilities to diffractometers. Powder diffractometers that are connected to computers often take a few to thirty minutes to identify basic minerals. However, gathering data might take hours or even days if incredibly accurate findings are desired (Dexter Perkins 2002).

### **3.5.4 IDENTIFICATION OF MINERALS FROM XRD DATA**

Since powder diffraction data are more challenging to interpret than single crystal data, powder patterns are often not employed to determine crystal structures. The powdered sample's crystals are represented by distinct X-ray peaks, and the results do not show the plane orientations that cause diffraction. The Rietveld method, a relatively recent method for deciphering powder patterns, may occasionally get around these issues and is becoming more and more well-liked these days. Mineralogists frequently utilize the list of d-values and peak intensities that powder patterns produce to identify minerals (Perkins, 2013). A set of planes corresponds to each d-value, and the number of atoms on each plane is indicated by the intensity. Every mineral produces a distinct pattern since they all have distinct atomic arrangements. We contrast measured d-values and intensities with reference data sets in order

to identify minerals. The International Centre for Diffraction Data has collected the most comprehensive reference, the X-ray Powder Diffraction File (PDF), which is accessible through electronic databases and includes information on about 6,000 minerals as well as tens of thousands of other crystalline compounds, both inorganic and organic.

Deviations might result from various samples, different sample preparation techniques, and a host of other factors. Strong peak d-values, on the other hand, will always match closely, even while the intensities are not exactly in the same sequence. The effort of finding a match in a big reference file may appear onerous once we have learned the d-values and intensities for an unknown mineral. Sometimes it is, but most of the time we simply need to take a close look at a handful of the strongest diffraction peaks. These days, most mineralogists utilize computer databases to match unknown patterns with PDF data, rather than conducting the matching by hand. There are two primary benefits to this: It is quick, and a lot more reference patterns are available for consideration. However, computer searches are "black box" methods that don't further our comprehension of powder diffractometry (Perkins, 2013).. Furthermore, computers occasionally provide ludicrous responses that a person would have quickly dismissed. Because powder diffraction is not a precise method, there are a lot of reasons why X-ray patterns differ from those found in reference files. Accurate pattern extraction requires careful sample preparation. When a sample is not thoroughly ground or when the orientations of the powdered crystals are not genuinely random, problems might occur. Small compositional and crystal structural differences can alter Xray patterns, which is a second issue that affects natural materials more than manufactured ones. The PDF files offer sufficient reference patterns for the majority of mineralogical applications despite these difficulties.

.

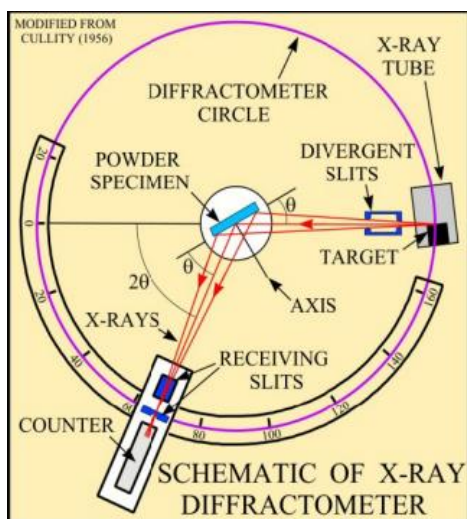


Fig.1: Schematic of X-ray diffractometer.  $\theta$  -angle between the incident beam and a lattice plane (Cullity 1956).

### 3.6 BULK MINERALOGY

The samples washed after treating with H<sub>2</sub>O<sub>2</sub> are emptied into a petridish leaving the centrifuge tube clean of any sediments. This can be achieved by using distilled water and draining the contents into the petridish. They are then kept in the oven at 60 °C for drying and after drying the samples are taken and powdered into fine particles with the help of a mortar and pestle. The grinded fine particles are transferred into a 2mm vials using butter- paper. The samples are then taken for XRD and each are filled into the slides, and evenly spread and made fine with a help of a glass slide and samples are run on XRD for 15min scanning an angle ranging from 5<sup>0</sup>-70<sup>0</sup> with a step size of 0.02mm. The data for XRD is obtained and the data is interpreted to understand the bulk composition of the sample using JCPDS files.

## 3.7 CLAY MINERALOGY

### 3.7.1 CLAY SEPRATION

Sedimentation methods can also be used to segregate clay particles according to their settling velocity. In these approaches, grains are allowed to sink through a column of water at a given. It is measured how long it takes for the grains to settle as well as the temperature in a settling tube. To determine the equivalent millimetre or phi size for coarser particles (granules, sand, and silt), the settling time of the particles is experimentally matched to a standard size-distribution curve (calibration curve). Particle shape has an impact on the settling velocity of particles. Compared to non-spherical particles of the same mass, spherical particles sink more quickly. As a result, measuring natural, non-spherical particle grain sizes using sedimentation methods could not produce accurate results matching those obtained by sieving. Using sedimentation techniques based on Stokes' Law, one may determine the grain size of tiny slit and clay particles. Stokes law pertains to the terminal fall velocity of a sphere in a fluid. If the settling velocity is known for a particular temperature, diameter (D) of the sphere can be calculated as

$$D = \sqrt{v} \sqrt{C}$$

V is the terminal velocity of the sphere.

Where C is a constant equaling  $C = (ds - df) / 18\mu$  And  $ds = 2.65 \text{ gm/cm}^3$  (density of quartz)

$df =$  the density of distilled water at the particular temperature

$$g = 980 \text{ cm/sec}^2$$

$\mu =$  the viscosity of distilled water at a particular

**Stokes law is only valid under the following conditions and limitations:**

- Particle must have reached terminal fall velocity
- Particles must be rigid
- Particles must be smooth
- No slippage or shear may take place between the particle and the fluid
- The fluid must be of infinite extent in relation to the particle
- Particle concentration must be less than 1%
- Particle must be greater than 0.5 micron in diameter
- Particle must be sphere (Carver, 1971)

The samples are collected in 1 litre measuring cylinder. The samples are thoroughly stirred and kept undisturbed for settling. 20ml of samples from the 10 cm is pipette out after 6 Hrs and 20 min. The temperature should maintain constant. The sample is collected in beakers and kept for settling for 36 Hrs (add 5 ml  $\text{CaCl}_2$  if the samples are not settling and wash the samples 3 or for times. Treat the samples with  $\text{AgNO}_3$  to find the presence of  $\text{CaCl}_2$  if ppt is coming then wash the sample again and continue).

### **3.7.2 Calcium Chloride SATURATION**

Add 10-15 ml of 1 M  $\text{CaCl}_2$  to the samples and shake it in the hand shaker for 3-5 min and put it in the rotatory shaker for 5-6 hrs and wash the samples with distilled water for 3-4 times and do the  $\text{AgNO}_3$  test in order to find the presence of  $\text{CaCl}_2$  if precipitate is coming wash the samples again now the samples are ready for preparation of slides.

### 3.7.3 PREPARATION OF SLIDES

Make the slides in the required dimension of the analysis it is 5 cm length, 3.5 cm width, 2mm thickness. Concentrate the samples in to 5 ml and shake it well and put the sample on the slide and keep the slide in a clean environment and dry it.

### 3.7.2 GLYCOLATION

1. Add an appropriate quantity of ethylene glycol to the desiccators reservoir ( 60% of reservoir capacity).
2. Place a disc in the desiccator.
3. Arrange the slides in numeric fashion 1,2,3, 4... N referring to landmark position on the disc with the clay layer facing upwards.
4. For Glycolation
  - Set the temperature of oven to 100<sup>0</sup>C. As the 100<sup>0</sup>C is attained place the desiccators in the oven for 1 hr. After this let it cool down for some time. Once it is sufficiently cool to hold the desiccator in your hand bring it to xrd lab.
  - Alternatively, the temperature within the oven could be set for 60<sup>0</sup>C and the desiccators be kept overnight for glycolation.

## 3.8 Quantitative Analysis – Calculation of Peak areas

The calculation of peak areas is done to determine roughly the peak intensities which ultimately help in determining the relative proportion of various clay minerals in the sample. The simplest case involves measuring the integrated areas of the peaks that have no interferences and are superimposed on flat linear backgrounds. Although these measurements can be done most accurately by using deconvolution techniques and computer methods, but in this case the intensity was measured by multiplying the peak

height above background (H) times the peak width (in  $2\theta$ ) at half the peak height (Full Width Half Maxima, or FWHM).

**Peak Intensity = H \* Full Width Half Maxima**

In case two peaks are incompletely resolved, we have to estimate the background and the shapes of the peaks in the overlap region and then apply the above formula. To determine the relative percentages of various minerals in the sample, we generally consider the area of the (001) peak of the mineral. Certain correction factors are applied to the minerals illite and chlorite+kaolinite. We multiply the area obtained for illite peak by a correction factor of 4 and that obtained for chlorite(002)+kaolinite(001) peak by a correction factor of 2.

Thereafter, following calculations are made (for a sample containing smectite, illite and chlorite+kaolinite):

$$1. \quad \% \text{ Smectite} = \frac{\text{Smectite}}{\text{Smectite (001)} + \text{Corrected Illite (001)} + \text{Corrected Chlo+Kaolinite}} \times 100$$

$$2. \quad \% \text{ Illite} = \frac{\text{Corrected Illite (001)}}{\text{Smectite (001)} + \text{Corrected Illite (001)} + \text{Corrected Chlo+Kaolinite}} \times 100$$

$$3. \quad \% \text{ Chlorite+Kaolinite} = \frac{\text{Corrected Chlo+Kaolinite}}{\text{Smectite (001)} + \text{Corrected Illite (001)} + \text{Corrected Chlo+Kaolinite}} \times 100$$

**CHAPTER IV**  
**RESULTS AND DISCUSSION**

## 4. Results

### 4.1 GRAIN SIZE DISTRIBUTION OF GRAVITY CORE (GC2)

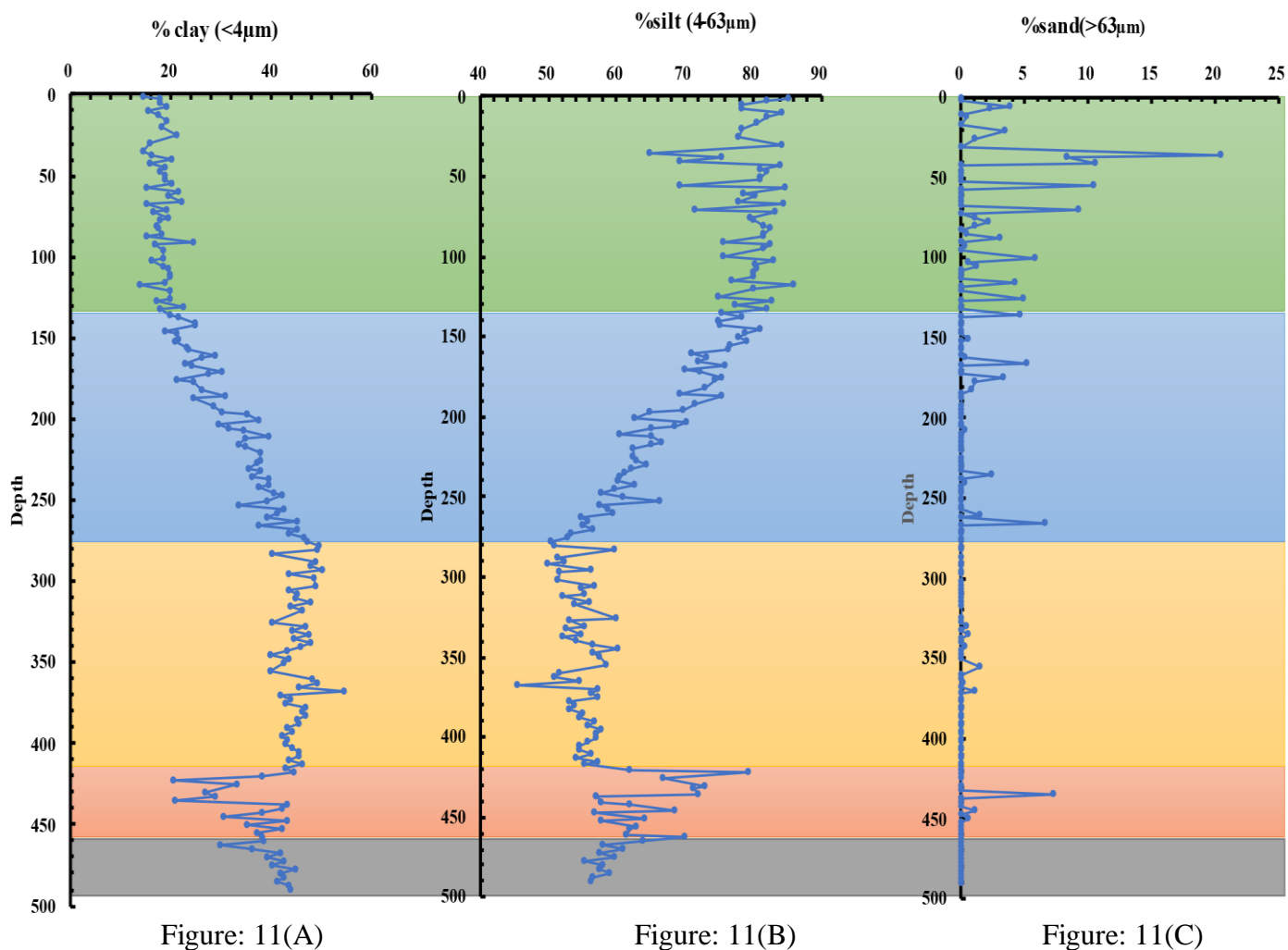


Fig 11 A - C: Grain Size Distribution of GC2 with depth (cm)

- We analyze the grain size variation of sand, silt, and clay in a gravity core, dividing it into five distinct zones based on depth. The core, spanning 490cm, provides valuable insights into sediment composition and depositional processes. By examining the distribution of different grain sizes,
- Zone One (490cm to 417cm): In this zone, the clay percentage ranges from 42% to 43%, while the silt percentage varies from 58% to 56%. The sand percentage is

consistently at 0%. This zone shows less variation in grain size distribution, and the graph indicates that the sand percentage tends to be nearly zero. This suggests that the sediment in this zone is predominantly composed of clay and silt particles, with little to no sand.

- Zone Two (467cm to 417cm): In this zone, there is a sudden decrease in clay percentage from 44% to 20%, followed by an increase to 41%. Correspondingly, the silt percentage shows a sudden increase from 55% to 79%, and then a decrease to 58%. The sand percentage remains close to zero throughout. This indicates a shift in grain size distribution, where the clay and silt content fluctuate abruptly, while the sand content remains negligible.
- Zone Three (417cm to 280cm): In this zone, the silt percentage ranges from 50% to 55%, while the clay percentage varies from 45% to 50%. The sand percentage is present in a minute amount. The grain size distribution shows relatively constant percentages of silt and clay, indicating a relatively stable sediment composition with a small presence of sand.
- Zone Four (280cm to 132cm): In this zone, there is a gradual decrease in clay percentage from 40% to 20%, while the silt percentage increases from 50% to 75%. The sand percentage remains at a very low level. This suggests a shift towards higher silt content and lower clay content, with only a minimal presence of sand.
- Zone Five (132cm to 0cm): In this zone, there is not much variation in clay percentage, ranging from 16% to 20%, while the silt percentage remains relatively high at 75% to 83%. The sand percentage is the highest in the overall core, ranging from 6% to 10%. This zone exhibits a relatively stable distribution of clay and silt, but with a notable increase in sand content compared to the other zones.

#### 4.2 GRAIN SIZE DISTRIBUTION OF MULTICORE (MANGALORE)

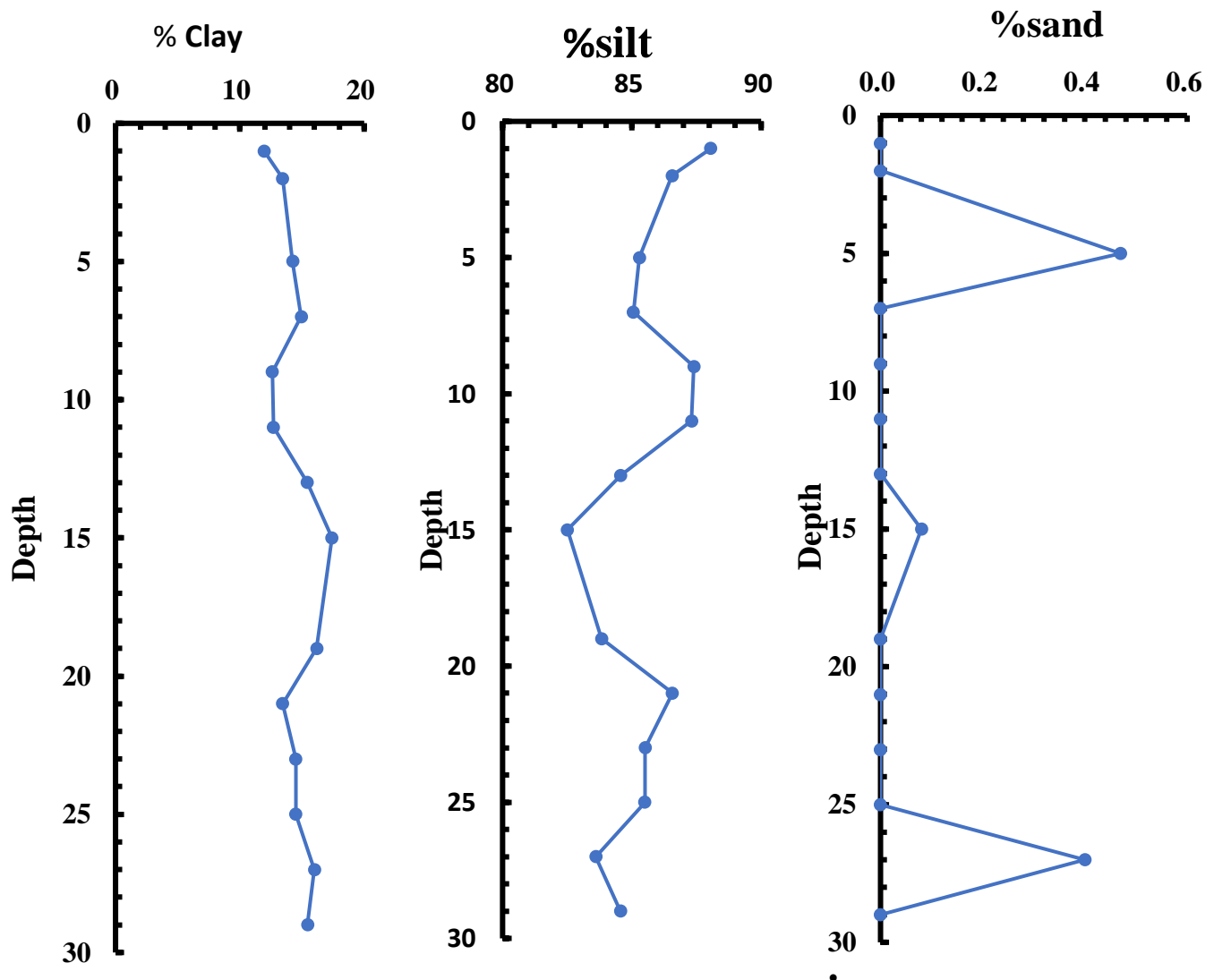


Figure:12(A)

Figure:12(B)

Figure:12(C)

Fig.12- Graphs of Grain Size Distribution of Multi Core with depth (cm)

- In the figure (9) The sediment sample analysed in this study exhibits a composition characterized by varying percentages of clay, silt, and sand. The clay content ranges from 12% to 15%, indicating a moderate presence within the sample. The silt fraction, on the other hand, accounts for a significant portion, with percentages ranging from

82% to 87%. Lastly, the sand component is relatively minimal, constituting only 0.5% of the sample. Overall, this composition suggests that the sediment is predominantly silt-dominated, with clay making up a smaller portion.

- The presence of a higher silt percentage indicates fine-grained particles, while the lower clay content suggests a relatively lesser influence of clay minerals. Additionally, the minimal sand percentage implies a limited contribution from coarser particles.

#### 4.3 DEPTH WISE VARIATION OF STATISTICAL DATA

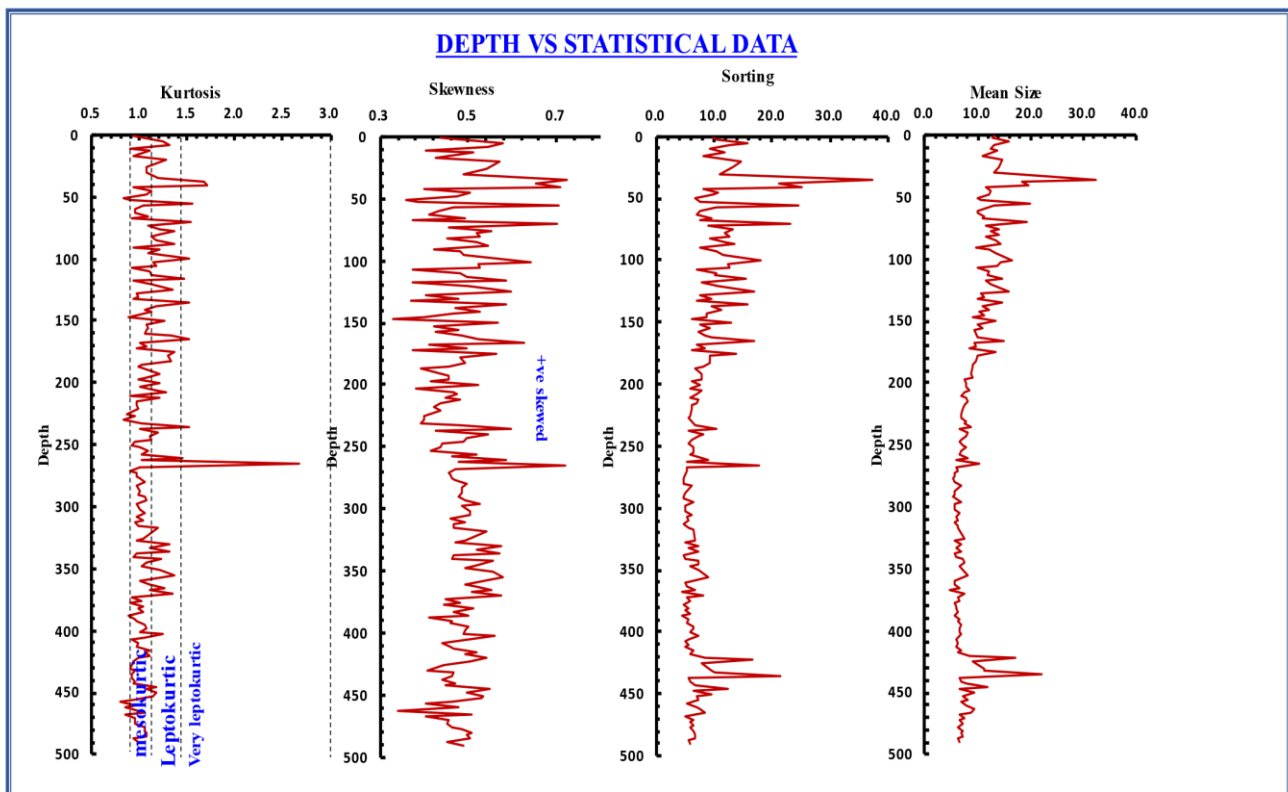


Fig.13- Plots of Statistical Data with depth in cm

The analysis of the sediment samples reveals that the majority of the data falls within the range of mesokurtic and leptokurtic distributions. This suggests a tendency towards moderate to high concentrations of sediment in the silt and clay fractions. The sediment

composition also exhibits a positive skewness, indicating a highly skewed distribution towards the coarser end of the particle size spectrum.

The positive skewness implies that there is a relatively higher concentration of larger particles (silt and clay) compared to smaller particles (sand). This skewed distribution could be attributed to various factors such as sediment transport processes, depositional dynamics, and local environmental conditions.

The presence of a higher concentration of silt and clay fractions suggests finer-grained sediments, which are often associated with low energy environments such as floodplains, estuaries, and deep marine settings. These sediments are typically transported and deposited by suspension settling or through slow sedimentation processes.

The analysis of grain size distribution with depth reveals that the sediment samples exhibit variations in size sorting. The overall trend indicates that the sediments fall within the category of very poorly sorted to poorly sorted.

Very poorly sorted sediments are characterized by a wide range of grain sizes, with significant variation and a lack of distinct size preference. This suggests a mixture of different-sized particles that have not undergone effective sorting processes. Poorly sorted sediments exhibit a similar trend, albeit with a relatively narrower range of grain sizes.

The presence of very poorly sorted to poorly sorted sediments suggests a complex depositional environment or multiple sediment sources. It indicates that the sediments have not experienced efficient sorting mechanisms, such as selective transport or sieving, which typically lead to better sorting and a narrower range of grain sizes.

The poor sorting of sediments can have various implications for sedimentary processes and environmental conditions. It can affect sediment stability, permeability, and the ability

of sediments to retain or transport fluids and contaminants. Additionally, it may influence sediment settling rates, bedform development, and sedimentation patterns.

## 4.4 GRAIN-SIZE STATISTICS

### 4.4.1 MEAN GRAIN SIZE VS SORTING

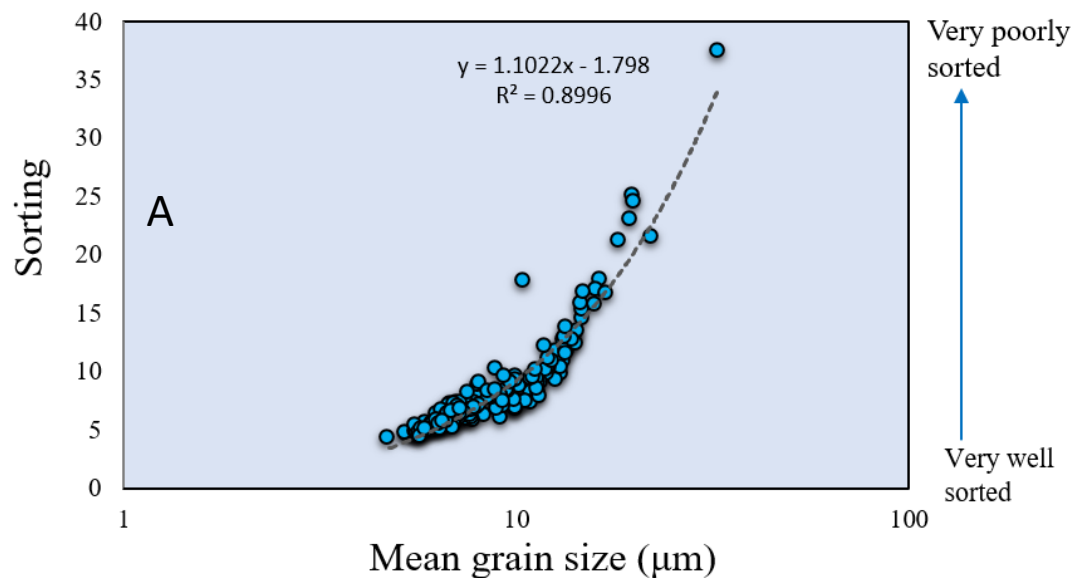


Fig.14 (A)- Plot of Mean Grain Size Vs sorting

The cross-plot of sorting against mean grain-size in the sediment samples reveals a negative relationship, indicating that increased grain-size is associated with poorer sorting. This means that as the mean grain-size increases, the sediment tends to exhibit lower levels of sorting.

Furthermore, the observation that all the samples fall within the category of poorly sorted confirms that the sediment in the studied area consistently displays inadequate sorting.

The negative relationship between grain-size and sorting is a common trend in sedimentary systems. Finer-grained sediments typically undergo more efficient sorting

processes due to their higher susceptibility to transport and selective settling. In contrast, coarser-grained sediments tend to experience less effective sorting due to their larger size and limited transportability.

The consistent presence of poorly sorted sediments suggests a dominant depositional environment or sedimentary process that has not facilitated sufficient grain-size segregation. This could be attributed to factors such as high-energy depositional conditions, rapid sedimentation rates, or the presence of mixed sediment sources.

#### 4.4.2 MEAN GRAIN SIZE VS SKEWNESS

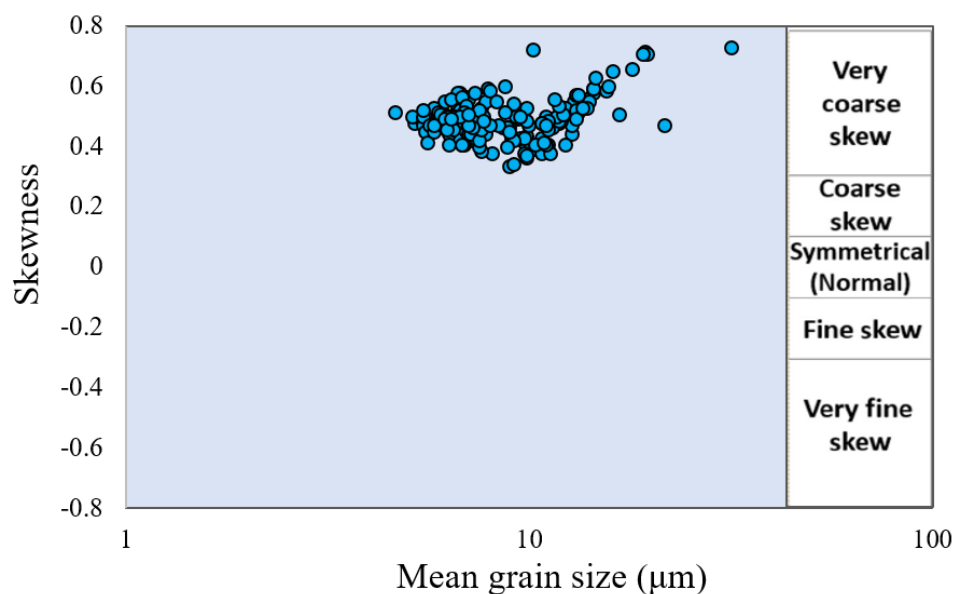


Fig.14 (B)- Mean Grain Size Vs Skewness

The analysis of mean grain size versus skewness in the sediment samples reveals that the data falls within the range of very coarse skew to coarse skew. This indicates that the grain sizes exhibit a skewed distribution towards the coarser (silt) end of the particle size spectrum.

A very coarse skew to coarse skew distribution suggests that there is a relatively higher concentration of larger grains (silt) compared to smaller grains (clay) in the sediment samples. The skewness parameter provides information about the asymmetry of the grain size distribution curve, with positive skewness indicating a tail towards larger grain sizes (silt).

The presence of such skewed distributions in the sediment samples may be influenced by several factors, including sediment transport processes, sediment sources, and depositional environments. High-energy environments and proximity to sediment sources can contribute to the dominance of coarser grains in the sediment samples.

Understanding the relationship between mean grain size and skewness provides valuable insights into the sedimentary dynamics and depositional processes. The dominance of larger grains and skewed distributions can impact sediment stability, permeability, and other geotechnical properties. Moreover, it may have implications for sediment transport, sedimentation patterns, and the interpretation of paleoenvironmental conditions

#### 4.4.3 MEAN GRAIN SIZE VS SORTING

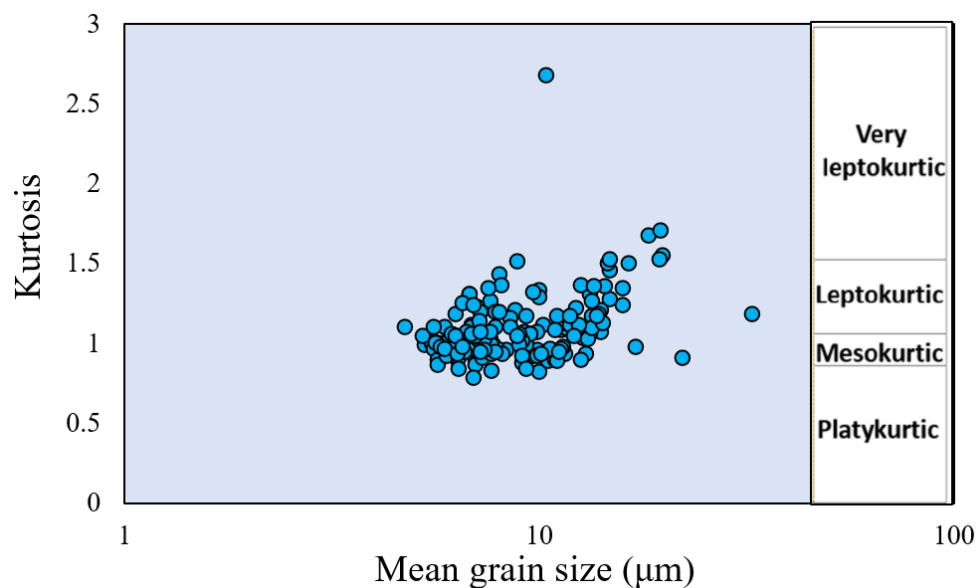


Fig.14 (C)- Mean Grain Size Vs Kurtosis

The analysis of mean grain size versus kurtosis reveals that the sediment samples exhibit a higher concentration of grain sizes around the mesokurtic to leptokurtic range. Kurtosis measures the peakedness or flatness of the grain size distribution curve. A mesokurtic distribution indicates a moderate level of peakedness, while a leptokurtic distribution indicates a higher degree of peakedness with heavier tails. The observation that the samples show a higher concentration of grain sizes around the mesokurtic to leptokurtic range suggests that the sediment is characterized by a relatively well-defined peak in the grain size distribution. This indicates a dominant grain size or a more pronounced mode in the sediment samples.

The presence of a peaked distribution can be influenced by various factors, including sediment sources, transport processes, and depositional environments. It suggests a preferential accumulation or preservation of certain grain sizes within the sediment.

## 4.5 BIVARIATE PLOTS OF VARIOUS STATISTICAL SIZE

### PARAMETERS

#### 4.5.1 BIVARIANT PLOTS AGAINST GRAPHIC SKEWNESS VS GRAPHIC

#### KURTOSIS

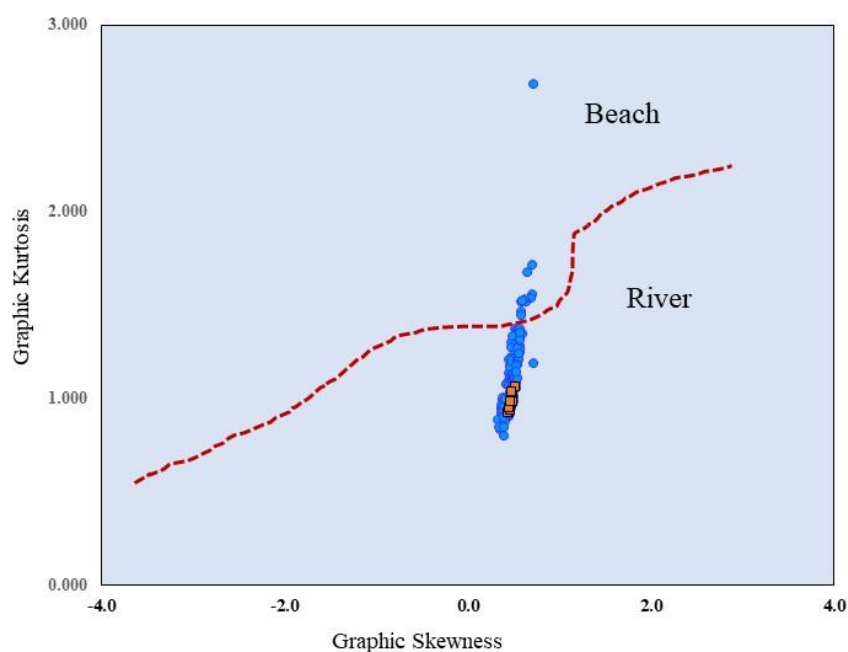


Fig.15 (A) Graphic Skewness vs Graphic Kurtosis

The analysis of the bivariate plot reveals that the majority of the samples fall within the region associated with river deposit processes. This indicates that these sediments are primarily influenced by fluvial transport and deposition. River deposits typically exhibit positive graphic skewness and higher graphic kurtosis values, reflecting a distribution skewed towards coarser grain sizes with a well-defined peak.

Additionally, a smaller portion of the grain size distribution falls within the region corresponding to beach processes. These sediments display characteristics such as lower graphic kurtosis values, indicating a distribution skewed towards finer grain sizes with a less pronounced peak. Beach processes are characterized by wave action and shoreline dynamics, which often result in the selective sorting and accumulation of finer sediments

#### 4.5.2 BIVARIANT PLOTS AGAINST GRAPHIC SKEWNESS VS SORTING

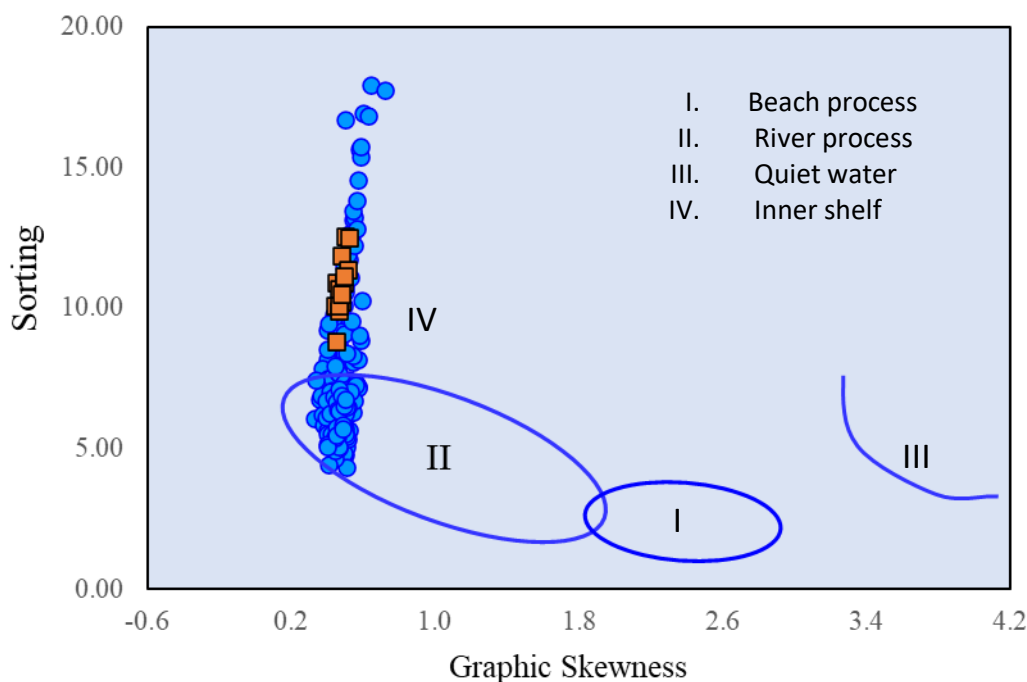


Fig. 15 (B) Graphic Skewness vs sorting

In the fig the dominance of samples falling within the region associated with river deposit processes confirms the significant role of fluvial transport and deposition in shaping the sedimentary environment of the studied area. The positive graphic skewness and poorer

sorting characteristics indicate the transport and accumulation of sediments with a wide range of grain sizes, likely influenced by upstream sediment sources and river dynamics.

Furthermore, the presence of samples falling within the region associated with inner shelf processes suggests the additional influence of wave action and longshore currents. These processes contribute to the selective sorting and accumulation of sediments on the inner shelf, resulting in a relatively better sorting pattern compared to river deposits. The Shepard ternary diagram reveals that the majority of sediment.

#### 4.6 Clay mineral XRD Graphs of GC2 Core (Mangalore)

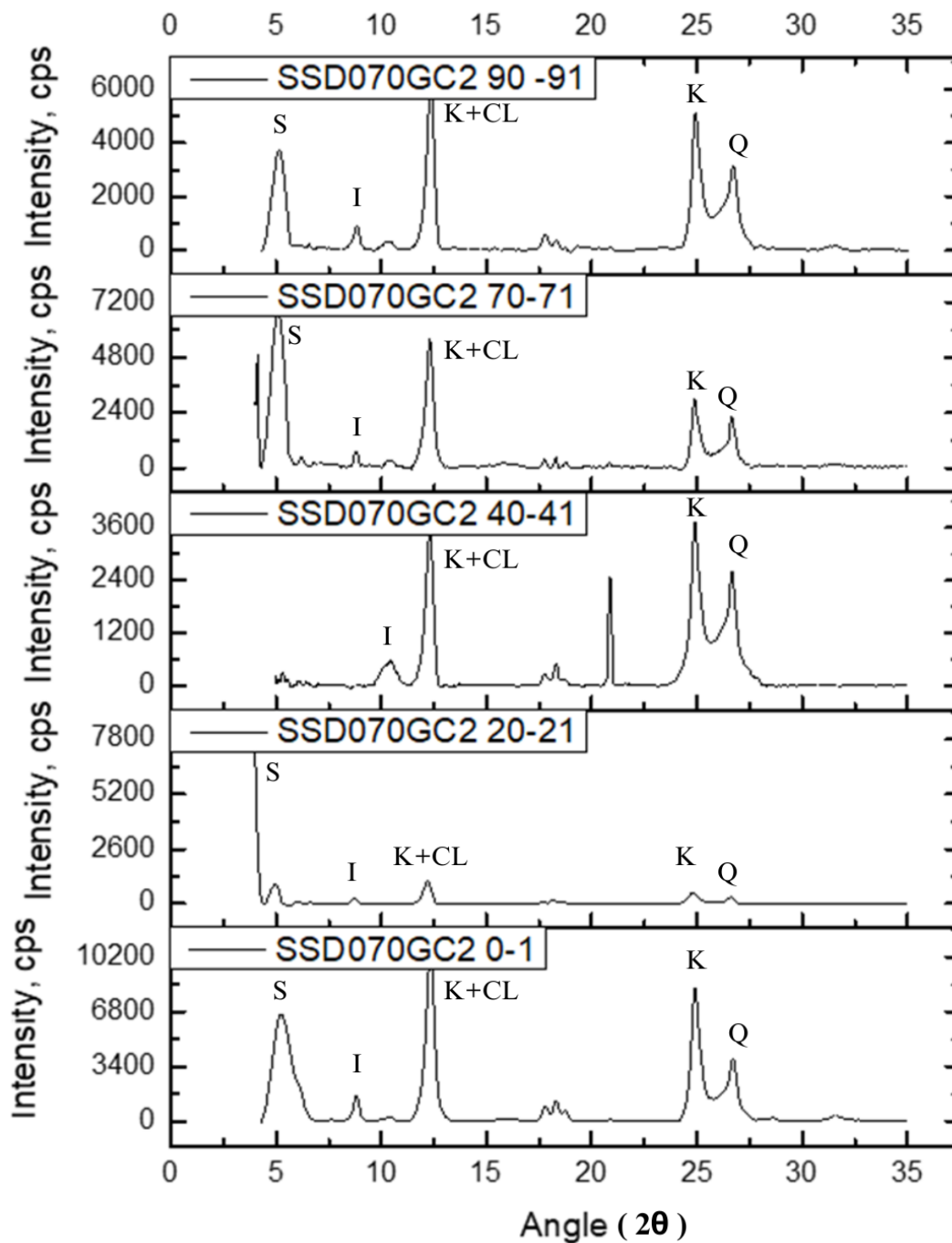


Fig. 16 (A): Clay mineral XRD Graph of GC2 0-91cm

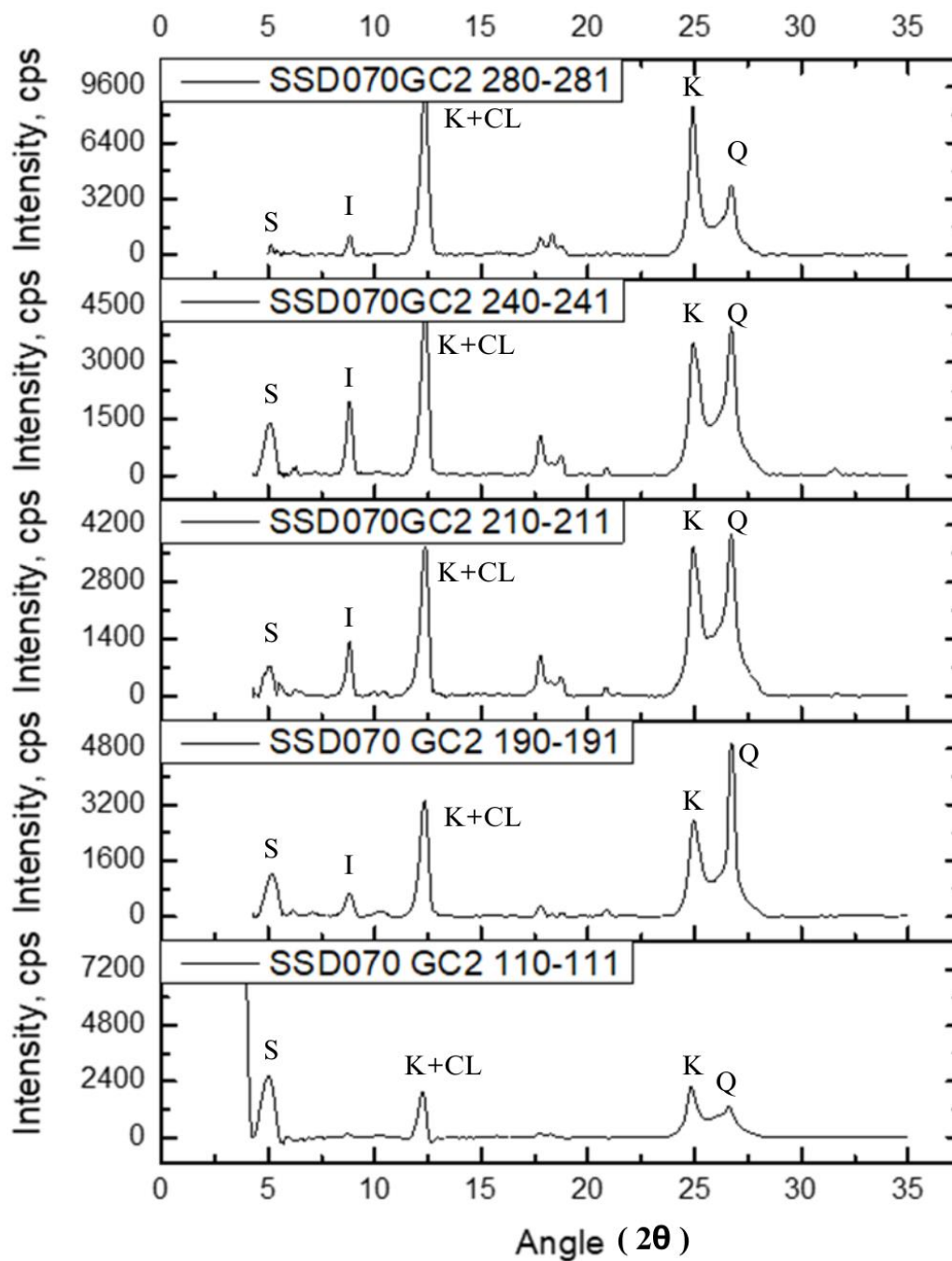


Fig. 16 (B): Clay mineral XRD Graph of GC2 110-281 cm

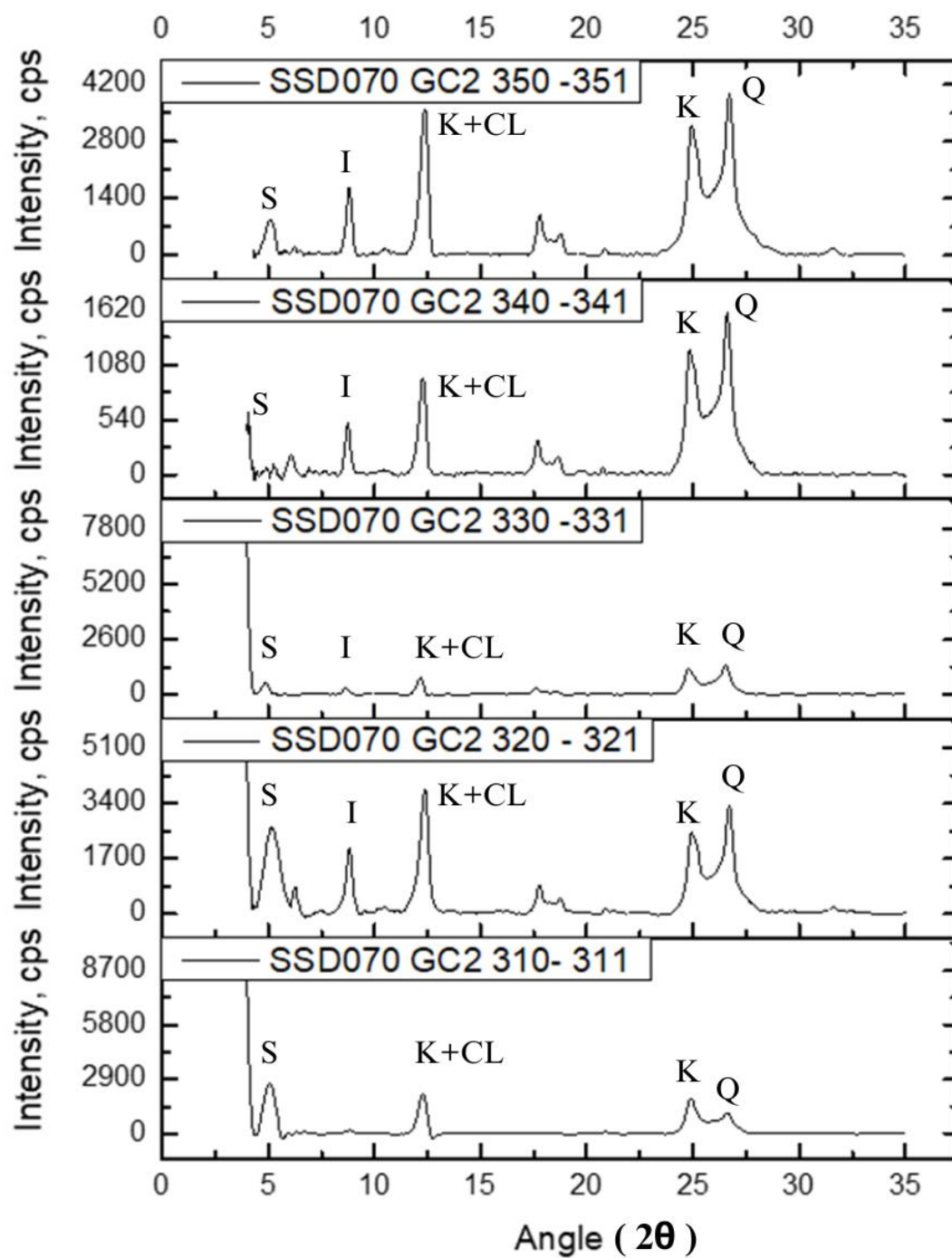


Fig. 16 (C): Clay mineral XRD Graph of GC2 310-351 cm

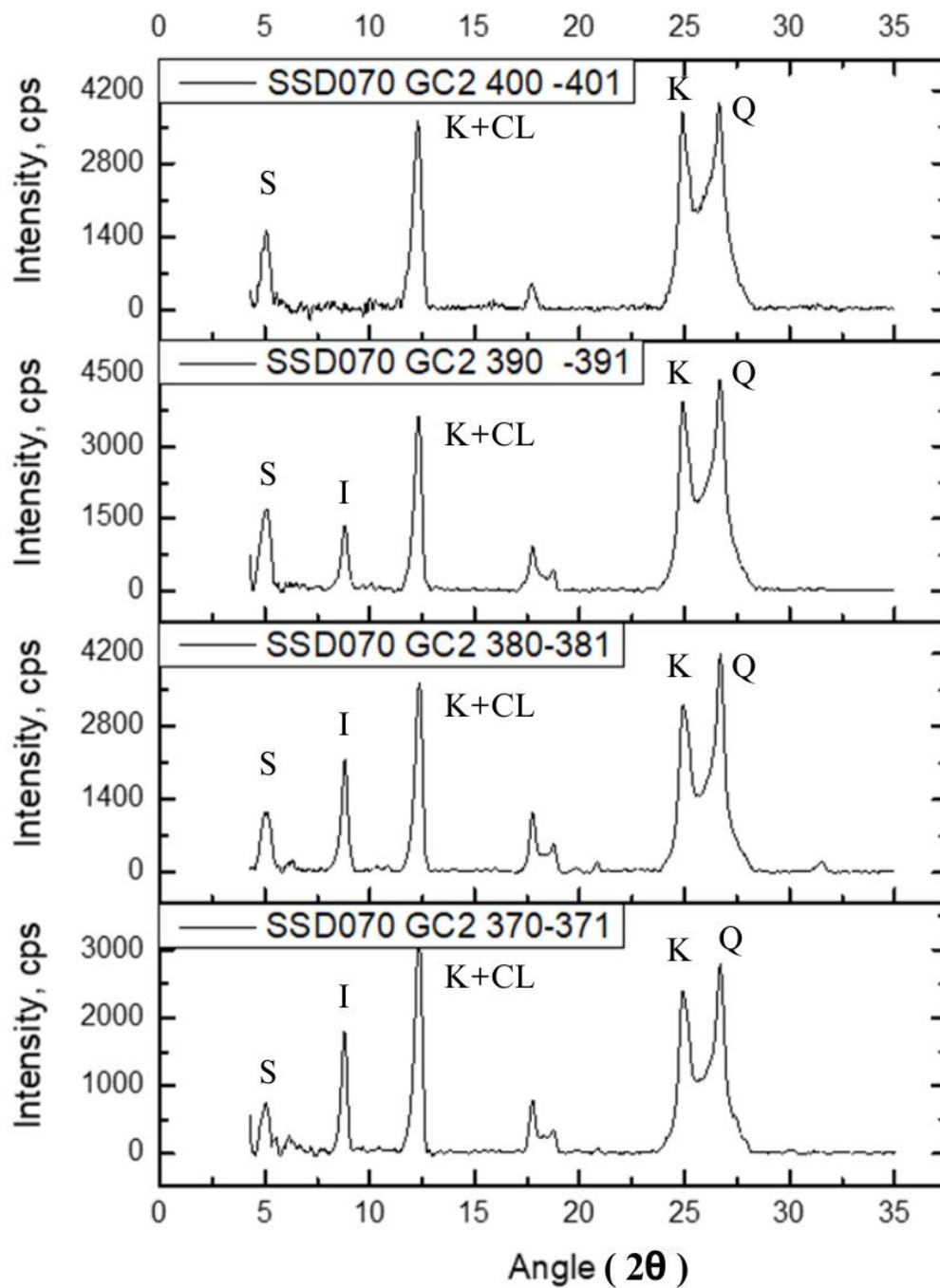


Fig. 16 (D): Clay mineral XRD Graph of GC2 370-401 cm

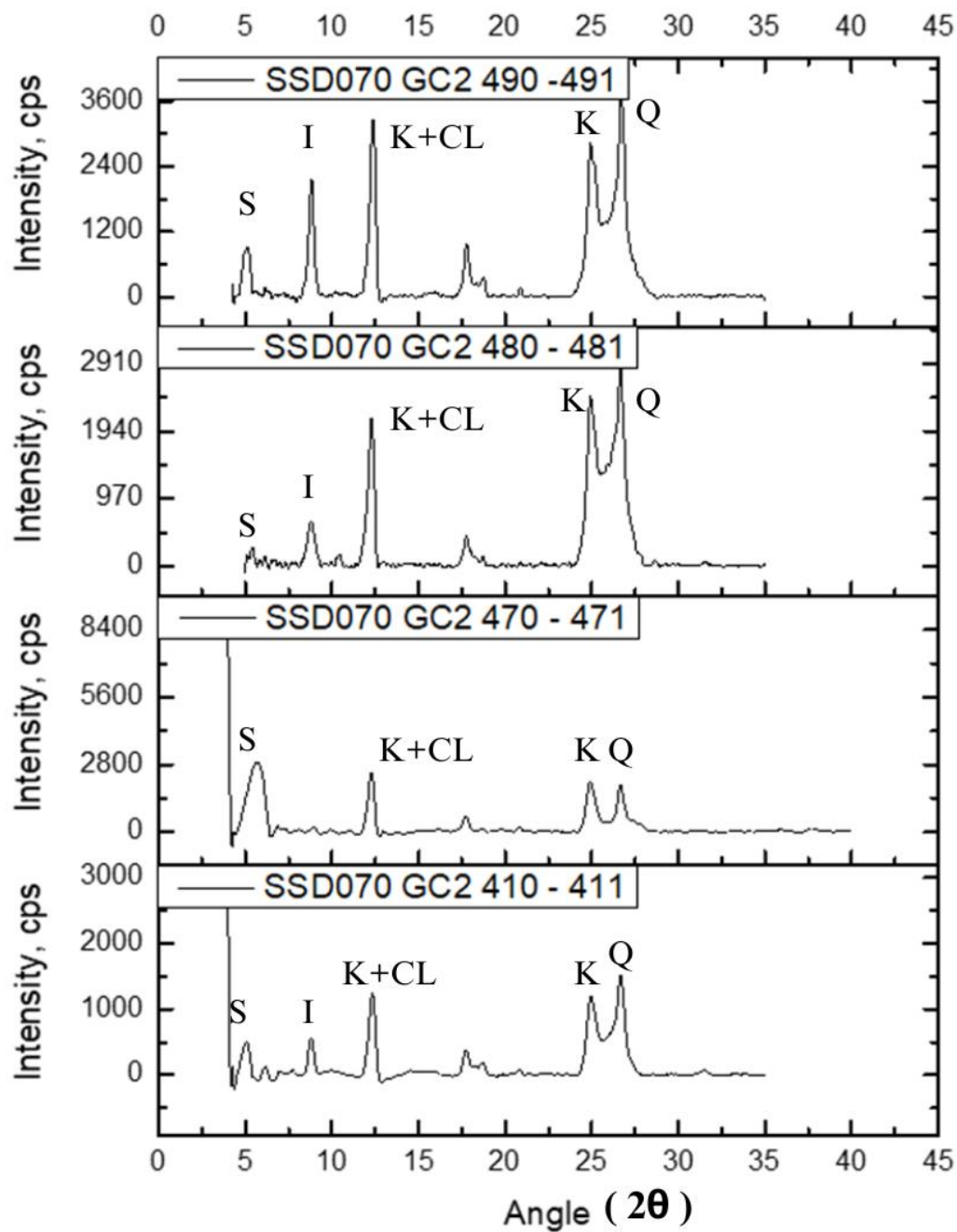


Fig. 16 (E): Clay mineral XRD Graph of GC2 410-491 cm

#### 4.6.1 PIE CHART DESCRIBING PERCENTAGES OF CLAY MINERALS IN GC2 SAMPLES

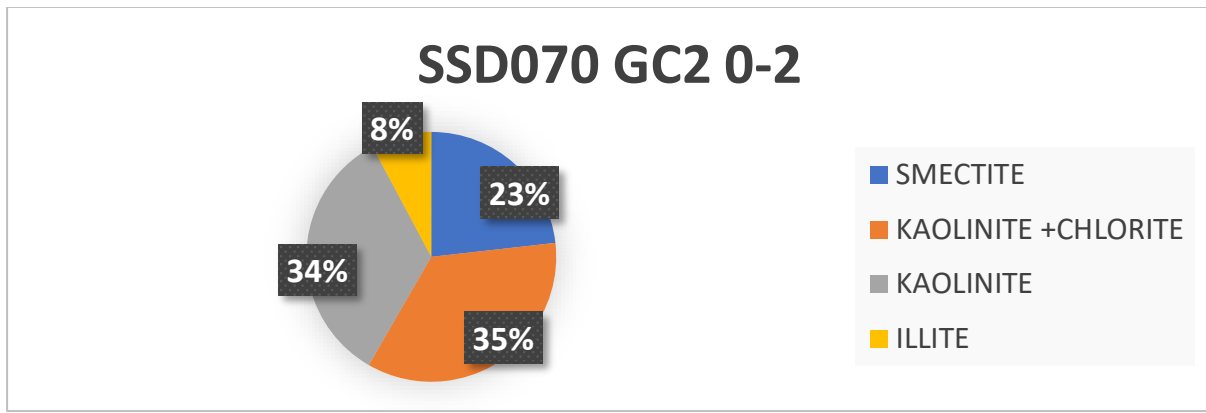


Fig 17 (A): Percentage of clay minerals in GC2 0-2 cm

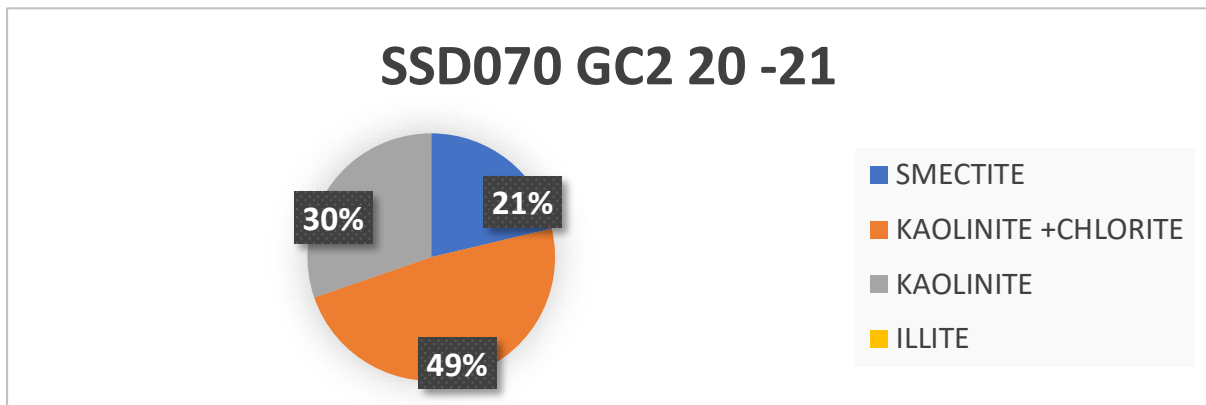


Fig 17 (B): Percentage of clay minerals in GC2 20-21 cm

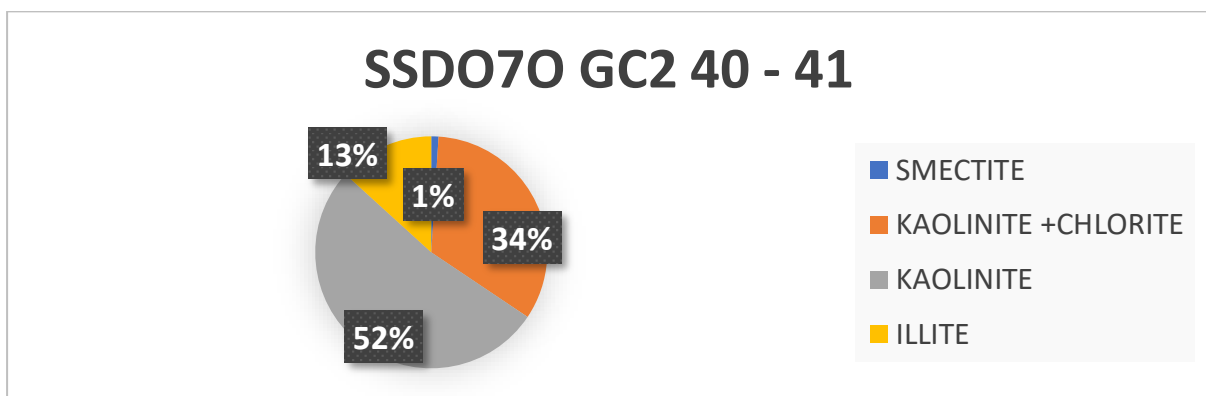


Fig 17 (C): Percentage of clay minerals in GC2 40-41 cm

### SSDO70 GC2 70 - 71

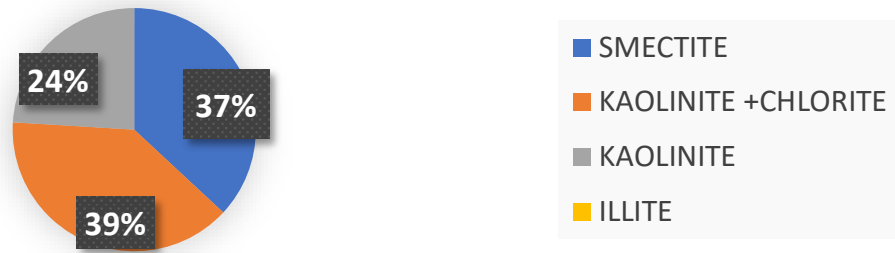


Fig 17 (D): Percentage of clay minerals in GC2 70-71 cm

### SSDO70 GC2 90 - 91

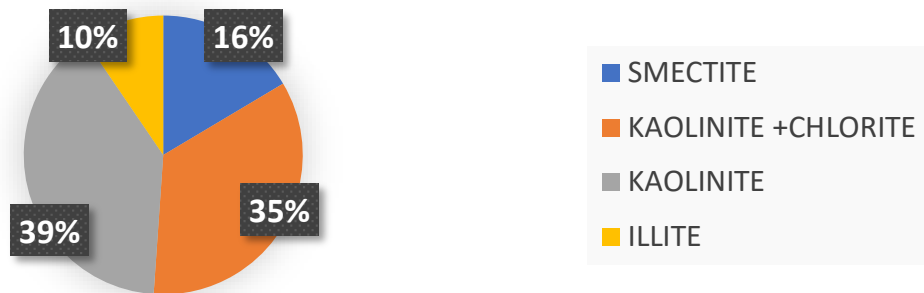


Fig 17 (E): Percentage of clay minerals in GC2 90-91 cm

### SSDO70 GC2 110 - 111



Fig 17 (F): Percentage of clay minerals in GC2 110-111 cm

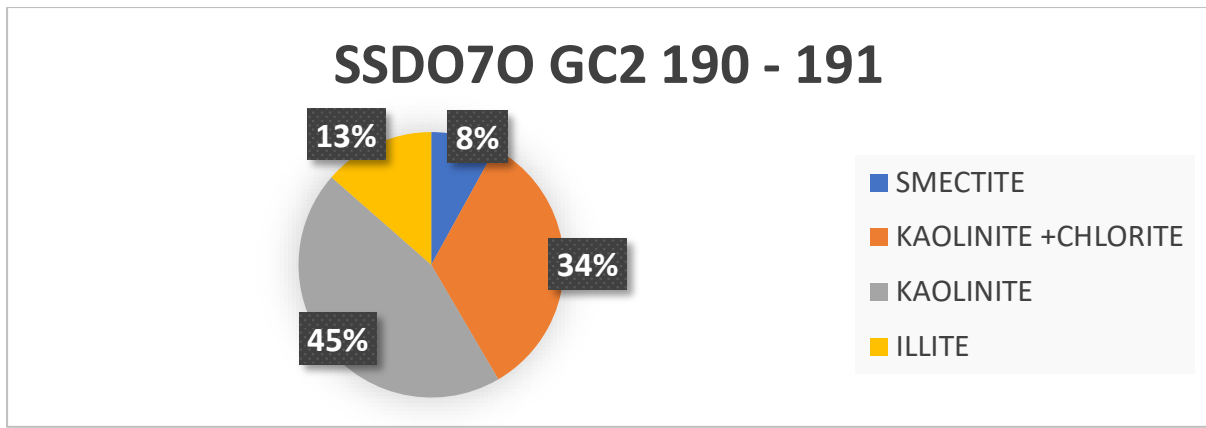


Fig 17 (G): Percentage of clay minerals in GC2 190-191 cm

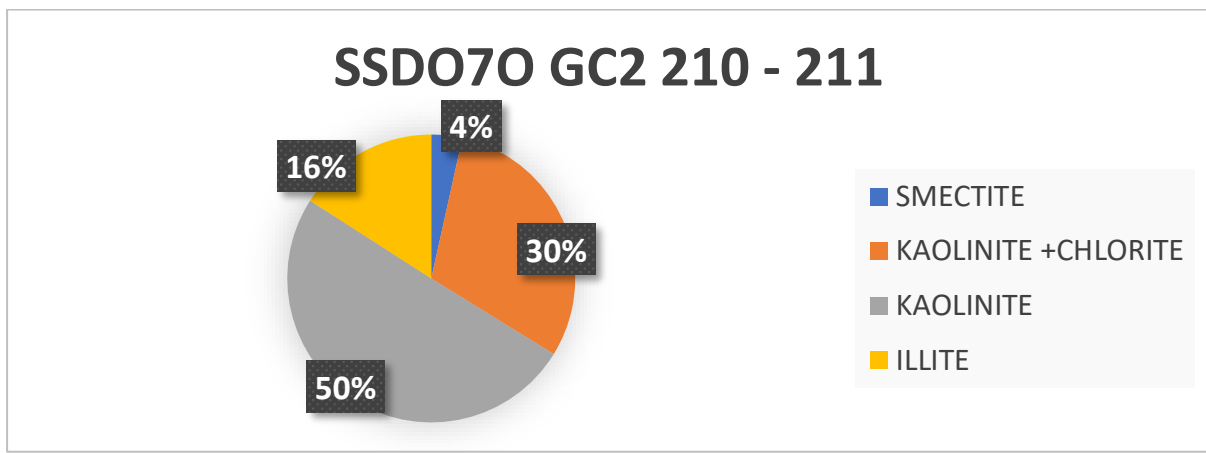


Fig 17 (H): Percentage of clay minerals in GC2 210-211 cm

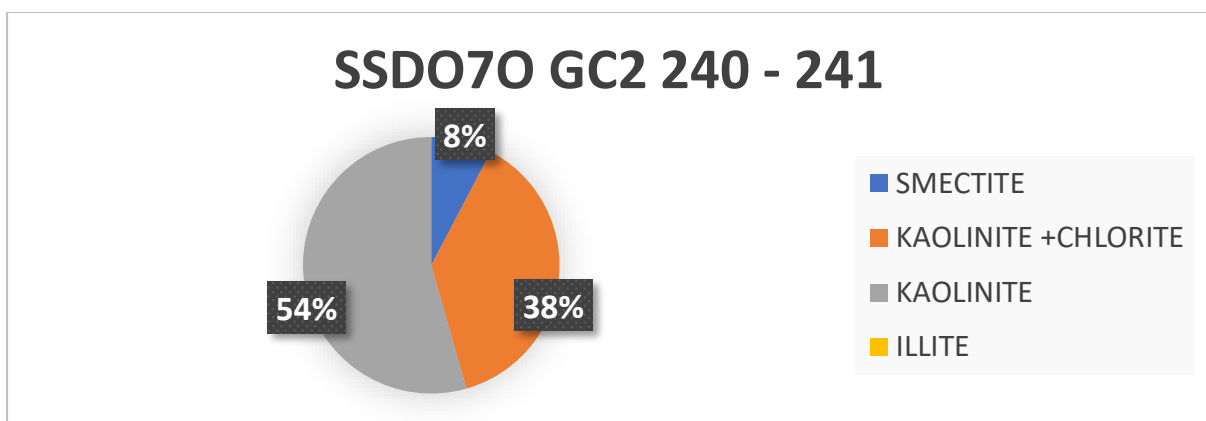


Fig 17 (I): Percentage of clay minerals in GC2 240-241 cm

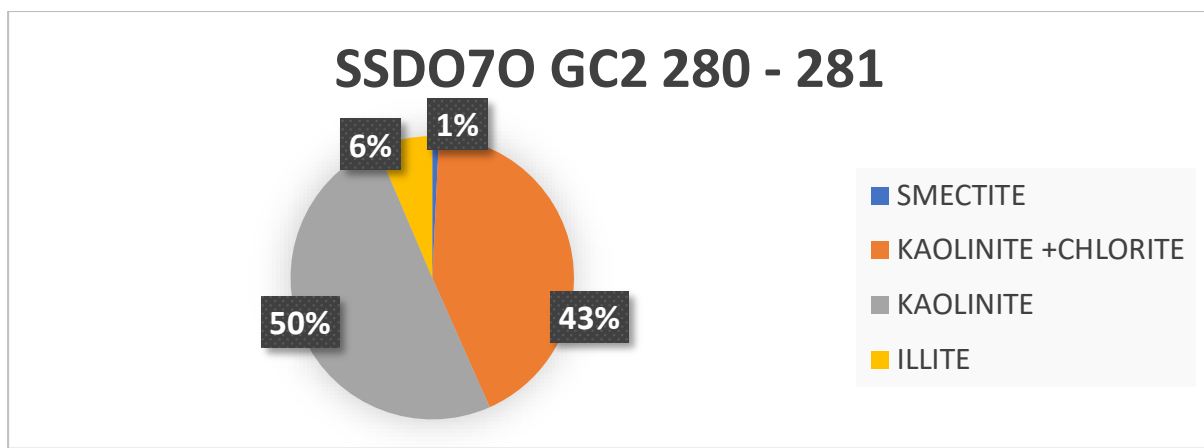


Fig 17 (J): Percentage of clay minerals in GC2 280-281 cm

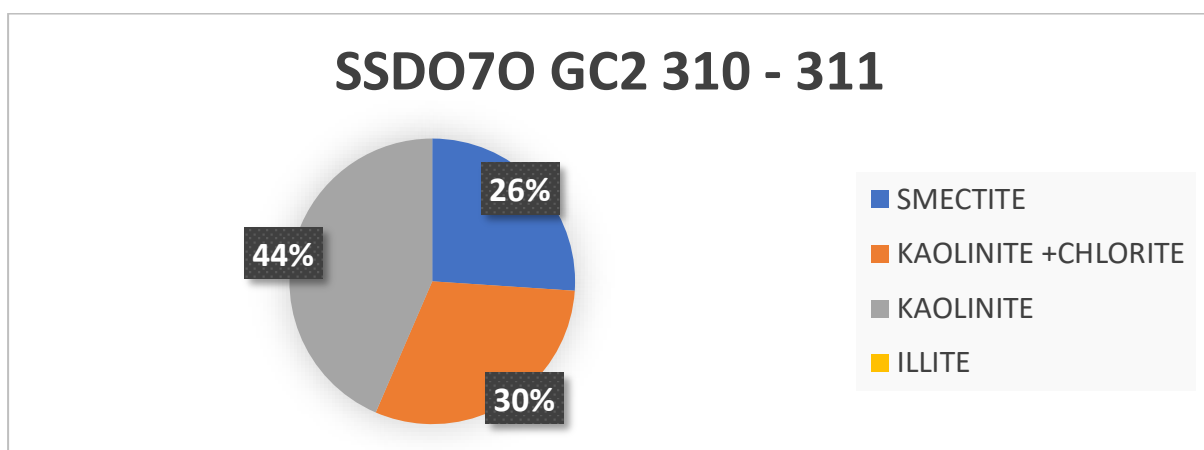


Fig 17 (K): Percentage of clay minerals in GC2 310-311 cm

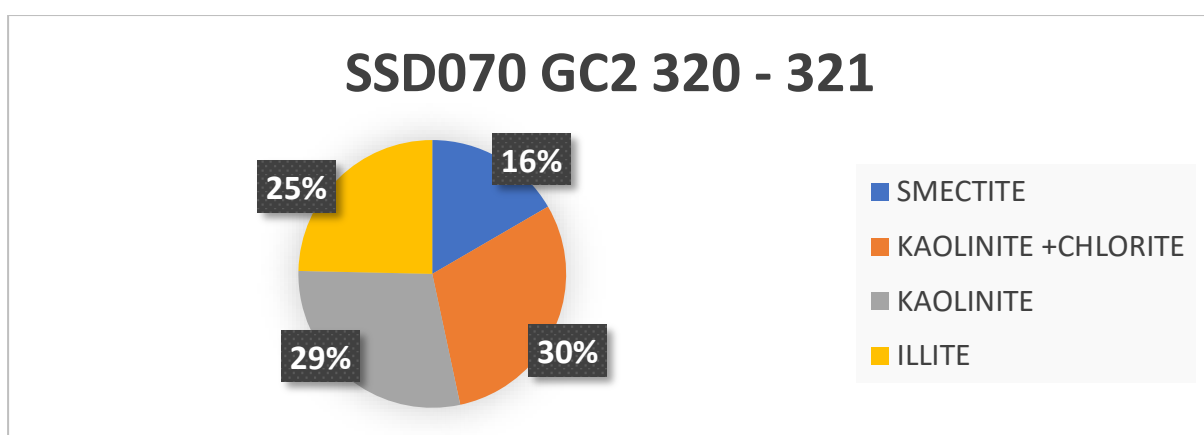


Fig 17 (L): Percentage of clay minerals in GC2 320-321 cm

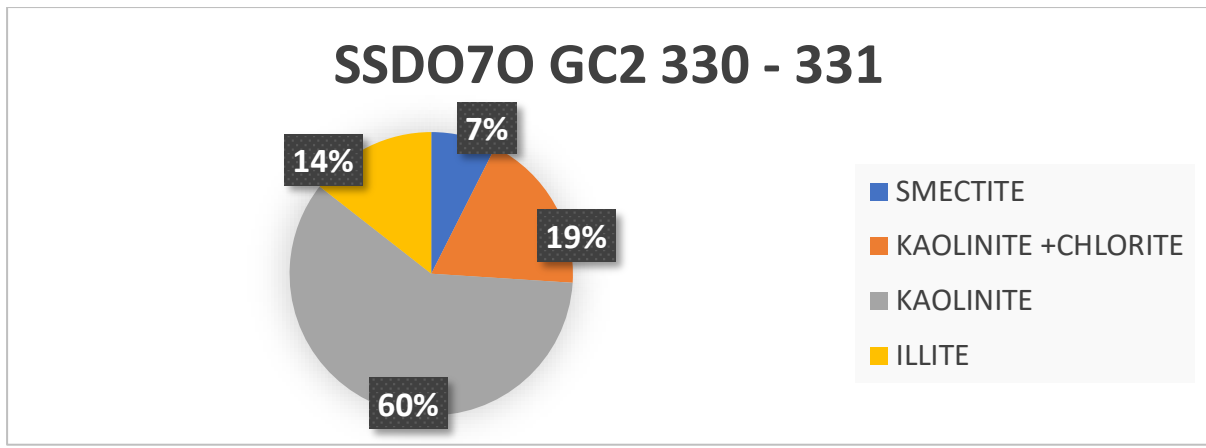


Fig 17 (M): Percentage of clay minerals in GC2 330-331 cm

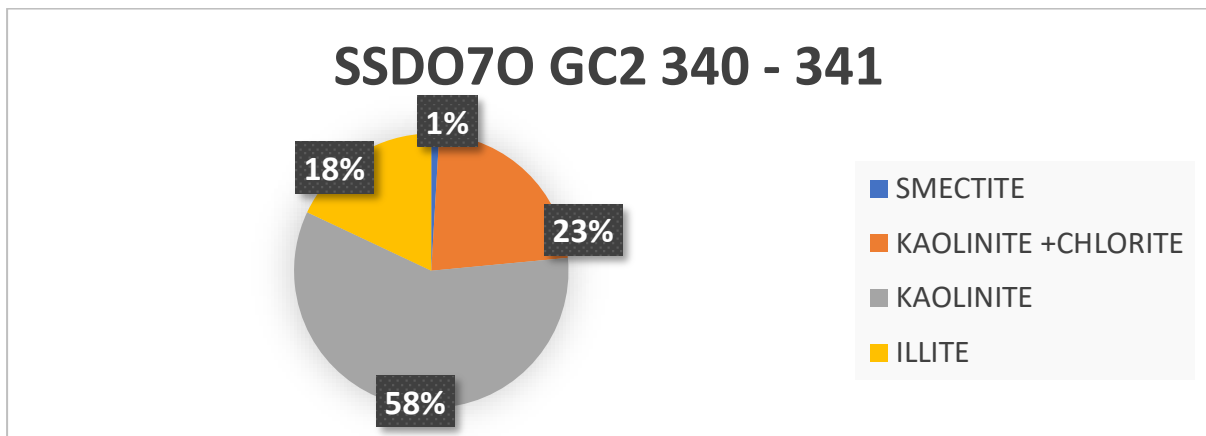


Fig 17 (N): Percentage of clay minerals in GC2 340-341 cm

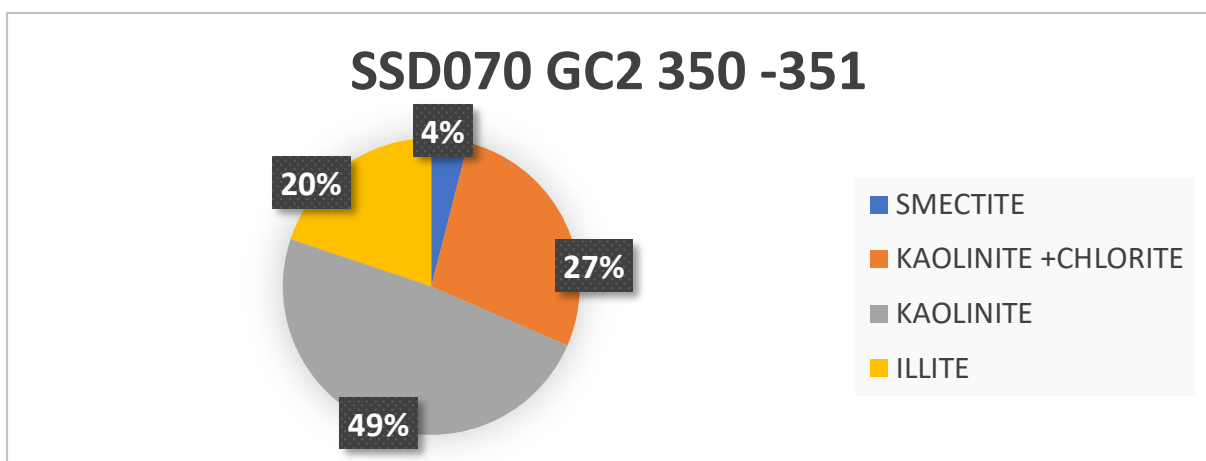


Fig 17 (O): Percentage of clay minerals in GC2 350-351 cm

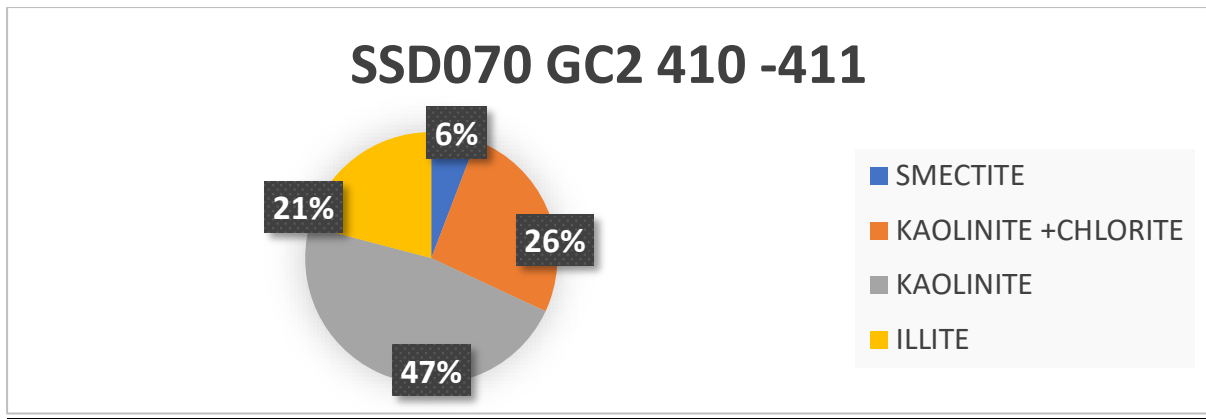


Fig 17 (P): Percentage of clay minerals in GC2 410-411 cm

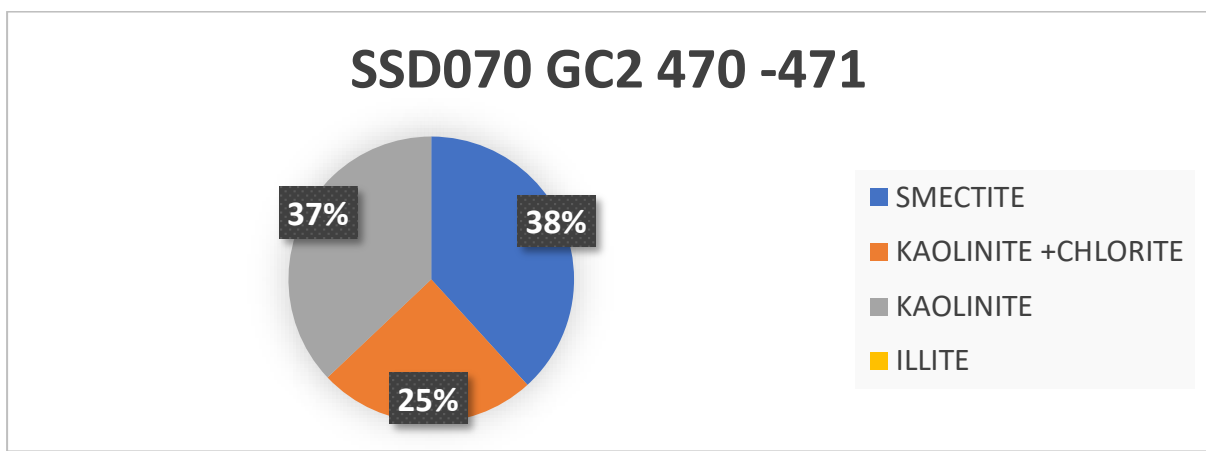


Fig 17 (Q): Percentage of clay minerals in GC2 470-471 cm

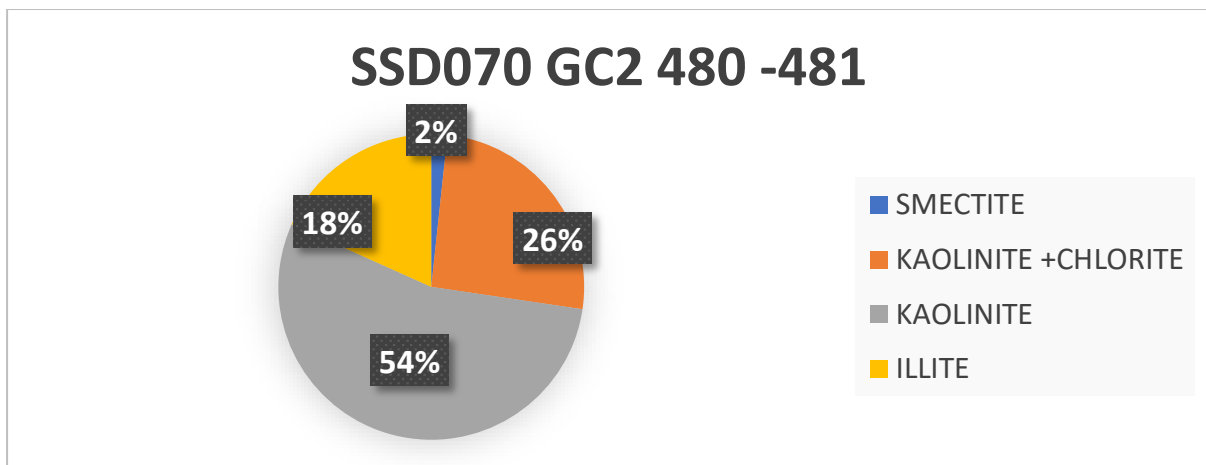


Fig 17 (R): Percentage of clay minerals in GC2 480-481 cm

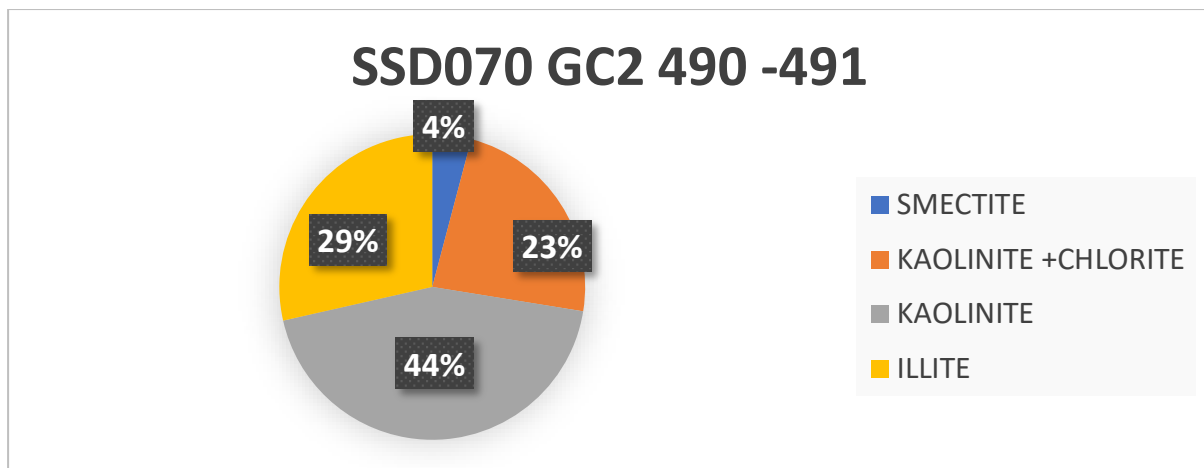


Fig 17 (S): Percentage of clay minerals in GC2 490-491 cm

#### 4.6.2 GC2 CORE BULK RD GRAPH (MANGALORE)

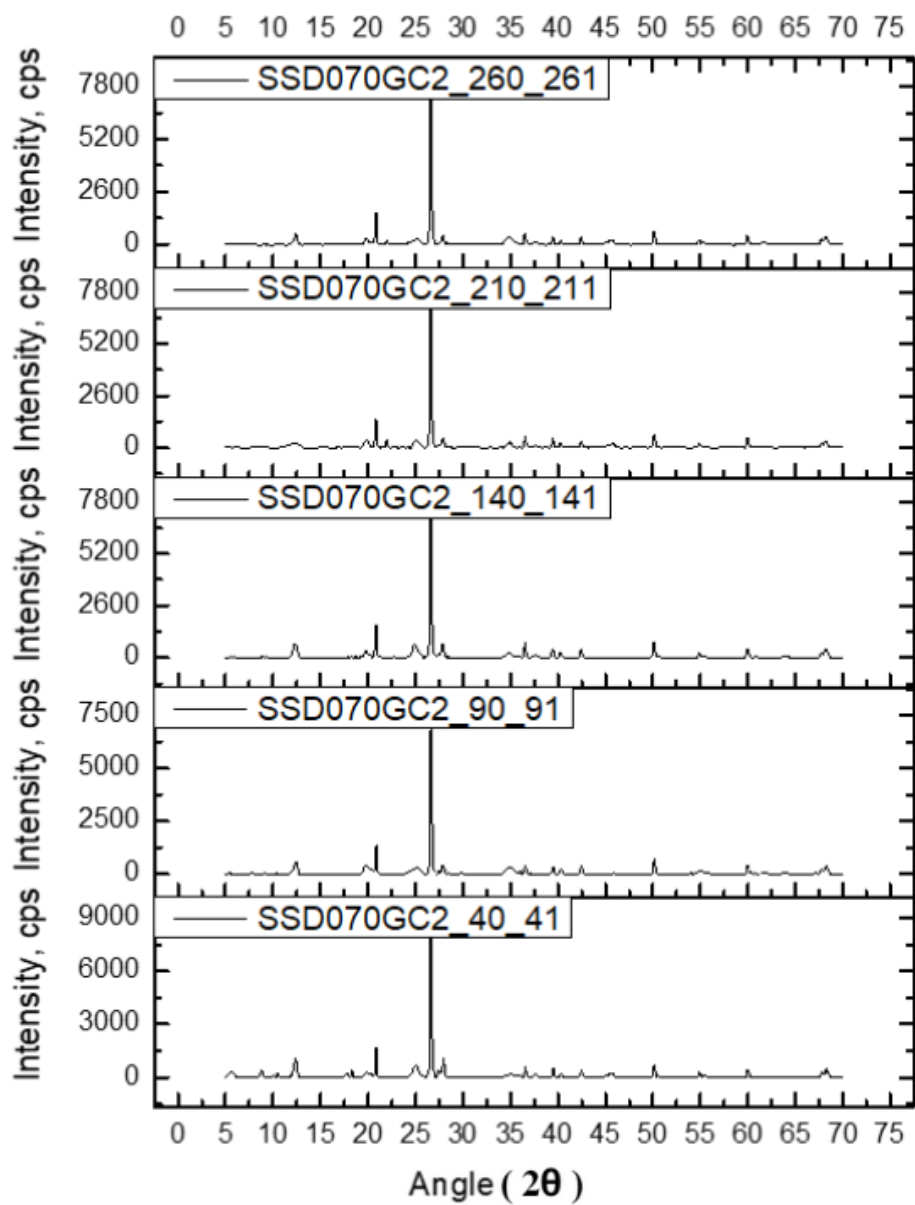


Fig. 18 (A): Bulk mineral XRD Graph of GC2 40-261 cm

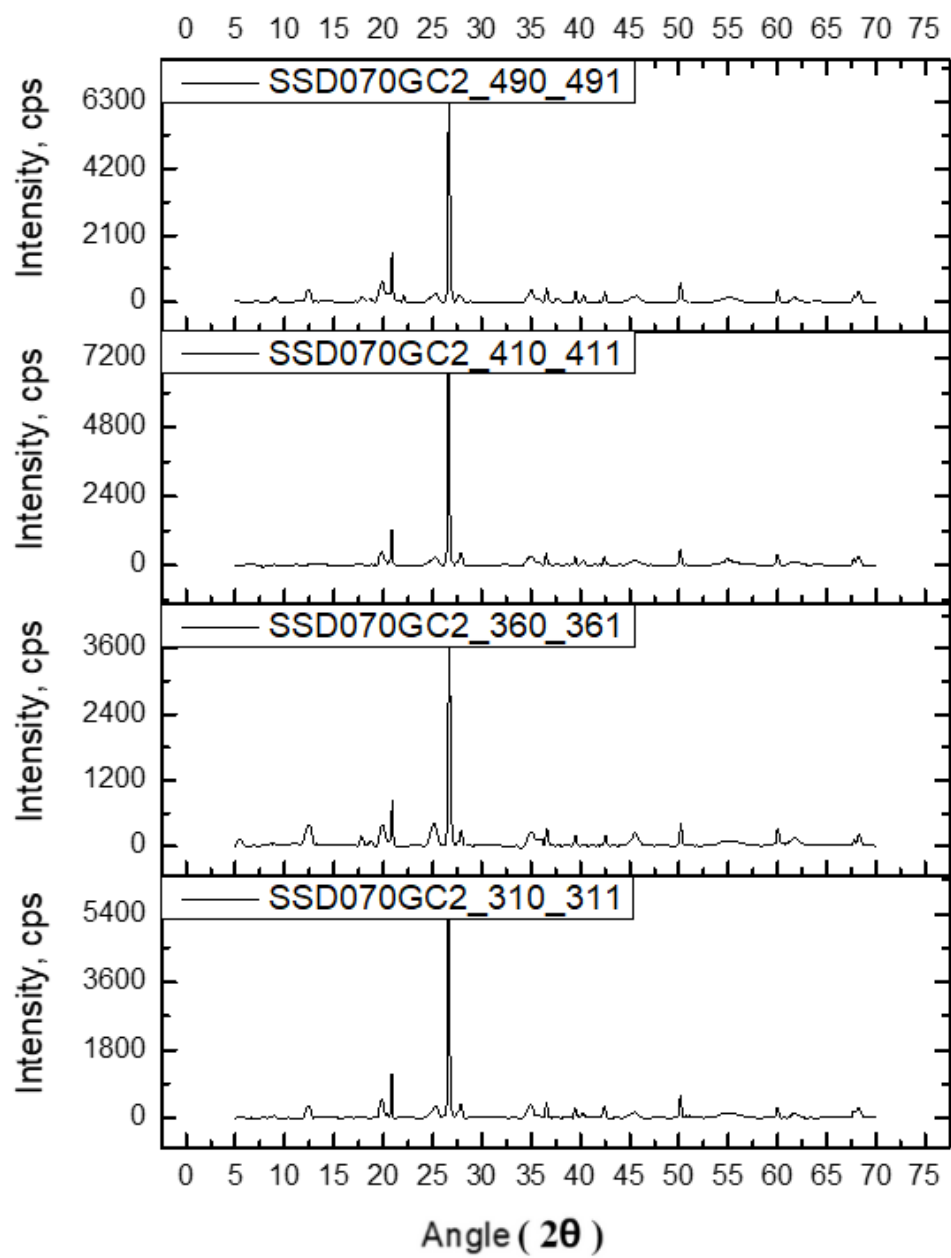


Fig. 18 (B): Bulk mineral XRD Graph of GC2 310-491 cm

## 4.6.3 PERCENTAGE OF CLAY MINERALS IN GC2 CORE

<b>SAMPLE NAME</b>	<b>SMECTITE %</b>	<b>KAOLINITE +CHLORITE%</b>	<b>KAOLINITE%</b>	<b>ILLITE%</b>
<b>SSD070 GC2 0-2</b>	<b>23.21790409</b>	<b>35.11533203</b>	<b>33.87907157</b>	<b>7.7876923</b>
<b>SSD070 GC2 20-21</b>	<b>21.297762</b>	<b>48.41939867</b>	<b>30.28283933</b>	<b>0</b>
<b>SSD070 GC2 40-41</b>	<b>1.008111944</b>	<b>33.40039753</b>	<b>52.33570695</b>	<b>13.255784</b>
<b>SSD070 GC2 70-71</b>	<b>36.92829997</b>	<b>39.03158326</b>	<b>24.04011677</b>	<b>0</b>
<b>SSD070 GC2 90-91</b>	<b>16.45303503</b>	<b>34.6462056</b>	<b>39.3864136</b>	<b>9.5143458</b>
<b>SSD070 GC2 110-111</b>	<b>27.98197896</b>	<b>24.05835051</b>	<b>47.95967053</b>	<b>0</b>
<b>SSD070 GC2 190-191</b>	<b>8.012733864</b>	<b>33.56239015</b>	<b>44.88937284</b>	<b>13.535503</b>
<b>SSD070 GC2 210-211</b>	<b>3.472963003</b>	<b>30.33363784</b>	<b>50.28346719</b>	<b>15.909932</b>
<b>SSD070 GC2 240-241</b>	<b>7.692615355</b>	<b>37.89210686</b>	<b>54.41527778</b>	<b>0</b>
<b>SSD070 GC2 280-281</b>	<b>0.765760256</b>	<b>42.58849052</b>	<b>50.24400044</b>	<b>6.4017488</b>
<b>SSD070 GC2 310-311</b>	<b>26.05140651</b>	<b>30.43151887</b>	<b>43.51707462</b>	<b>0</b>
<b>SSD070 GC2 320-321</b>	<b>16.62317776</b>	<b>30.02149824</b>	<b>28.7086047</b>	<b>24.646719</b>
<b>SSD070 GC2 330-331</b>	<b>7.448517904</b>	<b>18.57106382</b>	<b>59.535391</b>	<b>14.445027</b>
<b>SSD070 GC2 340-341</b>	<b>0.935856219</b>	<b>22.56648334</b>	<b>58.5069978</b>	<b>17.990663</b>
<b>SSD070 GC2 350-351</b>	<b>4.005354682</b>	<b>27.5158627</b>	<b>48.65852327</b>	<b>19.820259</b>

SSD070 GC2 410- 411	5.833069826	26.1003712	47.15211706	20.914442
SSD070 GC2 470- 471	38.23986712	24.70160582	37.05852706	0
SSD070 GC2 480- 481	1.696278896	25.64256005	54.37445385	18.286707
SSD070 GC2 490- 491	4.117987804	23.4340594	43.90907965	28.538873

Table 2: Percentage of clay minerals in GC2 core

#### 4.7 SP CORE BULK XRD GRAPH

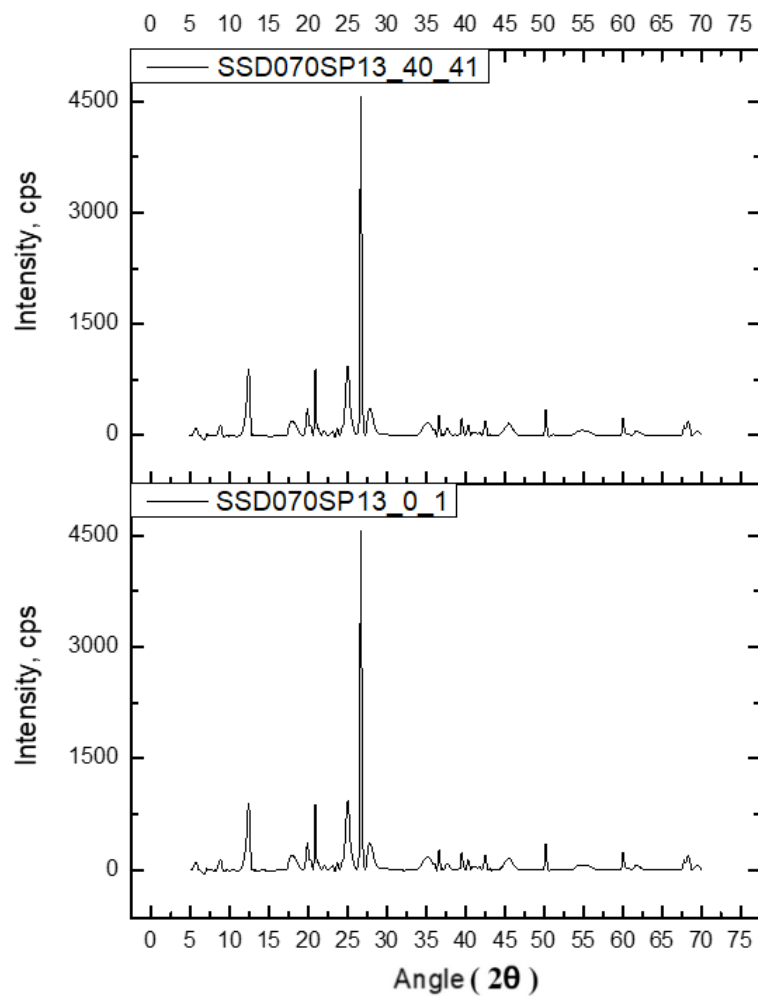


Fig. 19: Bulk mineral XRD Graph of SP 13 0-1 cm, 40-41 cm

#### 4.8 MC CORE BULK XRD GRAPH

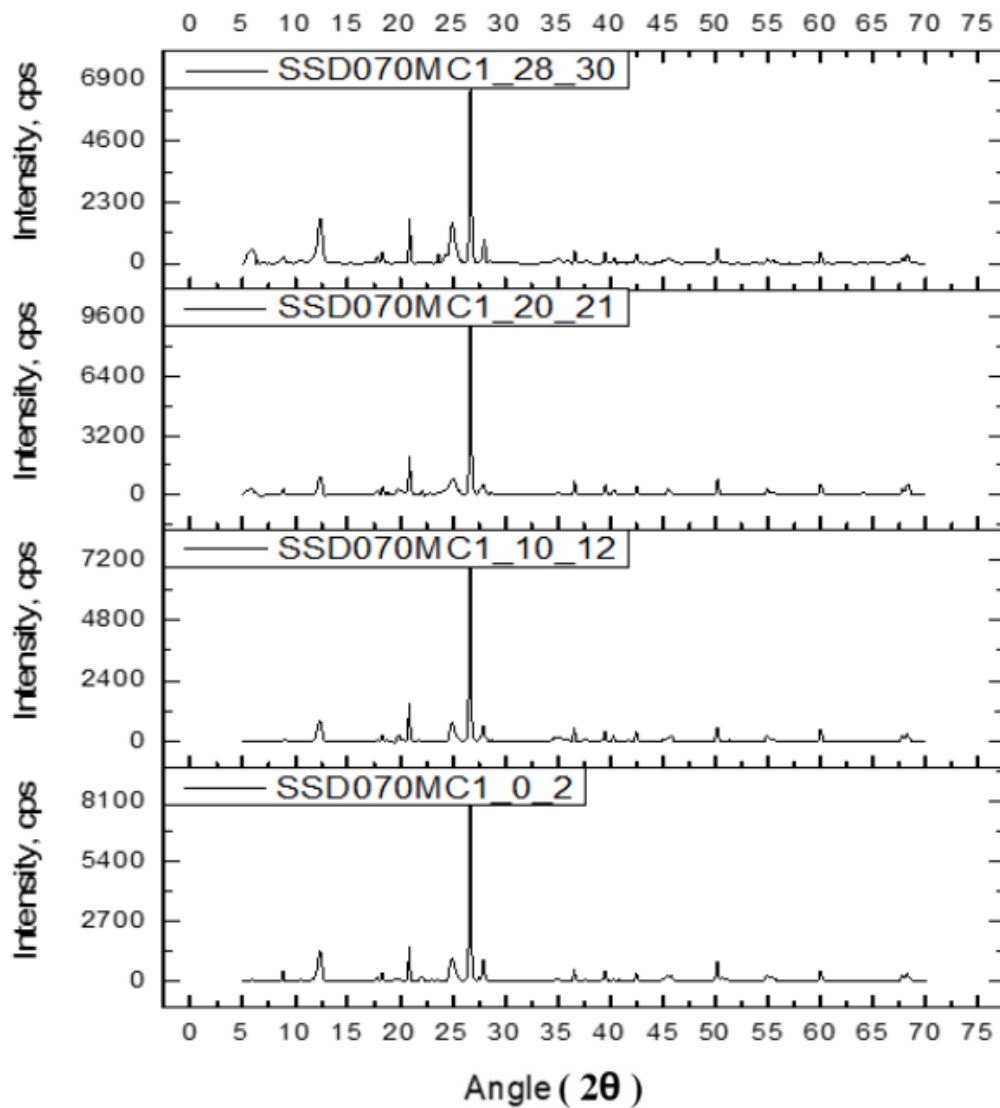


Fig. 20: Bulk mineral XRD Graph of MC1 0-30 cm

## 4.9 CLAY MINERAL XRD GRAPH GC6 CORE

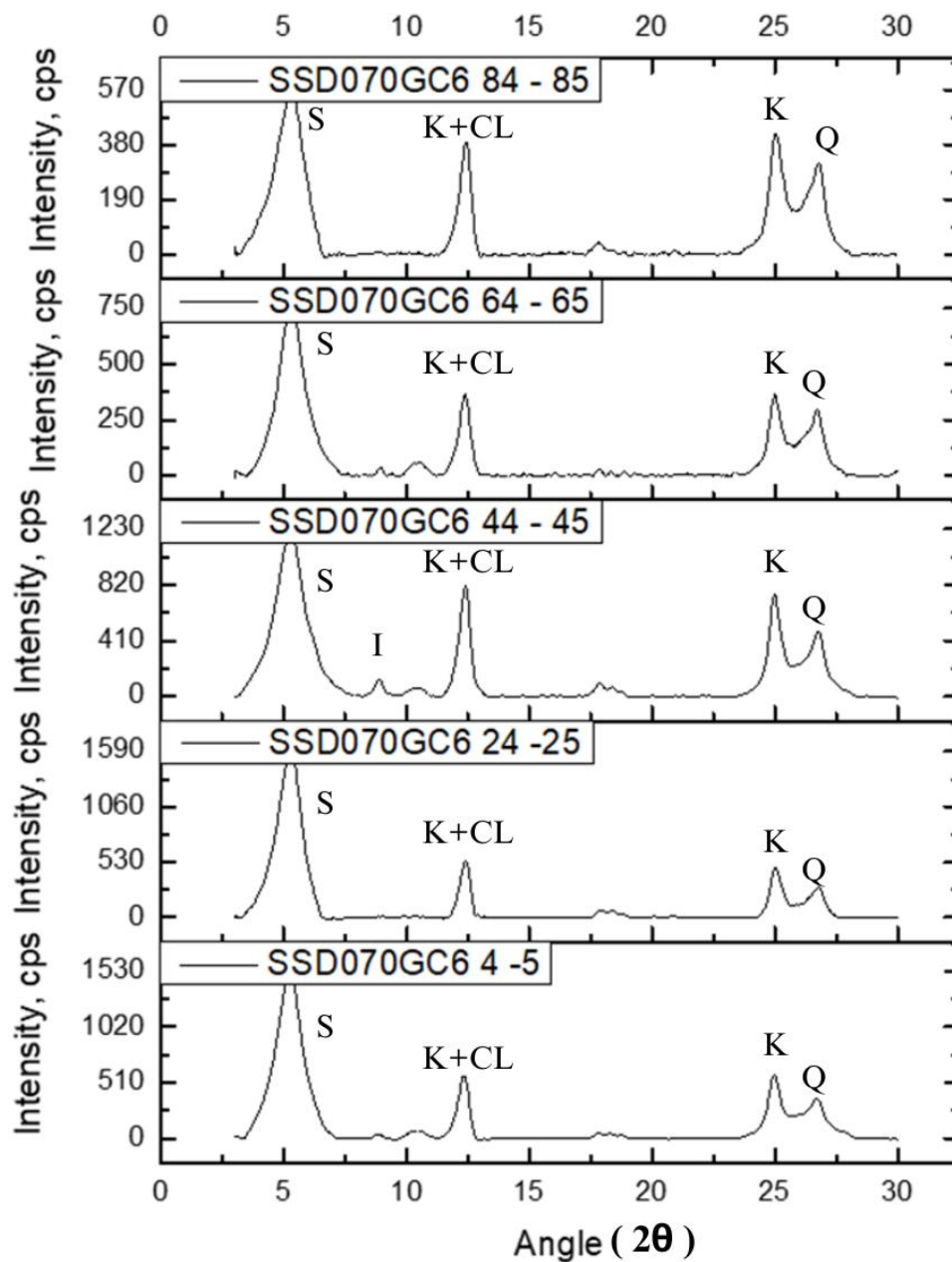


Fig. 21 (A): Clay mineral XRD Graph of GC6 4-85 cm

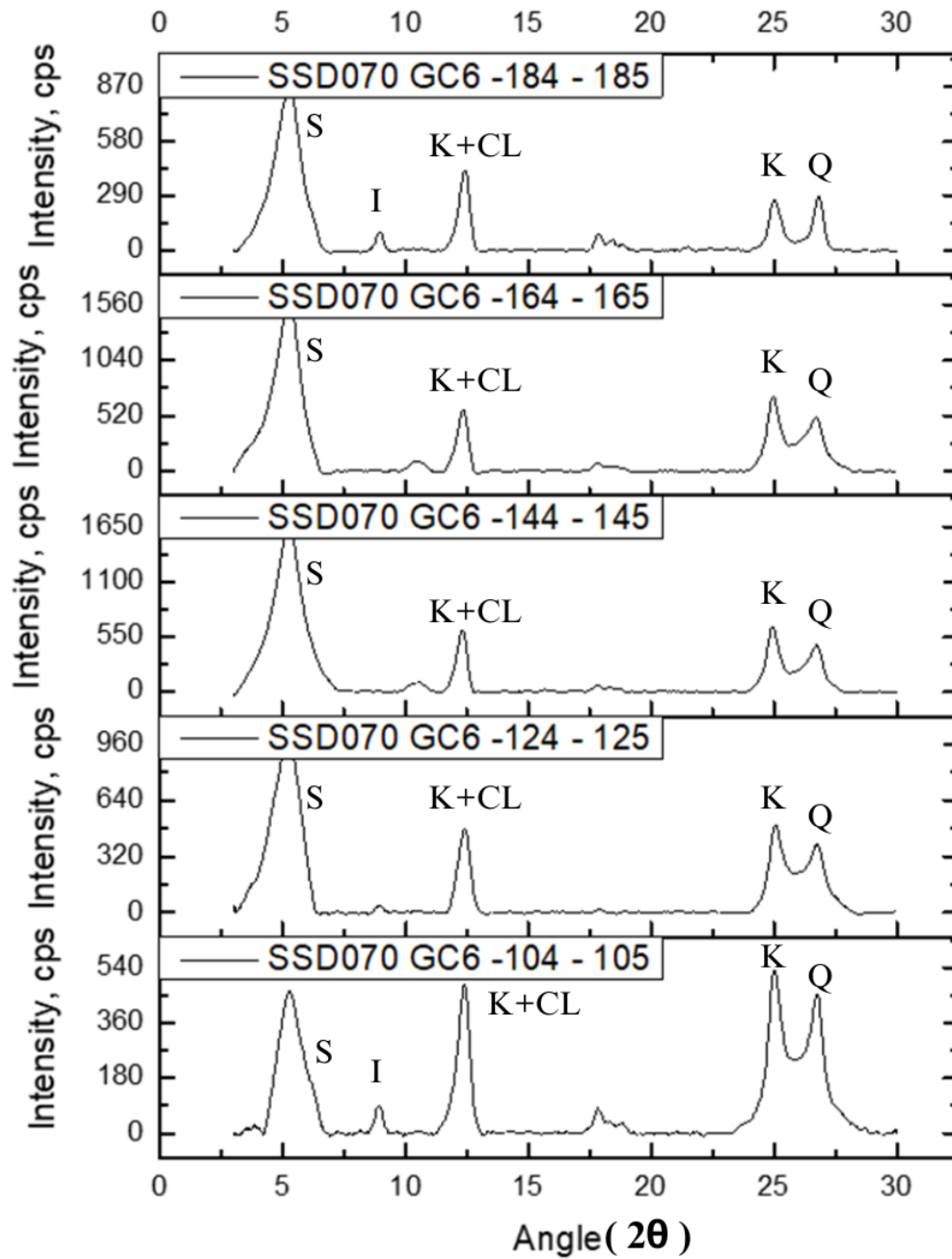


Fig. 21 (B): Clay mineral XRD Graph of GC6 104-185 cm

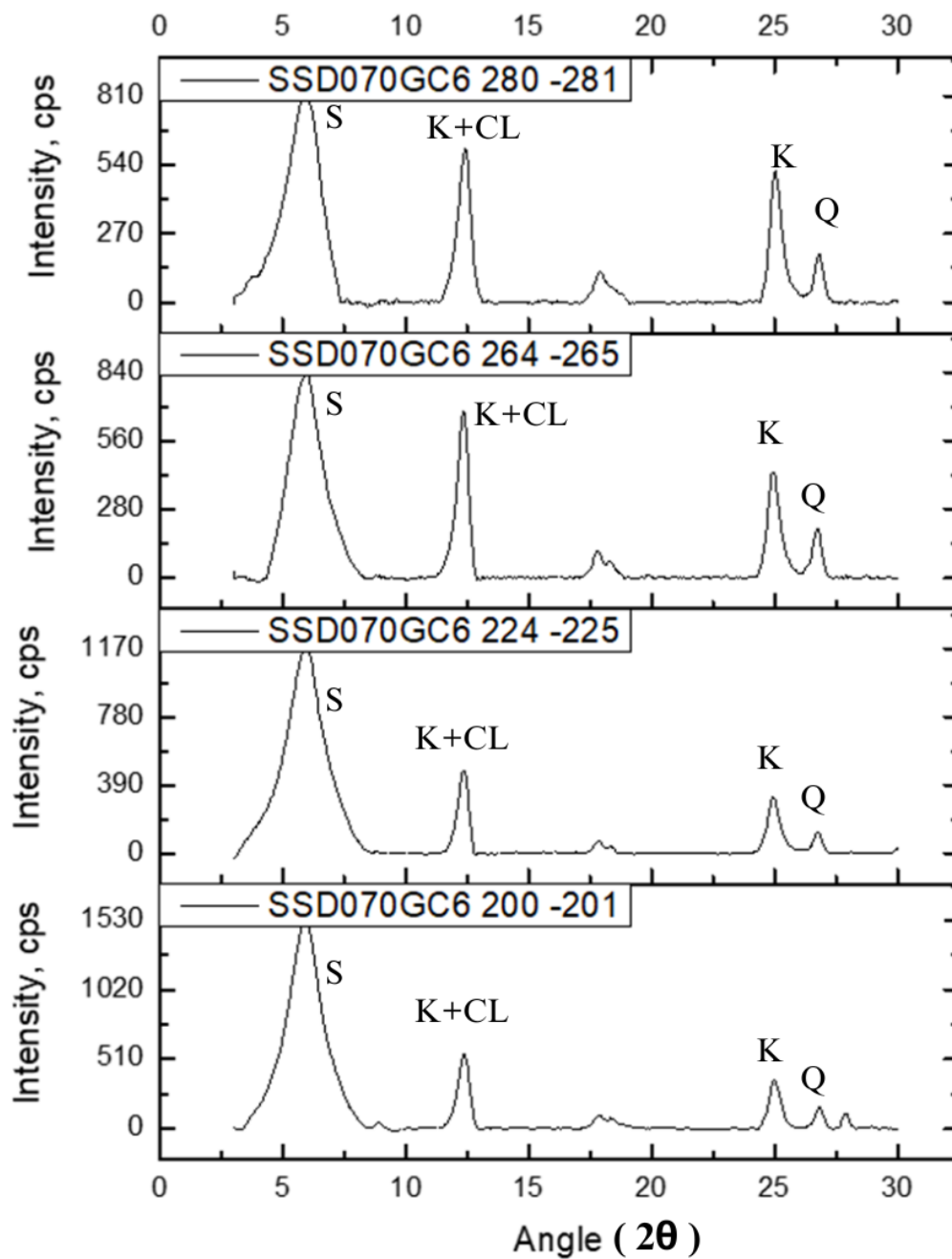


Fig. 21 (C): Clay mineral XRD Graph of GC6 200-281 cm

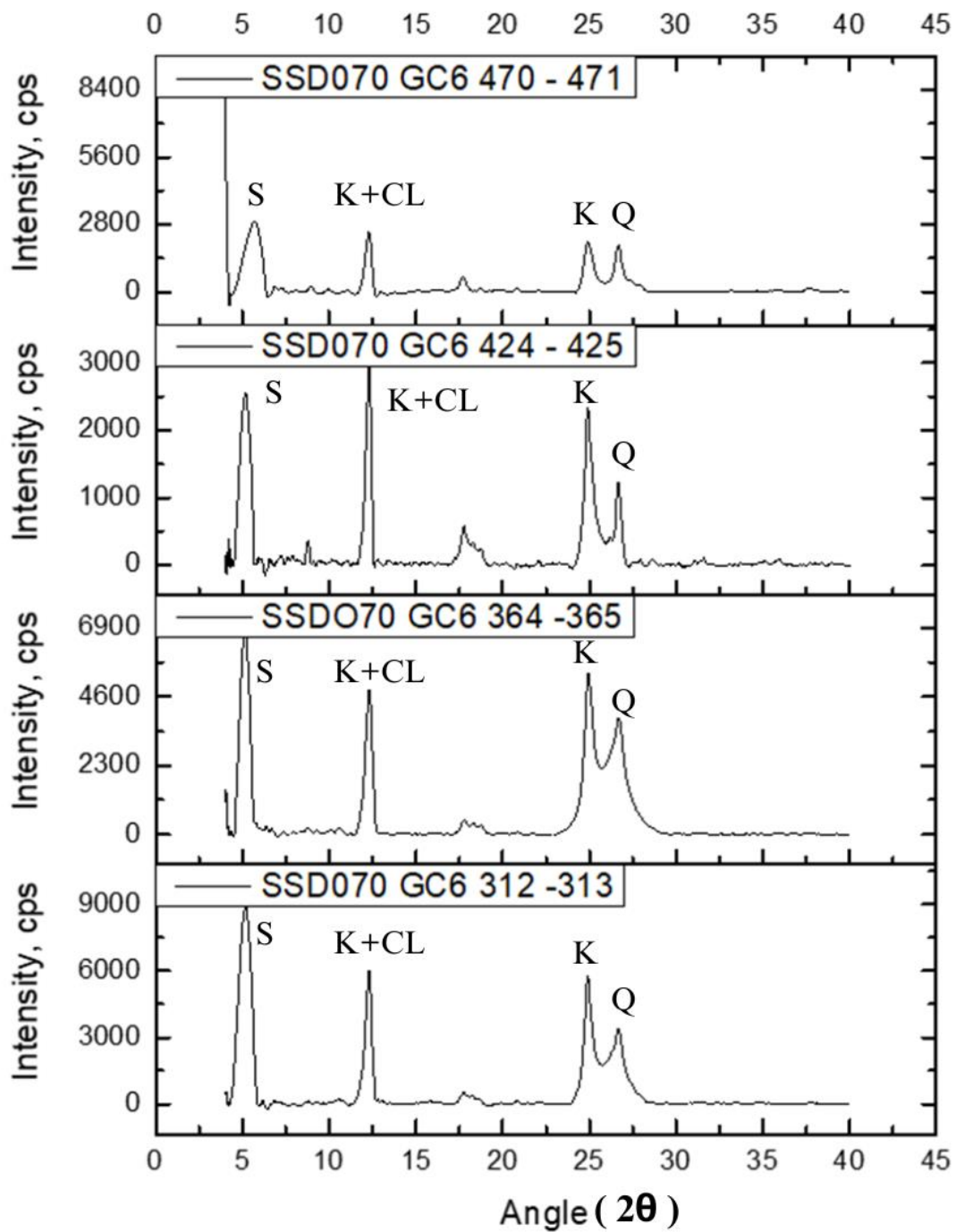


Fig. 21 (D): Clay mineral XRD Graph of GC6 312-471 cm

#### 4.9.1 PIE CHART DESCRIBING PERCENTAGES OF CLAY MINERALS IN GC6 SAMPLES

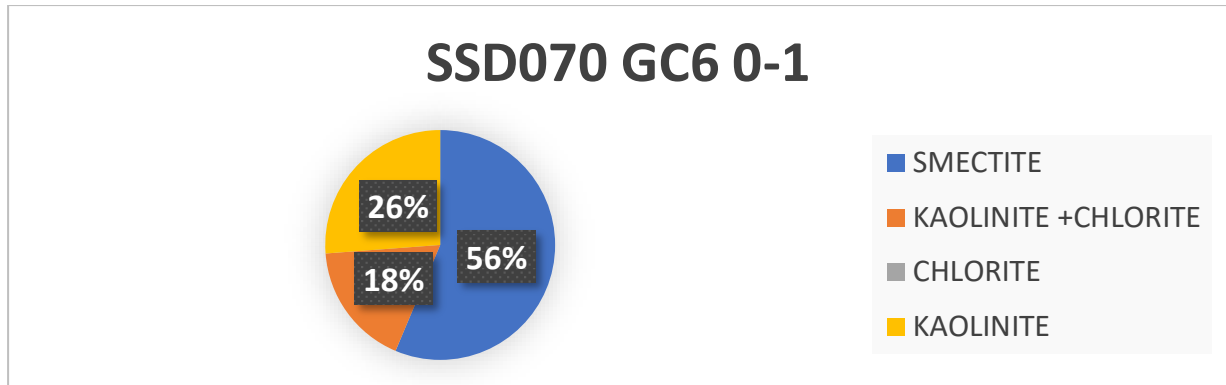


Fig 22 (A): Percentage of clay minerals in GC6 0-1 cm

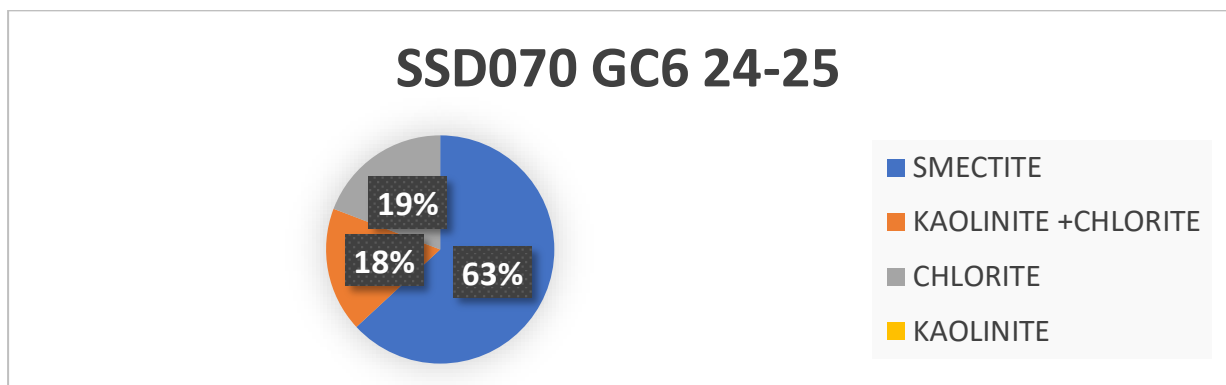


Fig 22 (B): Percentage of clay minerals in GC6 24-25 cm

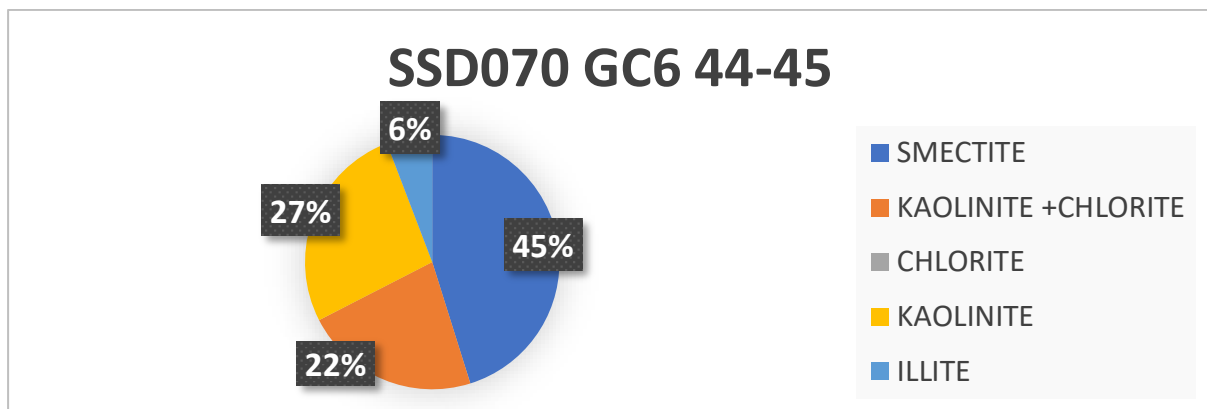


Fig 22 (C): Percentage of clay minerals in GC6 44-45 cm

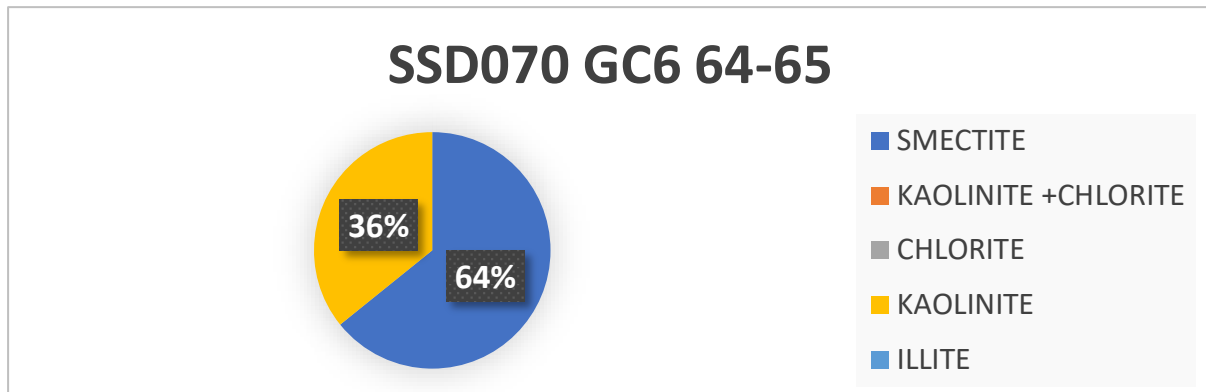


Fig 22 (D): Percentage of clay minerals in GC6 64-65 cm

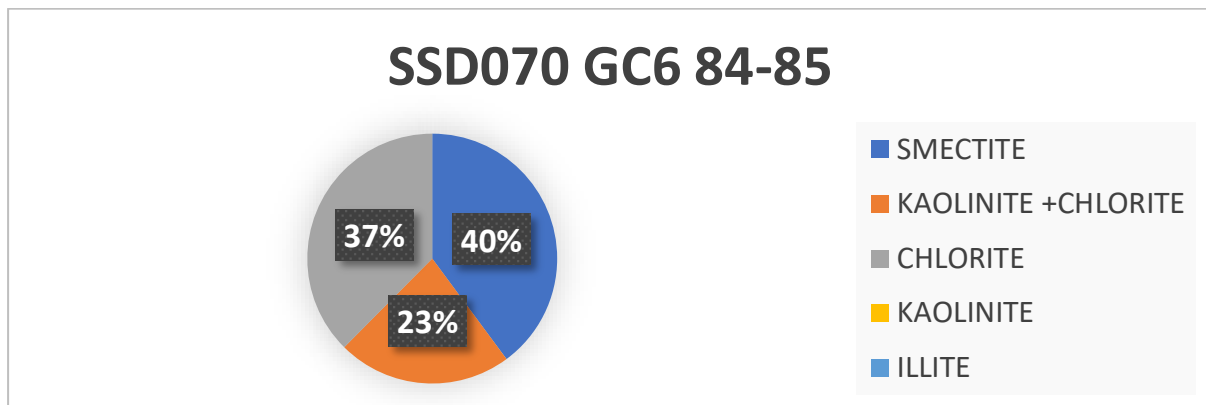


Fig 22 (E): Percentage of clay minerals in GC6 84-85 cm

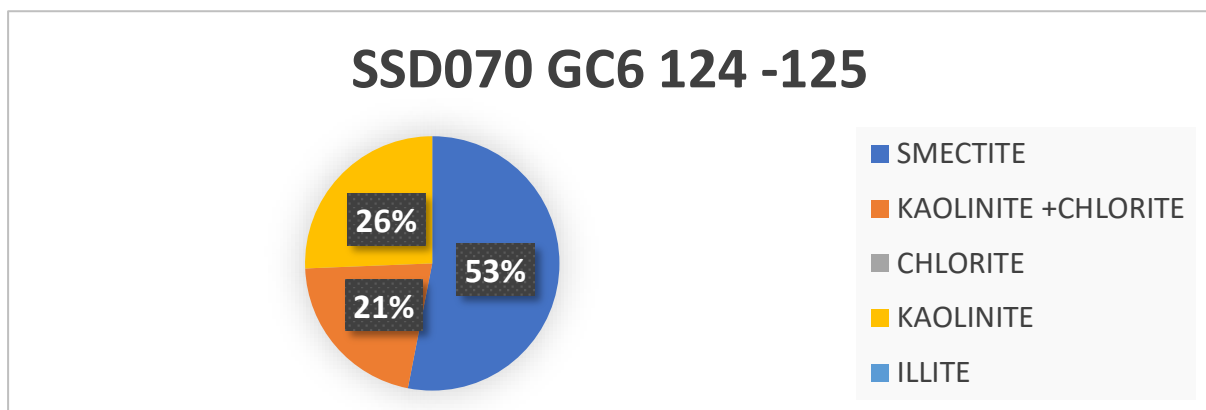


Fig 22 (F): Percentage of clay minerals in GC6 124-125 cm

### SSD070 GC6 144 -145



Fig 22 (G): Percentage of clay minerals in GC6 144-145 cm

### SSD070 GC6 164 -165



Fig 22 (H): Percentage of clay minerals in GC6 164-165 cm

### SSD070 GC6 184 -185



Fig 22 (I): Percentage of clay minerals in GC6 184-185 cm

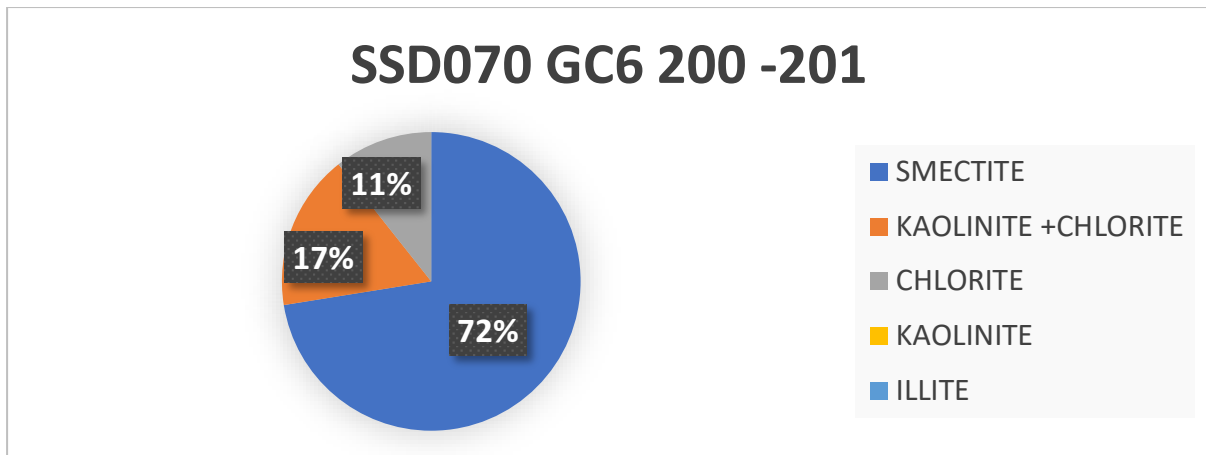


Fig 22 (J): Percentage of clay minerals in GC6 200-201 cm

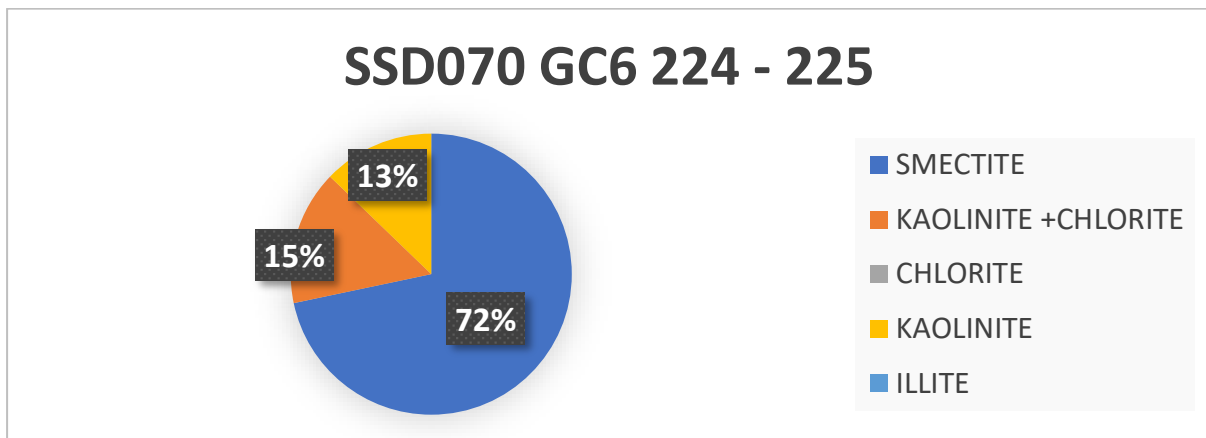


Fig 22 (K): Percentage of clay minerals in GC6 224-225 cm

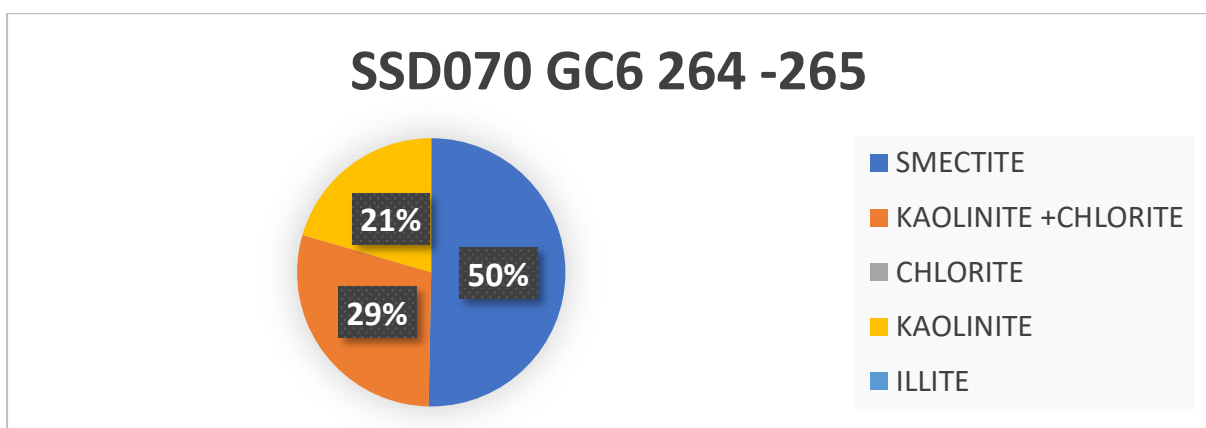


Fig 22 (L): Percentage of clay minerals in GC6 264-265 cm

### SSD070 GC6 280 -281

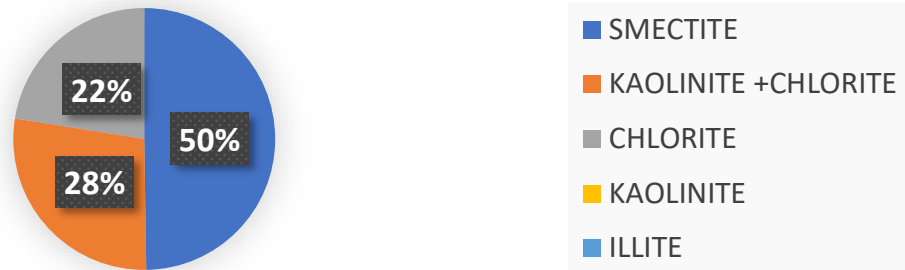


Fig 22 (M): Percentage of clay minerals in GC6 280-281 cm

### SSD070 GC6 312 -313

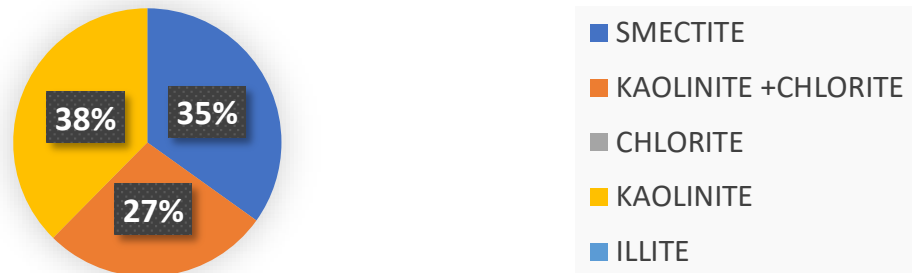


Fig 22 (N): Percentage of clay minerals in GC6 312-313 cm

### SSD070 GC6 364 -365

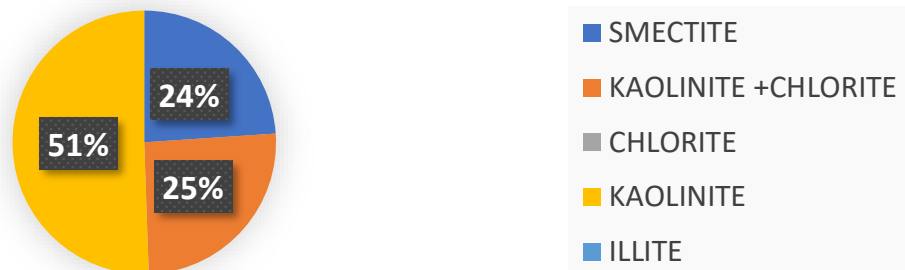


Fig 22 (O): Percentage of clay minerals in GC6 364-365 cm

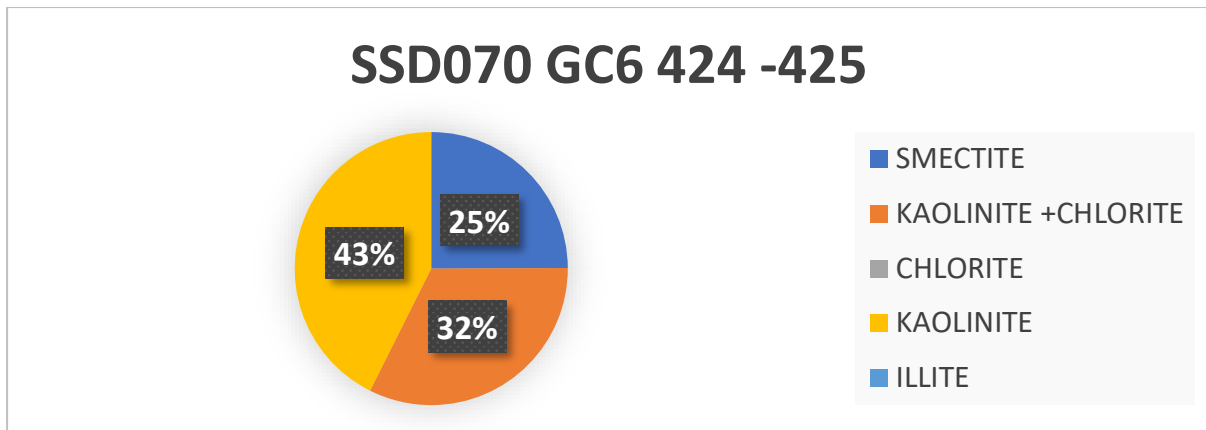


Fig 22 (P): Percentage of clay minerals in GC6 424-425 cm

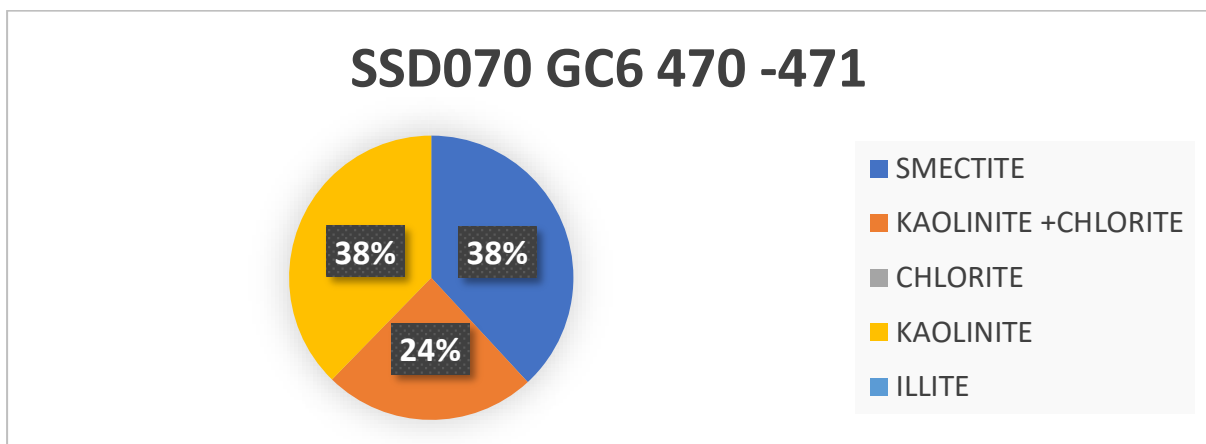


Fig 22 (Q): Percentage of clay minerals in GC6 470-471 cm

## 4.9.3 PERCENTAGE OF CLAY MINERALS IN GC6 CORE

SAMPL E NAME	SMECTIT E %	KAOLINITE +CHLORITE %	CHLORITE %	KAOLINITE %	ILLITE%
SSD070 GC6 0-1	56.3510539	17.46564877	0	26.18329724	0
SSD070 GC6 24- 25	63.1164928	17.68505984	19.19844728	0	0
SSD070 GC6 44- 45	45.1592057	22.29295083	0	26.73869839	5.80914501 3
SSD070 GC6 64- 65	64.2019004	0	0	35.79809953	0
SSD070 GC6 84- 85	39.8715484	22.57199453	37.556457	0	0
SSD070 GC6 104-105	24.4547789	26.85037049	42.58179311	0	6.11305747 7
SSD070 GC6 124-125	49.0660099	19.69012567	31.24386434	0	0
SSD070 GC6 144-145	60.7030325	15.60182146	0	23.695146	0
SSD070 GC6 164-165	56.5241461	15.75093958	0	27.72491429	0
SSD070 GC6 184-185	55.7028241	21.55872927	16.55170446	0	6.18674216 5
SSD070 GC6 200-201	72.463678	16.87354087	10.66278113	0	0
SSD070 GC6 224-225	71.6923435	15.50993509	0	12.79772141	0
SSD070 GC6 264-265	50.3171177	29.18140263	0	20.50147966	0
SSD070 GC6 280-281	49.7579095	27.75110621	22.49098421	0	0

<b>SSD070 GC6 312-313</b>	<b>34.8829001 2</b>	<b>27.52196411</b>	<b>0</b>	<b>37.59513577</b>	<b>0</b>
<b>SSD070 GC6 364-365</b>	<b>23.9392180 1</b>	<b>25.51357044</b>	<b>0</b>	<b>50.54721156</b>	<b>0</b>
<b>SSD070 GC6 424-425</b>	<b>24.9324275 9</b>	<b>32.46299942</b>	<b>0</b>	<b>42.60457298</b>	<b>0</b>
<b>SSD070 GC6 470-471</b>	<b>38.1242478 4</b>	<b>24.1774073</b>	<b>0</b>	<b>37.69834486</b>	<b>0</b>

Table 3: Percentage of clay minerals in GC6 core

#### 4.9.2 GC6 CORE BULK XRD GRAPH (GOA)

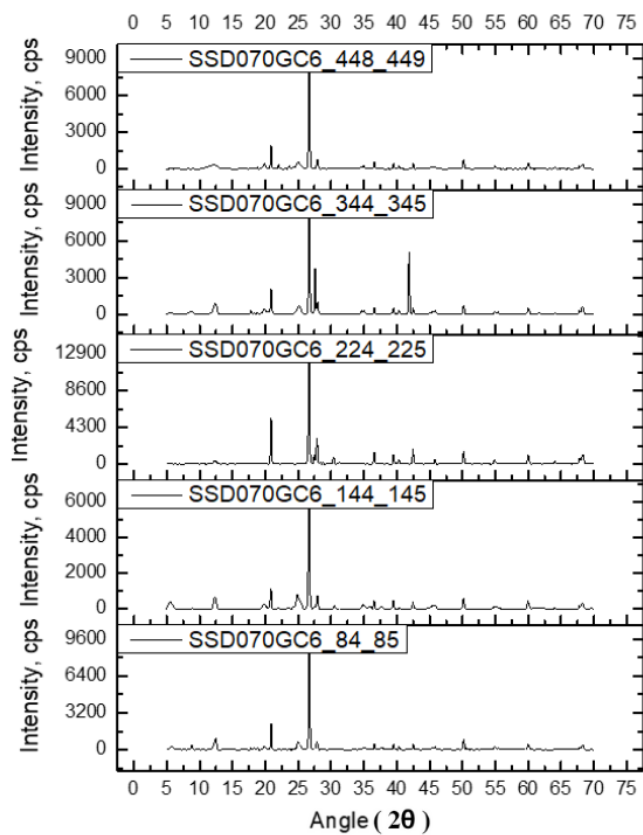


Fig. 23: Bulk mineral XRD Graph of SSD070 GC6 84-449 cm

#### 4.10 List of Bulk Minerals XRD

Sno.	Name	2θ
1	Smectite	4-5.5
2	Illite	8.8-9.0
3	Kaolinite + Chlorite	12.2-12.5
4	Gibbsite	18.3
5	Quartz	20.7-20.9, 26.6, 68.32
6	Kaolinite	24.8-24.9
7	Chlorite	25.1-25.2
8	Feldspar	27.98, 59.98
9	Magnetite	35.62
10	Hematite	36.58
11	Calcite	39.5

Table 4: List of Bulk Minerals XRD

#### 4.11 Clay minerals and their 2θ values

<b>Sno.</b>	<b>Name</b>	<b>2<math>\theta</math></b>
<b>1</b>	<b>Smectite</b>	<b>4-5.5</b>
<b>2</b>	<b>Illite</b>	<b>8.8-9.0</b>
<b>3</b>	<b>Kaolinite + Chlorite</b>	<b>12.2-12.5</b>
<b>4</b>	<b>Kaolinite</b>	<b>24.8-24.9</b>
<b>5</b>	<b>Chlorite</b>	<b>25.1-25.2</b>

Table 5: List of clay minerals and their 2 $\theta$  values

#### Other clay sized minerals

<b>Sno.</b>	<b>Name</b>	<b>2<math>\theta</math></b>
<b>1</b>	<b>Quartz</b>	<b>20.7-20.9, 26.6</b>

Table 6: List of other clay sized minerals

#### 4.12 OVERALL COMPARISON BETWEEN GC2 AND GC6 CORE CLAY MINERALOGY

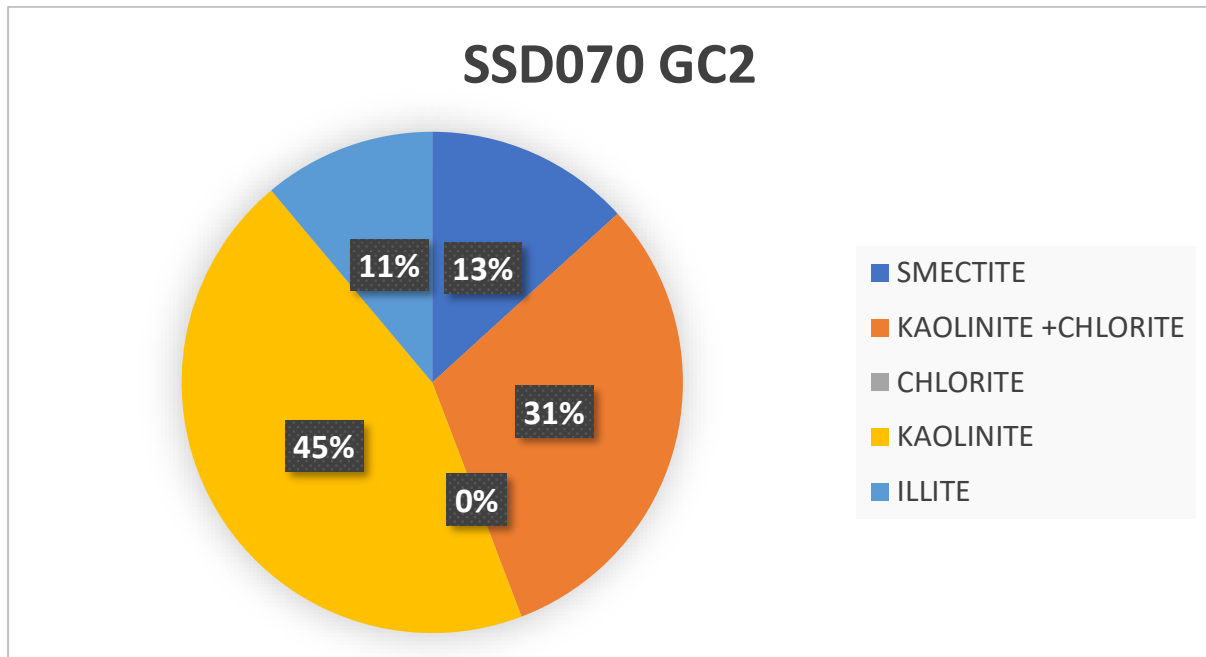


Fig 24 (A): Overall percentage of clay minerals in GC2 core

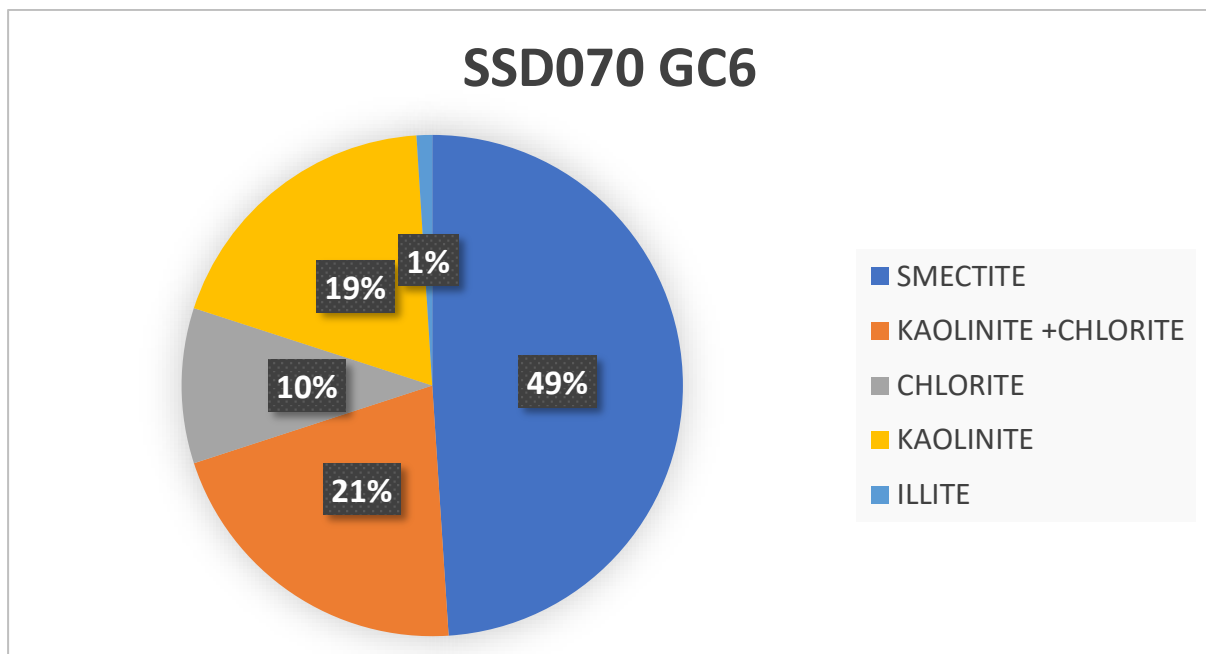


Fig 24 (B): Overall percentage of clay minerals in GC6 core

### 4.13 Variation in clay minerals from the offshore samples

The overall bulk mineralogy of the Gravity Core samples (GC) is prominently Quartz (20.7-20.9, 26.6). The prominent clay minerals smectite, kaolinite + chlorite (12.2-12.5) is prominent in both GC6 and GC2. Illite (8.8) is the least abundant clay mineral observed in the overall mineralogy of the sample. Presence of other minerals like magnetite (35.62), hematite (36.58) and calcite (39.5) are observed in smaller peaks within both the sample. These minerals are not quantified as the study focusses on the study of clay minerals in the sample.

#### 4.13.1 GC2 CORE SAMPLE(MANGALORE)

Kaolinite, Chlorite, Smectite and Illite are the major clay minerals found under this study within this sample. The Smectite concentration varies from varies from 1 to 38% with an average of 13.2%. the highest Smectite concentration was observed in the sample **SSD070 GC2 470-471** at 37% and the lowest in samples **SSD070 GC2 40-41**, **SSD070 GC2 280-281**, **SSD070 GC2 340-341** (1%). Although not very prominent, a cyclic increasing and then decreasing trend of smectite with depth within the core sample is observed.

Kaolinite and chlorite are generally studied together as they have very closely associated 2 theta peak values. In general, the kaolinite + chlorite values trend between 19 to 49% averaging about 31.3% within the sample.

Another kaolinite peak was observed which is not associated with the chlorite peaks, and concentration of these kaolinites are also significant. The concentrations vary from 24 to 59% averaging about 44.6% within the sample.

Illite is the least abundant clay minerals observed within the sample. Varying from 7 to 28% and averaging about 11.1% within the sample.

#### **4.13.2 GC6 CORE SAMPLE (GOA)**

Smectite, Kaolinite, Chlorite and Illite are also the major clay minerals found under this study within this sample. Smectite concentration varies from 72 to 24% averaging about 48.9% within the sample. No particular patterns or trends were observed within this sample. Kaolinite + Chlorite varies between 15 to 32%. The average value comes to be about 21%. A general cyclic increasing and decreasing trend can be observed within the sample. Chlorite varies from 16 to 42% averaging about 10% overall within the sample while kaolinite varies from 12 to 50% averaging just over 18%. Illite remains the least abundant clay mineral with very few occurrences within the sample. Illite is observed to present only in the upper sections of the core sample and absent in the subsequent samples below. The concentration of illite varies only from 5 to 6% in the entire sample.

#### **4.13.3 SP CORE BULK SAMPLE (MANGALORE)**

Smectite (4-5.5) and illite (8.8) are the prominent bulk minerals in the sample. This trend is followed by Kaolinite + chlorite (12.2-12.5) which are the remaining abundant minerals in the sample.

#### **4.13.4 MC CORE BULK SAMPLE(MANGALORE)**

Quartz (20.7-20.9, 26.6) is the most prominent mineral observed in the bulk mineralogy of the sample. Kaolinite + chlorite (12.2-12.5) peaks are the abundant clay minerals observed in the sample.

#### 4.14 DISCUSSION

Two major gravity core samples were collected from the Arabian off Mangalore and Goa coasts. The LPSA (Laser Particle Size Analyser) data of the sample was based on the size variation of sand, silt and clay within the gravity core, dividing it into five distinct zones based on depth. In the deepest zone (490-417cm) Zone One, Silt size particles are predominant (58% to 56%) followed by clay (42% to 43%) and no sand (0%). The second zone (467cm to 417cm) Zone Two, is characterized by initial increase in silt percentage (55% to 79%) followed by a decline (58%) and a significant decrease from 44% to 20% in clay percentage and then a sudden increases to 41%, while sand percentage remains almost zero. In Zone Three (417cm to 280cm) the silt percentage varies from 50% to 55%, while the clay percentage varies from 45% to 50%, while sand still remains negligible. In Zone Four (280cm to 132cm), a decrease in clay percentage from 40% to 20% is observed, while the silt percentage increases from 50% to 75%, with little sand content. Zone Five (132cm to 0cm) composes of clay varying from 16% to 20%, silt percentage varying from 75% to 83% and sand from 6% to 10%.

In the multicore sample, the clay percentage varies from 12% to 15%, the silt percentage ranges from 82% to 87%, and the sand percentage is minimal at 0.5%. This composition suggests a sediment dominated by silt and a relatively lower presence of clay.

The particle size studies on the multicore sample revealed that clay sized particles vary from 12% to 15%, while the silt size particle range from 82% to 87%, and sand ranges only about 0.5% of the sample. Much variability in percentage is not observed in clay sized particles. Silt particles are observed to have a cyclic increase and decrease in percentage with depth within the sample. Sand sized particles only observed between 0 to 10 cm and 25 to 30 cm.

The Mangalore coast has great amount of Kaolinite and Chlorite content, which could be associated with result of the possible chemical weathering due to precipitation in this region.

Kaolinite must have been transported from the chemical weathering product of the hinterland. Smectite and Illite and comparatively less in the Mangalore coast. Minerals such as smectite, illite, and chlorite have been observed, indicating a possible terrestrial source of origin.

In the Goa Coast sample, Smectite was found to be the most abundant clay mineral. Some of the smectite may have originated via the cross-shelf movement of sediments from the Deccan trap source. The presence of illite and chlorite in the sample further suggests that longshore transport currents carried it from the Indus River. (Rao & Rao, 1995).

Kaolinite is observed to be found in similar abundances in both Mangalore and Goa, suggesting their derivation from the gneissic rocks of the region. The source of the very little Illite and Chlorite present in the samples of both coasts could possibly be from the derived from the Western Ghats by the weathering in the humid tropical climate. (Rao & Rao, 1995). Since illite is often produced by physical weathering in cool, dry climates, and kaolinite is typically formed by severe chemical weathering in warm, humid climates, the kaolinite to illite ratio is a good proxy for paleoclimatic reconstruction. This suggests an overall warmer, more humid climate of depositions of these sediments. (SS Das et. al, 2013)

The contribution of terrigenous non-clay minerals, such as feldspar and quartz, was appreciable. Even though quartz may be produced from a wide range of source rocks in a variety of weathering scenarios, feldspar was better preserved in drier climates. The increased terrigenous influx during this time frame suggests sediments that were trapped on the continental shelf during the high stand of sea were being eroded. large quartz abundances are likely a result of coarse particle sizes and large terrigenous sediment influxes throughout the Pleistocene and Holocene eras. We assume that quartz is mostly extracted from Pre Cambrian granitic gneisses and other metamorphic rocks that are exposed in western India's interior and

coastal regions, and that many little rivers that drain the region eventually carry the mineral to the Arabian Sea.

**CHAPTER V**

**CONCLUSION**

## 5. CONCLUSION

- The particle size studies suggested that much of the gravity core sample is composed of silt, followed by clay and sand. The only significant quantity of sand was observed in of the shallow deposits of Zone Five, between 132cm to 0cm. This indicates a downward fining of sediments within the core.
- The particle size studies on the multicore sample revealed that clay sized particles vary from 12% to 15%, while the silt size particle range from 82% to 87%, and sand ranges only about 0.5% of the sample. Silt particles are observed to have a cyclic increase and decrease in percentage with depth within the sample. Sand sized particles only observed between 0 to 10 cm and 25 to 30 cm. This again suggests that sand sized particles are less abundant in these sedimentary core sample.
- Most of the samples fall within the range of mesokurtic and leptokurtic distributions, suggesting a tendency towards moderate to high concentration of sediment in the silt and clay fractions.
- The sediment composition shows a positive skewness (very coarse skewed).
- Cross-plot of sorting against mean grain-size reveals that increased grain-size have a negative relationship with sorting. All the samples are poorly sorted.
- Mean grain size versus skewness. grain sizes show a coarse tail.
- Mean grain size versus kurtosis. Shows a higher concentration of grain sizes around the mesokurtic to leptokurtic
- They may also be present on the continental shelf, where they compete with other processes, such as wind or tidal-driven circulation, which may have an even greater effect on sediment deposition
- The silt and clay of these samples are modern and brought to this environment by the present-day drainage pattern

- Grain size distribution shows that the inner-shelf is dominated with clay silt and silty clay with minor amounts of sand. The analysed sediments are characteristically poorly sorted, and dominantly positively skewed with leptokurtic and Mesokurtic nature.
- The prevalence of poorly sorted sediments indicates near source region. However, considerable number of moderately sorted sediment samples reveal continuous reworking of sediments by waves and currents
- The decreasing sorting trend as grain sizes increase to is interpreted to be due to increasing rates of bioturbation and sediment mixing, also indicates weak bottom currents which capable of transporting only the finest silts and clays in suspension.
- A larger percentage of silt and clay fractions indicates finer-grained sediments, which are commonly found in low-energy environments such as floodplains, estuaries, and deep marine settings. These sediments are often transported and deposited by suspension settling or slow sedimentation processes.
- The examination of particle size distribution with depth demonstrates that sediment samples vary in size sorting. The general pattern reveals that the sediments range from very poorly sorted to poorly sorted.
- The gravity core sample GC2 composes of the minerals Kaolinite, Chlorite, Smectite and Illite in the descending order of their abundance.
- The gravity core sample GC6 composes of the minerals Smectite, Kaolinite, Chlorite and Illite in the descending order of their abundances.

**CHAPTER VI**

**REFERENCES**

## 6. REFERENCES

adsorbed additive and time-dependent behavior. *Rheologica Acta*, 50, 29-38.

Ao, H., & Xiao, G. (2012). History and Prediction of the Asian Monsoon and Glacial Terminations, Based on Records from the South China Sea. In *International Perspectives on Global Environmental Change*. IntechOpen.

Aoki, S., Oinuma, K., & Sudo, T. (1974, April). The distribution of clay minerals in the recent sediments of the Japan Sea. In *Deep Sea Research and Oceanographic Abstracts* (Vol. 21, No. 4, pp. 299-310). Elsevier.

Biscaye, P. E. (1965). Mineralogy and sedimentation of recent deep-sea clay in the Atlantic Ocean and adjacent seas and oceans. *Geological Society of America Bulletin*, 76(7), 803-832.

Biscaye, P. E. (1965). Mineralogy and sedimentation of recent deep-sea clay in the Atlantic Ocean and adjacent seas and oceans. *Geological Society of America Bulletin*, 76(7), 803-832.

Blatt, H., Middleton, G., and Murray, R., 1980, *Origin of sedimentary rocks* (2d ed.): Englewood Cliffs, N.J., Prentice-Hall, 766 p.

Blott, S. J., & Pye, K. (2001). GRADISTAT: a grain size distribution and statistics package for the analysis of unconsolidated sediments. *Earth surface processes and Landforms*, 26(11), 1237-1248.

Carver, R. E. (1971). *Procedures in sedimentary petrology*.

Chauhan, O. S., & Gujar, A. R. (1996). Surficial clay mineral distribution on the southwestern continental margin of India: evidence of input from the Bay of Bengal. *Continental Shelf Research*, 16(3), 321-333.

Chester, R. (1990). 1.1 Setting the background: a unified 'process-orientated' approach to marine geochemistry.

Chester, R., & Chester, R. (1990). The transport of material to the oceans: The atmospheric pathway. *Marine geochemistry*, 83-134.

Cullity, B. D. (1956). *Elements of X-ray Diffraction*. Addison-Wesley Publishing.

Das, S. S., Rai, A. K., Akaram, V., Verma, D., Pandey, A. C., Dutta, K., & Prasad, G. R. (2013). Paleoenvironmental significance of clay mineral assemblages in the southeastern Arabian Sea during last 30 kyr. *Journal of earth system science*, 122, 173-185.

Das, S. S., Rai, A. K., Akaram, V., Verma, D., Pandey, A. C., Dutta, K., & Prasad, G. R. (2013). Paleoenvironmental significance of clay mineral assemblages in the southeastern Arabian Sea during last 30 kyr. *Journal of earth system science*, 122, 173-185.

Diju, S., & Thamban, M. (2006). Clay mineral and textural variations in the sediments of Chandragiri River, estuary and shallow marine realms off Kasaragod, Kerala. *JOURNAL-GEOLOGICAL SOCIETY OF INDIA*, 67(2), 189.

Fagel, N. (2007). Chapter four clay minerals, deep circulation and climate. *Developments in marine geology*, 1, 139-184.

Folk, R. L. (1980). *Petrology of sedimentary rocks*. Hemphill publishing company.

Folk, R. L., & Ward, W. C. (1957). Brazos River bar [Texas]; a study in the significance of grain size parameters. *Journal of sedimentary research*, 27(1), 3-26.

Garrison, T. (2010). *Oceanography: an invitation to marine science*.

Goh, R., Leong, Y.K. and Lehane, B. (2011) Bentonite slurries-zeta potential, yield stress,

Gribble, C. D. (Ed.). (2012). *Optical mineralogy: principles and practice*. Springer Science & Business Media.

Griffin, J. J., & Goldberg, E. D. (1975). The fluxes of elemental carbon in coastal marine sediments. *Limnology and oceanography*, 20(3), 456-463.

Griffin, J. J., Windom, H., & Goldberg, E. D. (1968, August). The distribution of clay minerals in the world ocean. In *Deep Sea Research and Oceanographic Abstracts* (Vol. 15, No. 4, pp. 433-459). Elsevier.

Gupta, P. K., & Pant, M. C. (1983). Chemical composition of surface sediments in a eutrophic lake: Naini Tal (UP, India). *Environmental Pollution Series B, Chemical and Physical*, 6(2), 95-107.

Hamann, Y., Ehrmann, W., Schmiedl, G., & Kuhnt, T. (2009). Modern and late Quaternary clay mineral distribution in the area of the SE Mediterranean Sea. *Quaternary Research*, 71(3), 453-464.

Hashimi, N. H., Nigam, R., Nair, R. R., & Rajagopalan, G. (1995). Holocene sea level fluctuations on Western Indian continental margin: an update. *Journal of geological Society of India*, 157-162.

Inman, D. L., & Jenkins, S. A. (1999). Climate change and the episodicity of sediment flux of small California rivers. *The Journal of geology*, 107(3), 251-270.

Karisiddaiah, S. M., & Veerayya, M. (2002). Occurrence of pockmarks and gas seepages along the central western continental margin of India. *Current Science*, 52-57.

Karisiddaiah, S. M., Veerayya, M., & Vora, K. H. (2002). Seismic and sequence stratigraphy of the central western continental margin of India: late-Quaternary evolution. *Marine Geology*, 192(4), 335-353.

Kessarkar, P. M., Rao, V. P., Ahmad, S. M., & Babu, G. A. (2003). Clay minerals and Sr–Nd isotopes of the sediments along the western margin of India and their implication for sediment provenance. *Marine Geology*, 202(1-2), 55-69.

Kolla, V., Kosteki, J. A., Robinson, F., Biscaye, P. E., & Ray, P. K. (1981). Distributions and origins of clay minerals and quartz in surface sediments of the Arabian Sea. *Journal of Sedimentary Research*, 51(2), 563-569.

Kolla, Venkatarathnam, Allan WH Bé, and Pierre E. Biscaye. "Calcium carbonate distribution in the surface sediments of the Indian Ocean." *Journal of Geophysical Research* 81.15 (1976): 2605-2616.

Konta, J. (1985). Mineralogy and chemical maturity of suspended matter in major rivers sampled under the SCOPE/UNEP project. *Transport of carbon and minerals in major world rivers, Part, 3*, 569-592.

Luis, A. J., & Kawamura, H. (2004). Air-sea interaction, coastal circulation and primary production in the eastern Arabian Sea: a review. *Journal of Oceanography*, 60, 205-218.

Mattait, B., Peters, J., & Eckhardt, F. J. (1973). Results of petrographic analysis on sediments from the Indian Pakistan continental margin (Arabian Sea)(German). *Meteor” Forsch Ergebrisse Reiche*, (14), 1-50.

Mazumdar, A., Peketi, A., Dewangan, P., Badesab, F., Ramprasad, T., Ramana, M. V., ... & Dayal, A. (2009). Shallow gas charged sediments off the Indian west coast: Genesis and distribution. *Marine Geology*, 267(1-2), 71-85.

Middelburg, J. J. (1989). A simple rate model for organic matter decomposition in marine sediments. *Geochimica et Cosmochimica acta*, 53(7), 1577-1581.

Nair, R. R., & Pylee, A. B. R. A. H. A. M. (1968). Size distribution and carbonate content of the sediments of the western shelf of India. *B Natl Inst Sci India*.

Nair, R. R., Hashimi, N. H., & Purnachandra, V. (1982). Distribution and dispersal of clay minerals on the western continental shelf of India. *Marine Geology*, 50(1-2), M1-M9.

Nair, R. R., Hashimi, N. H., & Rao, V. P. (1982). On the possibility of high-velocity tidal streams as dynamic barriers to longshore sediment transport: evidence from the continental shelf off the Gulf of Kutch, India. *Marine Geology*, 47(1-2), 77-86.

Pearson, M.N. (2003). *The Indian Ocean* (1st ed.). Routledge.  
<https://doi.org/10.4324/9780203414132>

Perkins, D. (2013). *Mineralogy: Pearson New International Edition*. Pearson.

Poppe, L. J., Paskevich, V. F., Hathaway, J. C., & Blackwood, D. S. (2001). A laboratory manual for X-ray powder diffraction. *US Geological Survey open-file report*, 1(041), 1-88.

Rao, V. P., & Rao, B. R. (1995). Provenance and distribution of clay minerals in the sediments of the western continental shelf and slope of India. *Continental Shelf Research*, 15(14), 1757-1771.

Rao, V. P., & Wagle, B. G. (1997). Geomorphology and surficial geology of the western continental shelf and slope of India: A review. *Current Science*, 330-350.

Reddy, N. P. C., & Rao, K. M. (2001). Heavy sediment influx during early Holocene: Inference from clay mineral studies in a core from the Western Bay of Bengal. *Current science*, 1361-1364.

Schott, F. (1983). Monsoon response of the Somali Current and associated upwelling. *Progress in oceanography*, 12(3), 357-381.

Shetye, S. R., Gouveia, A. D., Shenoi, S. S. C., Michael, G. S., Sundar, D., Almeida, A. M., & Santanam, K. (1991). The coastal current off western India during the northeast monsoon. *Deep Sea Research Part A. Oceanographic Research Papers*, 38(12), 1517-1529.

Shetye, S. R., Shenoi, S. S. C., Gouveia, A. D., Michael, G. S., Sundar, D., & Nampoothiri, G. (1991). Wind-driven coastal upwelling along the western boundary of the Bay of Bengal during the southwest monsoon. *Continental Shelf Research*, 11(11), 1397-1408.

Siddiquie, H. N., Rao, D. G., Vora, K. H., & Topgi, R. S. (1981). Acoustic masking in sediments due to gases on the western continental shelf of India. *Marine Geology*, 39(1-2), M27-M37.

Sirocko, F., & Lange, H. (1991). Clay-mineral accumulation rates in the Arabian Sea during the late Quaternary. *Marine Geology*, 97(1-2), 105-119.

Socher, R., Pennington, J., Huang, E. H., Ng, A. Y., & Manning, C. D. (2011, July). Semi-supervised recursive autoencoders for predicting sentiment distributions. In *Proceedings of the 2011 conference on empirical methods in natural language processing* (pp. 151-161).

Stanley, D. J., & Liyanage, A. N. (1986). Clay-mineral variations in the northeastern Nile Delta, as influenced by depositional processes. *Marine Geology*, 73(3-4), 263-283.

Subramanian, V. (1980). Mineralogical input of suspended matter by Indian rivers into the adjacent areas of the Indian Ocean. *Marine Geology*, 36(3-4), M29-M34.

Thamban, M., Rao, V. P., & Schneider, R. R. (2002). Reconstruction of late Quaternary monsoon oscillations based on clay mineral proxies using sediment cores from the western margin of India. *Marine Geology*, 186(3-4), 527-539.

Torsvik, T. H., Müller, R. D., Van der Voo, R., Steinberger, B., & Gaina, C. (2008). Global plate motion frames: toward a unified model. *Reviews of geophysics*, 46(3).

Vinu, P., & Narayana, A. C. (2012). *Sedimentological and Geotechnical Studies of Coastal Sediments of Central Kerala* (Doctoral dissertation, Cochin University of Science And Technology).

Weaver, C. E. (1989). *Clays, muds, and shales*. Elsevier.

Wentworth, C. K. (1922). A scale of grade and class terms for clastic sediments. *The journal of geology*, 30(5), 377-392.

Windom, H., Gardner, W., Stephens, J., & Taylor, F. (1976). The role of methylmercury production in the transfer of mercury in a salt marsh ecosystem. *Estuarine and Coastal Marine Science*, 4(5), 579-583.